Mutations in protein kinase A catalytic subunit as a cause of adrenal Cushing´s syndrome: mechanisms and functional consequences

Mutationen in der katalytischen Untereinheit von Proteinkinase A als Ursache des adrenalen Cushing Syndroms: Mechanismen und funktionelle Konsequenzen

Doctoral thesis for a doctoral degree
at the Graduate School of Life Sciences,
Julius-Maximilians-Universität Würzburg,
Section Biomedicine

submitted by

Kerstin Bathon

from

Aschaffenburg

Würzburg, 2018

Submitted on: ……..……..

Office stamp

Members of the *Promotionskomitee*:

Chairperson: Prof. Alexander Buchberger

Primary Supervisor: Prof. Davide Calebiro

Supervisor (Second): Prof. Martin Fassnacht

Supervisor (Third): Prof. Caroline Kisker

Date of Public Defence: ……..……

Date of Receipt of Certificates: ……..

Affidavit

I hereby declare that my thesis entitled

‘Mutations in protein kinase A catalytic subunit as a cause of adrenal Cushing´s syndrome: mechanisms and functional consequences‘

is the result of my own work. I did not receive any help or support from commercial consultants. All sources and / or materials applied are listed and specified in the thesis. Furthermore, I confirm that this thesis has not yet been submitted as part of another examination process neither in identical nor similar form.

Würzburg, …….. ……

Date Kerstin Bathon

Eidesstattliche Erklärung

Hiermit erkläre ich an Eides statt, die Dissertation

„Mutationen in der katalytischen Untereinheit von Proteinkinase A als Ursache des adrenalen Cushing Syndroms: Mechanismen und funktionelle Konsequenzen”

eigenständig, d.h. insbesondere selbständig und ohne Hilfe eines kommerziellen Promotionsberaters, angefertigt und keine anderen als die von mir angegebenen Quellen und Hilfsmittel verwendet zu haben. Ich erkläre außerdem, dass die Dissertation weder in gleicher noch in ähnlicher Form bereits in einem anderen Prüfungsverfahren vorgelegen hat.

Würzburg, …….. ……

Datum Kerstin Bathon

Mutations in protein kinase A catalytic subunit as a cause of adrenal Cushing´s syndrome: mechanisms and functional consequences

Doctoral thesis by
Kerstin Bathon

Table of contents

Abbreviations

3β-HSD	3β-Hydroxysteroid dehydrogenase/Δ^{5-4} isomerase
ACTH	adrenocorticotropic hormone
ADP	adenosine diphosphate
AGC	automatic gain control
AIMAH	ACTH-independent macronodular adrenal hyperplasia
AKAP	A kinase anchoring protein
ANOVA	analysis of variance
APA	aldosterone-producing adenomas
ATF	activating transcription factor
ATP	adenosine triphosphate
BCA	bicinchoninic acid
C subunit	catalytic subunit
cAMP	cyclic-adenosine monophosphate
Cas	CRISPR associated protein
CFP	cyan fluorescent protein
CIT	citron rho-interacting kinase
CNB	cyclic nucleotide binding site
CNBA	cyclic nucleotide binding site A
CNBB	cyclic nucleotide binding site B
Co-IP	co-immunoprecipitation
CPA	cortisol-producing adrenocortical adenoma
CREB	cAMP response element-binding protein
CRH	corticotropin-releasing hormone
CRISPR	clustered regularly interspaced short palindromic repeats
crRNA	CRISPR RNA
CS	Cushing's syndrome
Cy2	fluorescence tag
CYP11A1	mitochondrial cholesterol side-chain cleavage enzyme
CYP11B1	cytochrome P450 11B1
CYP17	cytochrome P450 17A1
CYP21	steroid 21-hydroxylase
Cα	catalytic subunit α
D/D domain	dimerization/docking domain
ddH_2O	double distilled water

DNA	deoxyribonucleic acid
DNAJB1	gene coding for a member of the heat shock 40 protein family
dNTPs	deoxynucleotide triphosphates
E. coli	*Escherichia coli*
Epac	exchange protein directly activated by cAMP
ERK	extracellular signal-regulated kinase
FACS	fluorescence activated cell sorting
FDR	false-discovery rate
FLAG-tag	tag with amino acid sequence: DYKDDDDK
FL-HCC	fibrolamellar hepatocellular carcinoma
FRET	Förster resonance energy transfer
FSK	forskolin
GFP	green fluorescent protein
GH-oma	growth-hormone secreting adenomas
Glu	glutamate
GPCR	G-protein coupled receptor
GRM4	gene encoding for metabotropic glutamate receptor 4
H1.2	histone 1.2
H1.4	histone 1.4
HA-tag	protein tag derived from hemagglutinin
HCD	higher-energy collisional dissociation
HDR	homology directed repair
HPA	hypothalamic-pituitary-adrenal
HPRT	gene coding for hypoxanthine-guanine phosphoribosyltransferase
HyD	hybrid detector
indel	random insertions and deletions
IP	immunoprecipitation
IQR	interquartile range
LB medium	lysogeny broth medium
LHR	luteinizing hormone receptor
MAPK	mitogen-activated protein kinase
MCR2	melanocortin receptor 2
MEK	mitogen-activated protein kinase
Mg	magnesium
mGlu4	metabotropic glutamate receptor 4
mGlu5	metabotropic glutamate receptor 5

MS	mass spectrometry
MS/MS	tandem mass spectrometry
nanoLC-MS/MS	nanoscale liquid chromatography coupled to tandem mass spectrometry
NES	nuclear export signal
PAGE	polyacrylamide gel electrophoresis
PAM	protospacer adjacent motif
PCR	polymerase chain reaction
PDB	protein data bank
PDE	phosphodiesterase
PEP	posterior error probability
PKA	protein kinase A
PKI	protein kinase inhibitor
PPNAD	primary pigmented nodular adrenocortical disease
PRKACA	gene encoding for the catalytic subunit α of protein kinase A
PRKACB	gene encoding for the catalytic subunit β of protein kinase A
PRKARIA	gene encoding for the regulatory subunit Iα of protein kinase A
PrKX	protein kinase X
PRS1/2	peripheral recognition sites
PVDF	polyvinylidene difluoride
R subunit	regulatory subunit
Raf	rapidly accelerated fibrosarcoma
Ras	rat sarcoma
RNA	ribonucleic acid
RNP	ribonuclear protein
SDS-PAGE	sodium dodecyl sulfate polyacrylamide gel electrophoresis
sgRNA	Single guide RNA
SILAC	stable isotope labeling by amino acids in cell culture
SNAPf	self-labeling protein tag
Sp	*Streptococcus pyogenes*
SpCas9	*Streptococcus pyogenes* CRISPR-associated proteins
Src	cellular sarcoma
STAR	steroidogenic acute regulatory protein
T	temperature
t	time
TF	transcription factor
Tm	melting temperature

TOM34	mitochondrial import receptor subunit
tracrRNA	trans-activating crRNA
TSHR	thyrotropin receptor
WT	wild-type
YFP	yellow fluorescent protein
α/β-GSK	glycogen synthase kinase 3 alpha/beta

1 Introduction

1.1 Cushing's syndrome

Cushing's syndrome was first described by Harvey Cushing in 1932 as a clinical manifestation of the pituitary gland[1]. Typical symptoms associated with Cushing's syndrome are moon facies and facial plethora[1, 2, 3, 4]. However, patients also present catabolic symptoms, like muscle weakness, skin fragility, osteoporosis, and severe metabolic complications such as obesity, diabetes and hypertension[1, 2, 3, 4]. Cushing's syndrome is a rare disease with 2.3 cases per million per year[5]. However, if untreated, about 50% of the patients die within 5 years mainly due to infections, cardiovascular complications or neoplastic diseases[6].

1.1.1 Adrenal Cushing's syndrome

Cushing's syndrome is caused by chronic cortisol excess[7]. Under normal conditions, cortisol production is under the strict control of the hypothalamic–pituitary–adrenal (HPA) axis[7]. In the hypothalamus, the corticotropin-releasing hormone (CRH) is secreted in portal circulation and transported to the pituitary gland. In the pituitary gland, CRH stimulates release of the adrenocorticotropic hormone (ACTH), which stimulates cortisol production and release in the adrenal gland[7]. Circulating cortisol controls its own endocrine axis by inducing a negative feedback on hypothalamic CRH and pituitary ACTH secretion (Figure 1)[2, 7].

The most common presentation of Cushing's syndrome is ACTH dependent and is termed as Cushing's disease (60-80% of cases)[2, 4, 5]. It is often caused by an ACTH secreting pituitary adenoma[2, 4, 5] and in very rare cases by ectopic (extra pituitary) ACTH secreting tumors[2, 3, 4]. Less frequently, Cushing's syndrome can be ACTH independent, which is then caused by adrenocortical tumors (15-30% of cases)[3, 5]. This type of syndrome is termed adrenal Cushing's syndrome. Another very rare cause of Cushing's syndrome are CRH secreting tumors[2, 3, 4].

In all these types of Cushing's syndrome, the control system for cortisol secretion is disturbed. In the case of an ACTH secreting pituitary adenoma, increased ACTH secretion enhances cortisol secretion, which has a negative feedback on CRH, but not on ACTH secretion, due to the resistance of the tumor[2, 7](Figure 1). Consequently, this leads to excess cortisol production and release[2, 7]. Contrary to this, both CRH and ACTH are low in adrenal Cushing's syndrome, but there is a supraphysiological cortisol secretion from the adrenal gland[4, 7](Figure 1).

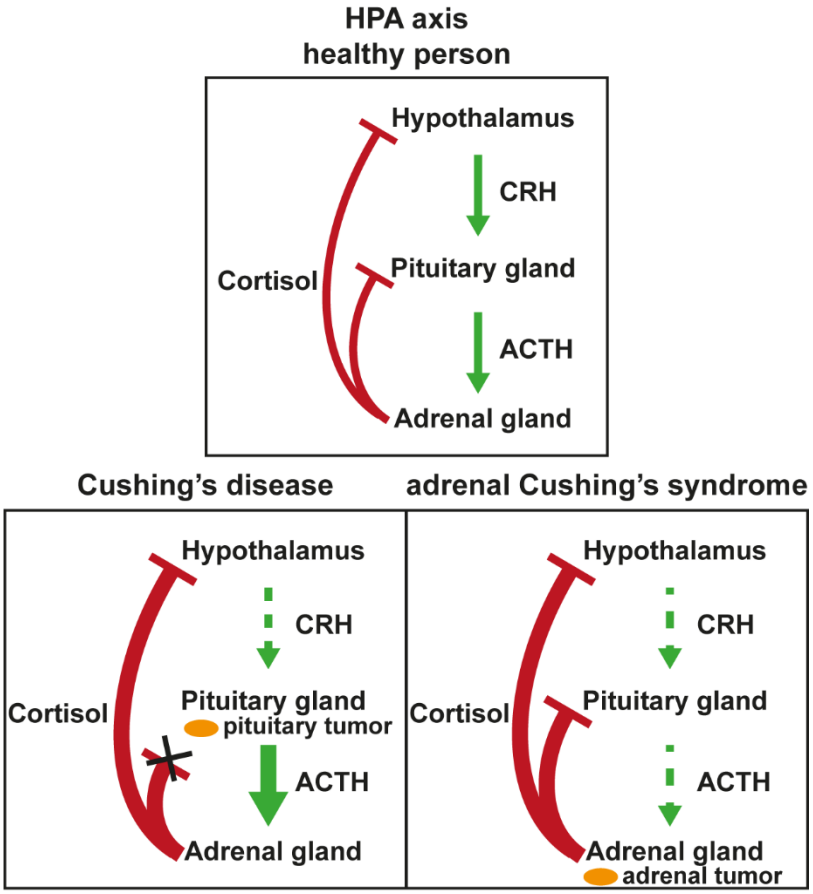

Figure 1: The hypothalamic–pituitary–adrenal (HPA) axis. Cortisol production in the adrenal gland is under the strict control of corticotropin-releasing hormone (CRH) and adrenocorticotropic hormone (ACTH). Under normal conditions, circulating cortisol in the bloodstream gives a negative feedback on hypothalamic CRH and pituitary ACTH production. Tumors can disturb this system. For example, in Cushing's disease, an ACTH secreting pituitary tumor and in adrenal Cushing's syndrome a cortisol producing adrenal tumor lead to excess cortisol production.

1.1.2 Cortisol synthesis in the adrenal gland

The adrenal gland is composed of the adrenal cortex which is the outermost layer and the *medulla* which is at the center[7]. The *medulla* represents only 10-20% of the adrenal gland and is responsible for epinephrine and norepinephrine secretion[7]. The adrenal cortex comprises the major part of the adrenal gland (80-90%)[7] and can be divided into three zones, each with specific functions[7, 8]. The outer zone is called *zona glomerulosa* and is responsible for production of the steroid hormone aldosterone[7, 8]. The middle part is named *zona fasciculata* and is the thickest zone in the adrenal cortex (>70% of the adrenal cortex)[7, 8]. It is responsible for the production of glucocorticoids like cortisol[7, 8]. The innermost zone of the adrenal cortex, at the border of *medulla* is defined as *zona reticularis*[7, 8] and is responsible for androgen production[7, 8].

Cortisol synthesis and secretion in the *zona fasciculata* is controlled by ACTH and involves two distinct responses which can be distinguished temporally as acute and chronic[9]. In both responses, the cyclic-adenosine monophosphate (cAMP)/protein kinase A (PKA) pathway plays an important role. Signaling via this pathway is initiated by ACTH binding to the melanocortin receptor 2 (MCR2)[10, 11], a G protein-coupled receptor (GPCR). Following this binding and the ensuing receptor and G protein conformational changes, adenylyl cyclase is activated which converts adenosine triphosphate (ATP) to cAMP[11, 12, 13]. The second messenger cAMP activates PKA by binding to the regulatory (R) subunits of PKA, which undergo a conformational change and release the catalytic (C) subunits[14, 15]. The C subunit is then able to phosphorylate its targets in the cytosol (*e.g*. StAR[16]) and in the nucleus (*e.g.* transcription factors like cAMP response element-binding protein (CREB)[17]) which ultimately leads to cortisol synthesis and secretion (Figure 2).

PKA phosphorylation of targets in the cytosol is involved in the acute response of ACTH, which occurs rapidly, within seconds or minutes[18]. This response mobilizes cholesterol, a precursor of cortisol, to the mitochondrial cholesterol side-chain cleavage enzyme (CYP11A1)[18]. This involves (i) the rapid mobilization of cholesterol esters from lipid droplets, (ii) the hydrolysis of cholesterol esters in the lipid droplets and finally (iii) the transfer of cholesterol into mitochondria where the cholesterol side-chain cleavage enzyme (CYP11A1) is located[9]. The first phase is regulated by the stimulation of low-density lipoprotein receptors[19] and the second phase is controlled by protein kinase A dependent activation of cholesterol esterases[20]. The last phase is the rate-limiting step of steroidogenesis and mediated by the steroidogenic acute regulatory (StAR) protein[21]. StAR is activated by PKA mediated phosphorylation[16] and its transcription is also induced via the cAMP/PKA pathway which is part of the chronic response[21, 22].

In the chronic response of ACTH, the phosphorylation of nuclear targets by PKA plays a relevant role[23]. Here PKA mediates the activation of transcription factors of the activating transcription factor (ATF)/CREB family[17]. This leads to increased levels of steroidogenic enzymes like 3β-hydroxysteroid dehydrogenase/Δ^{5-4} isomerase (3β-HSD)[24], steroid 21-hydroxylase (CYP21)[25], cytochrome P450 17A1 (CYP17)[26], cytochrome P450 11B1 (CYP11B1)[27], Cyp11A1[28] and StAR[29, 30] (Figure 2).

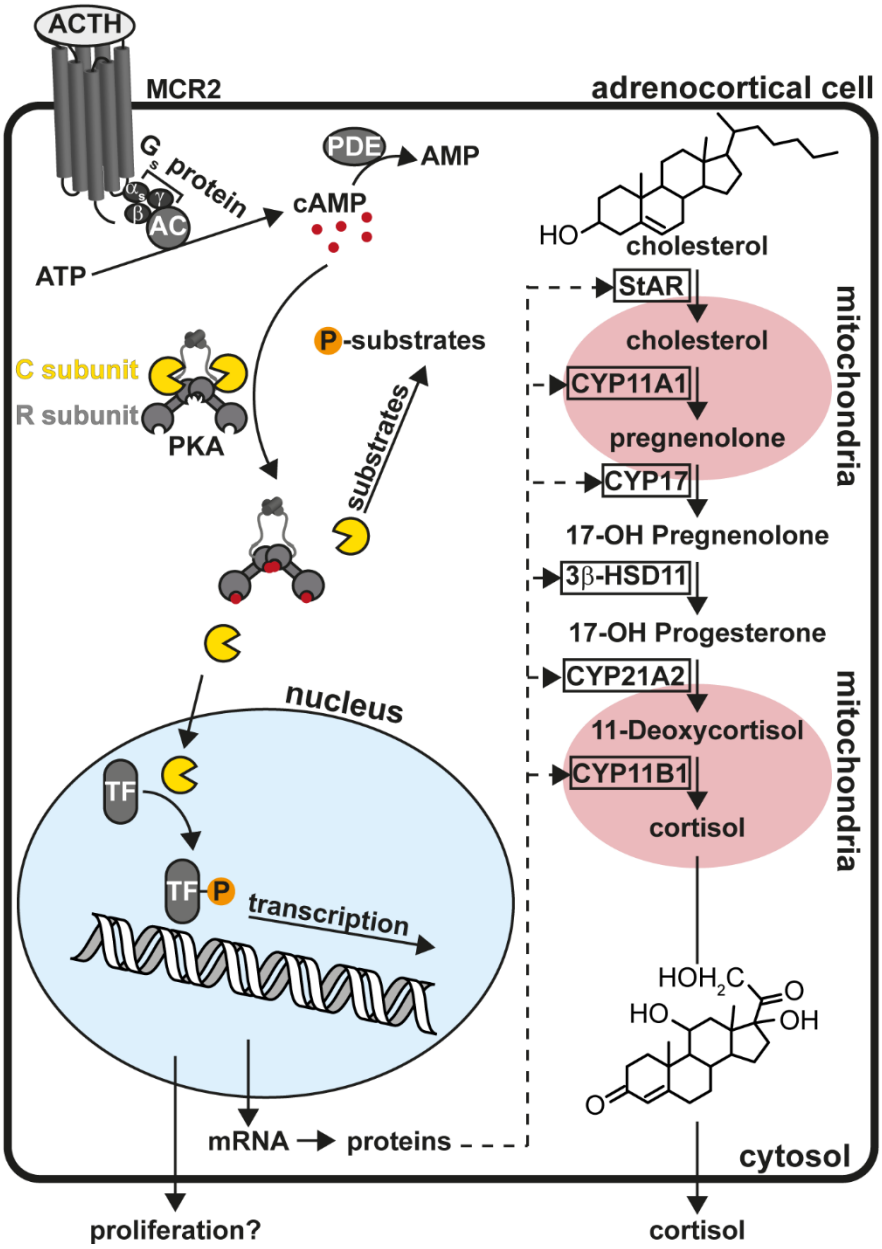

Figure 2: cAMP/PKA pathway mediating ACTH response in adrenal cells. Steroidogenesis and proliferation in adrenal cells is under the strict control of adrenocorticotropic hormone (ACTH). Upon ACTH binding to the melanocortin receptor 2 (MCR2), adenylyl cyclase (AC) is activated which converts adenosine triphosphate (ATP) to cyclic-adenosine monophosphate (cAMP). Consequently, cAMP activates protein kinase A (PKA), which then phosphorylates targets in the cytosol and nucleus leading to increased steroidogenesis and proliferation.

1.1.3 Role of cAMP/PKA pathway in proliferation of adrenal cells

As mentioned, the cAMP/PKA pathway also plays a role in cell proliferation. This effect is achieved by a crosstalk with other intracellular signaling pathways like the extracellular signal-regulated kinases (ERK)/mitogen-activated protein kinase (MAPK) signaling pathway (Figure 3)[31]. The crosstalk with this pathway could explain the observed cell type specific inhibition or stimulation of proliferation by the cAMP/PKA pathway. For the ERK/MAPK signaling cascade, it was shown that it can be stimulated directly by cAMP through activation of exchange protein directly activated by cAMP (Epac)[32] or via PKA[33] stimulation of Src kinase[34] (Figure 3). In both cases, the expression of B-Raf controls the outcome of the pathway[31, 33, 35]. In the brain B-Raf is expressed only in neurons[36] but not in astrocytes[37]. Additionally, B-Raf was also found in many endocrine cells[38, 39], cells of neural crest origin[33, 40], endothelial cells[41] and prostate cells[42]. In addition to B-Raf expression, two B-Raf splicing variants and their expression pattern also play a role in controlling proliferation[31]. It was shown that the predominance of the N-terminally truncated 62 kDa B-Raf isoform leads to inhibition of proliferation, whereas the expression of the 95 kDa isoform leads to increased proliferation (Figure 3)[31, 35]. The expression of the two B-Raf isoforms is cell type specific and can also be dependent on the confluency of the culture[35]. This means, that crosstalk between the cAMP/PKA pathway and ERK/MAPK signaling can lead to inhibition or stimulation of proliferation, depending on the expression of B-Raf and its isoforms in the cells. This explains why the cAMP/PKA pathway was found to stimulate proliferation in many endocrine cells[43], where B-Raf is expressed. Whereas in others, for example in adipocytes, the cAMP/PKA pathway inhibited proliferation[44].

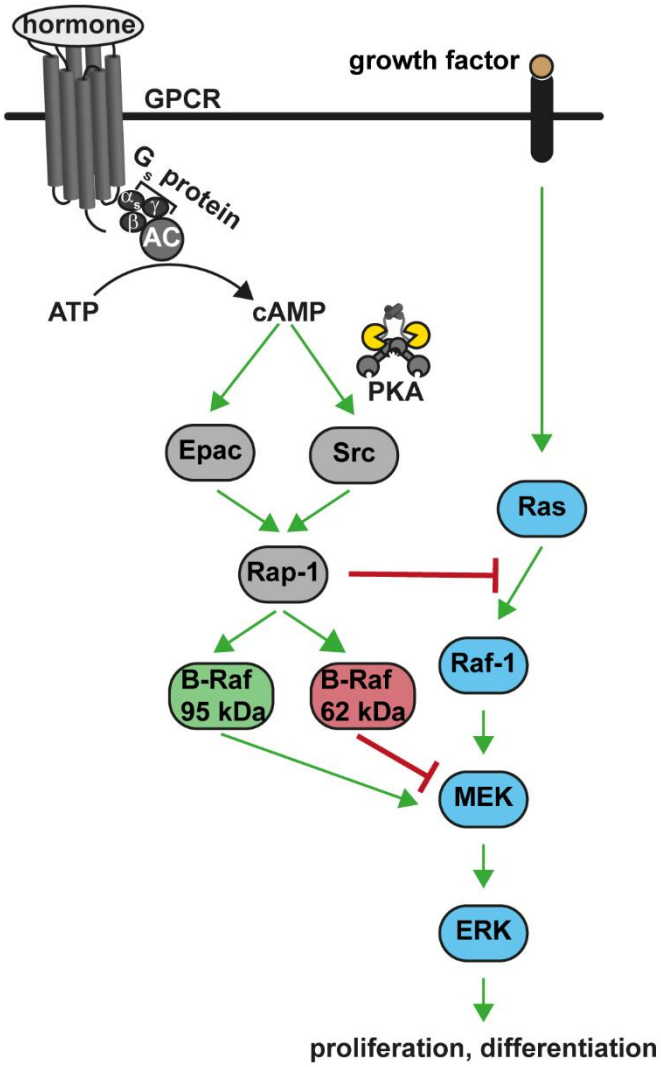

Figure 3: Extracellular signal-regulated kinases (ERK) signaling leading to proliferation and differentiation of cells. Growth factors activate the GTPase Ras which in turn binds and activates Raf-1. Raf-1 phosphorylates mitogen-activated protein kinase (MEK) which phosphorylates and activates extracellular signal-regulated kinase (ERK). This leads to cell proliferation and differentiation. cAMP can independently (via exchange protein directly activated by cAMP (Epac)) or dependently (via Src) from PKA activate Rap-1. Rap-1 has an inhibitory effect on Ras-binding of Raf-1 and therefore can inhibit cell growth. But Rap-1 also activates the two B-Raf isoforms, which can either activate or inhibit MEK and this stimulate or inhibit cell proliferation and differentiation respectively.

Whether or not ACTH stimulates the proliferation of adrenocortical cells is a matter of debate. An argument in favor of a proliferative effect of ACTH is the clinical picture observed in congenital adrenal hyperplasia, which is caused by inactivating mutations in genes encoding key enzymes involved in steroidogenesis[45]. The lack of cortisol due to the genetic defect results in increased ACTH levels which are associated with adrenal gland hyperplasia[45]. Additionally, germline inactivating mutations of MCR2 or the MCR2 accessory protein (MRAP), identified in familiar glucocorticoid deficiency, were found to be causative for adrenal hypoplasia[46, 47]. These mutations cause an impaired response to ACTH, resulting in low cortisol levels, which cause not only higher ACTH levels, but also lead to hypoplasia[46, 47, 48]. This is further supported by studies in mice lacking the MCR2 receptor[49] or proopiomelanocortin (POMC), a precursor of ACTH[50]. Both mouse models exhibit a survival rate of 25%[49, 50]. MCR2 knock-out mice develop adrenocortical hypoplasia with a normal architecture of the adrenal gland, even though the cells in *zona fasciculata* are atrophied[49]. Mice lacking POMC present obesity, pigmentation defects and adrenal insufficiency[50, 51, 52]. In addition, they show a disrupted adrenocortical architecture and adrenal hypoplasia[51]. Adrenal hypoplasia is also observed upon hypophysectomy or dexamethasone treatment in rats[53, 54]. Interestingly, treatment with an ACTH analogue is capable of restoring the normal architecture and weight of the adrenal gland[51]. This indicates that ACTH is essential for adrenal development in rodents[52].

On the other hand, several studies reported a paradox antiproliferative effect of ACTH on adrenal cells *in vitro*[55, 56, 57]. This was also supported by the observation that cAMP inhibits proliferation in adrenal tumor cells[56], which also lead to phase I/II clinical trials of cAMP analogs as anti-tumor drug[58]. It is noteworthy that experiments with selective cAMP analogs revealed a positive effect of PKA regulatory I (RI) and a negative effect of PKA regulatory II (RII) subunits on cell proliferation[59, 60]. Another argument against a proliferative effect of ACTH is that after unilateral adrenalectomy, ACTH treatment has been shown to inhibit the proliferative response of the remaining adrenal gland[54]. Interestingly, primary bovine adrenocortical cells have been reported to desensitize to the anti-proliferative effect of ACTH with chronic exposure and start growing in presence of ACTH[57]. Possibly at least partially reconciling these contrasting observations, a study in adrenal cancer cell lines (human NCI-H295 and mouse Y-1) suggested that POMC derived peptides other than ACTH might be responsible for pituitary-dependent proliferation of adrenocortical cells[61].

1.1.4 Mutations found in cAMP/PKA pathway causing endocrine diseases

Given the prominent role of the cAMP/PKA pathway in hormone production and proliferation of endocrine cells, alterations via inherited or acquired mutations of genes encoding enzymes implicated in this pathway account for a variety of endocrine diseases[62, 63, 64, 65, 66, 67, 68, 69, 70]. Those mutations, for example in the case of several GPCRs such as the thyroid stimulating hormone receptor (TSHR)[64] or luteinizing hormone receptor (LHR)[71, 72] and the MCR2[46], lead to either activation or inactivation of the cAMP/PKA pathway. The first mutation of a GPCR was identified in toxic thyroid adenomas[64]. Those mutations were found to render the TSHR constitutively active which lead to thyrotropin-independent activation of the cAMP/PKA pathway and therefore hyperfunction of the thyroid[64]. Loss-of-function mutations have also been identified in the TSHR leading to resistance to the natural agonist, thyroid stimulating hormone[73, 74], and may cause varying manifestations of mild to severe hypothyroidism[62]. This loss-of-function was found to be the result of reduced biological activity[74] or lower surface expression of the mutated receptor[73].

Another key protein involved in the cAMP/PKA signaling pathway is the $G\alpha_s$ protein and was found to be mutated in McCune-Albright syndrome[67], growth-hormone secreting adenomas (GH-oma)[66] and in ACTH-independent macronodular adrenal hyperplasia (AIMAH)[62, 75]. The identified mutations lead to an increased activity of the $G\alpha_s$ protein which causes increased cAMP formation[67]. These kind of activating mutations of the $G\alpha_s$ protein have been identified for the first time in GH-oma[66] and in AIMAH patients[75]. Recently, the crystal structure of the most frequent mutation occurring at arginine 201 in $G\alpha_s$ protein has been resolved[76] and revealed that the mutation results in an active $G\alpha_s$ in the GDP-bound state by stabilization of an intramolecular hydrogen bond network[76]. In addition to those activating mutations, cases of inactivating $G\alpha_s$ protein mutations were reported in Albright's hereditary osteodystrophy[77]. This syndrome is characterized by a short stature, obesity, subcutaneous ossifications, brachydactyly and mental deficiency[78].

In addition, phosphodiesterases (PDEs), which are responsible for degradation of cAMP to AMP[79], were found to be mutated in primary pigmented nodular adrenocortical disease (PPNAD)[80]. For example, two deletions leading to a frameshift (171delTfs41X and 1655_1657delTCT/insCCfs15X) and one base pair substitution (919C-T; R307X) in PDE11A were found to disrupt the expression of PDE11A and therefore cause elevated levels of cAMP[81].

One of the most prominent examples for mutations in genes of enzymes implicated in the cAMP/PKA pathway are mutations in the gene coding for the regulatory Iα (RIα) subunit of PKA (*PRKAR1A*) [69]. Those mutations were found to be responsible for Carney Complex, a multiple endocrine neoplasia syndrome[69]. This disease is characterized by PPNAD, cutaneous and neuronal tumors, cardiac myxomas and pigmented lesions of the skin and mucosae[69, 82]. The *PRKAR1A* mutations found in Carney Complex can lead to the production of a truncated, nonfunctional protein resulting in its reduced expression or increased degradation[83, 84, 85, 86]. This further impairs the function of the inhibitory RIα subunit and renders the catalytic subunit constitutively active[83, 84, 85, 86]. Additional *PRKAR1A* mutations have been identified in acrodysostosis, a syndrome characterized by skeletal abnormalities and resistance to multiple hormones[87, 88]. These mutations reduce the ability of cAMP to dissociate the RIα subunit from the holoenzyme and thus stabilize its interaction with the catalytic (C) subunit[87, 88].

More recently, we and other groups reported mutations in the gene coding for the catalytic α (Cα) subunit of PKA (*PRKACA*) in cortisol-producing adrenocortical adenomas (CPAs) of Cushing's syndrome patients. The identified mutations lead to constitutive activation of PKA Cα. This constitutively active PKA was linked to development of Cushing´s syndrome due to CPAs[89, 90, 91, 92, 93, 94]. Another mutation, leading to a fusion protein of DnaJ homolog subfamily B member 1 (DNAJB1) and PKA Cα was identified in fibrolamellar hepatocellular carcinoma (FL-HCC)[95]. This chimeric protein was shown to be expressed at higher levels than the wild-type PKA Cα subunit and to lack the binding domain of PKA R subunits[95]. The mutations identified in PKA C subunits are discussed in more detail in section 1.2.3.

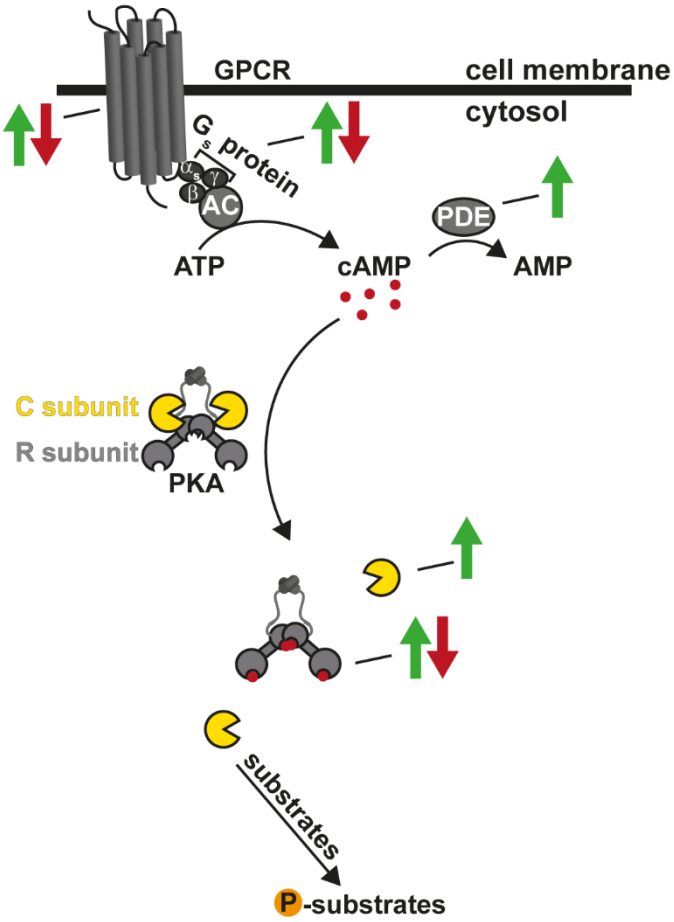

Figure 4: Summary of enzymes in the cAMP/PKA pathway affected by genetic alterations. Mutations leading to activation of the pathway are marked by green and mutations leading to inactivation of the pathway by red arrows.

1.2 Protein kinase A

One of the central components of the cAMP/PKA pathway is PKA. PKA is a key effector of the second messenger cAMP which is produced in response to activation of GPCRs by several hormones and neurotransmitters[96]. PKA is a serine/threonine kinase[97], which forms a holoenzyme composed of two regulatory (R) and two catalytic (C) subunits under basal condition (Figure 5)[97]. Three isoforms are known for the C subunit (Cα, Cβ, Cγ) and four are known for the R subunit (RIα, RIβ, RIIα, RIIβ)[97]. All of them are encoded by separate genes[97]. In addition to the three C subunit isoforms, the human protein kinase X (PrKX) can also form holoenzymes with the R subunits[98, 99]. In the tetrameric form, the C subunit is inactivated by the inhibitory sequence of the R subunit, which then is positioned in the active site of the C subunit[97, 100, 101]. Binding of cAMP to the two regulatory subunits causes dissociation of the C subunits, which are then able to phosphorylate several target proteins in the cytosol as well as in the nucleus[97]. Therefore, PKA plays a fundamental role in the regulation of key biological processes such as cell metabolism, hormone production, proliferation, differentiation and apoptosis [97, 102].

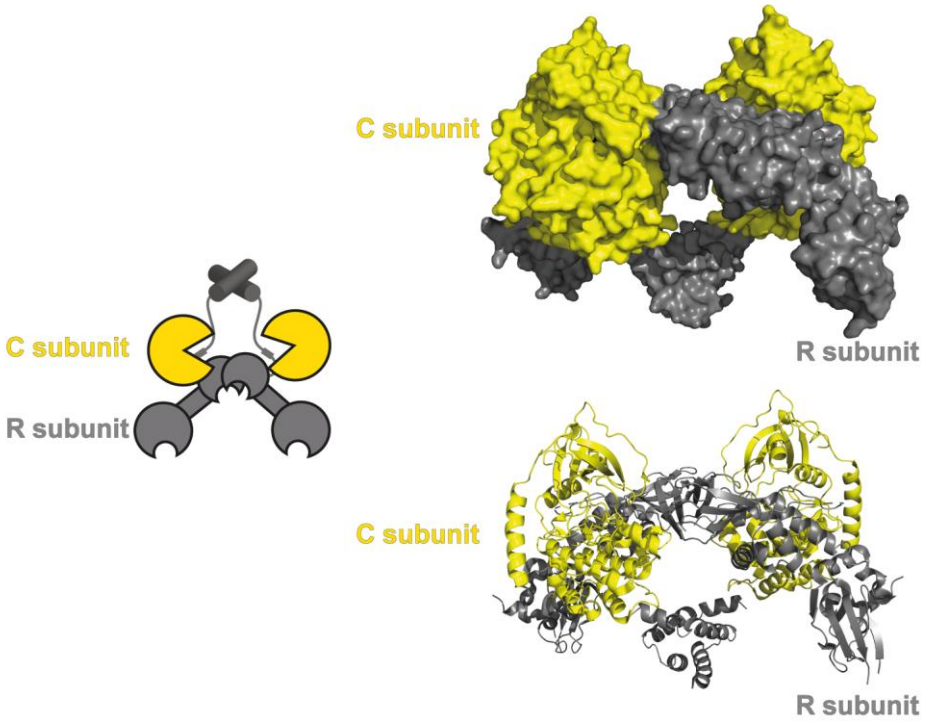

Figure 5: Protein kinase A holoenzyme. Schematic (left) and structural (right) depictions of the RIIβ$_2$:Cα$_2$ holoenzyme. The structure is shown with surface (right, top) and in cartoon style showing the different structure motifs (right, bottom). For the structure, protein data bank (PDB) entry 3TNP is used for the holoenzyme, the dimerization/docking (D/D) domain is taken from PDB entry 3IM4 and oriented as predicted by Zhang *et al.*[101].

1.2.1 Structure of the regulatory subunit

PKA is one of the simplest and best understood kinases[103]. Due to the fact that the structure of PKA was the first kinase structure to be solved[104], it is often used as a prototype for the entire kinase family[103]. As shown in figure 6, the regulatory subunits form dimers by interacting via an N-terminal four-helix bundle (dimerization/docking or D/D domain)[105]. Additionally, this domain creates a hydrophobic groove where the amphipathic helices of A kinase anchoring proteins (AKAPs) can bind with high affinity[106, 107]. With the help of this interaction, the AKAPs can target PKA to specific subcellular locations[105]. Most AKAPs are specific for RII subunits[105, 108, 109], but there are also some specific for RI subunits[110, 111, 112] or able to bind both types of R subunits[113]. The C-terminus of each R subunit has two cyclic nucleotide binding sites (CNB)[97]. These are joined to the D/D-domain by a flexible linker that includes an inhibitory sequence[97] (Figure 6A-C). In the absence of cAMP, this inhibitory sequence binds to the active site cleft of the C subunit[97]. An essential difference between the RI and RII subunits is that the inhibitory sequence of RI subunits is a pseudo-substrate with alanine or a glycine at the phosphosite[97, 105] and those of the RII subunits are both substrates and inhibitors, having a serine at the phosphosite[97, 105] (Figure 6D). Upon cAMP binding to the two CNB sites, the R subunit undergoes a conformational change and releases the C subunit which is then free to phosphorylate its targets[15, 114]. The different R subunit isozymes have unique inhibitory sequences (Figure 6D) but still, the inhibitory effect of RIIβ and RIα on the Cα subunit is similar (0.1 nM and 0.15 nM respectively) and also the affinity for both R subunits are similar (0.23 nM for RIα and 0.24 nM for RIIβ)[115]. But interestingly, the holoenzymes show different sensitivities to the cAMP concentration. The RIα_2Cα_2 holoenzyme is already activated at 101 nM cAMP concentration[116], whereas the RIIβ_2Cα_2 holoenzyme is activated at 584 nM cAMP concentration[101].

The C subunit is also inhibited by heat stable protein kinase inhibitor (PKI), which is another physiological inhibitor of PKA. PKI binds also with high affinity (<1 nM) to free C subunits[117]. PKI is a pseudosubstrate (Figure 6D) and helps to export the C subunit from the nucleus[118]. Due to a nuclear export signal (NES) at the carboxyl-terminus of PKI, which is exposed after binding of the C subunit, the complex of C subunit and PKI is exported from the nucleus[118].

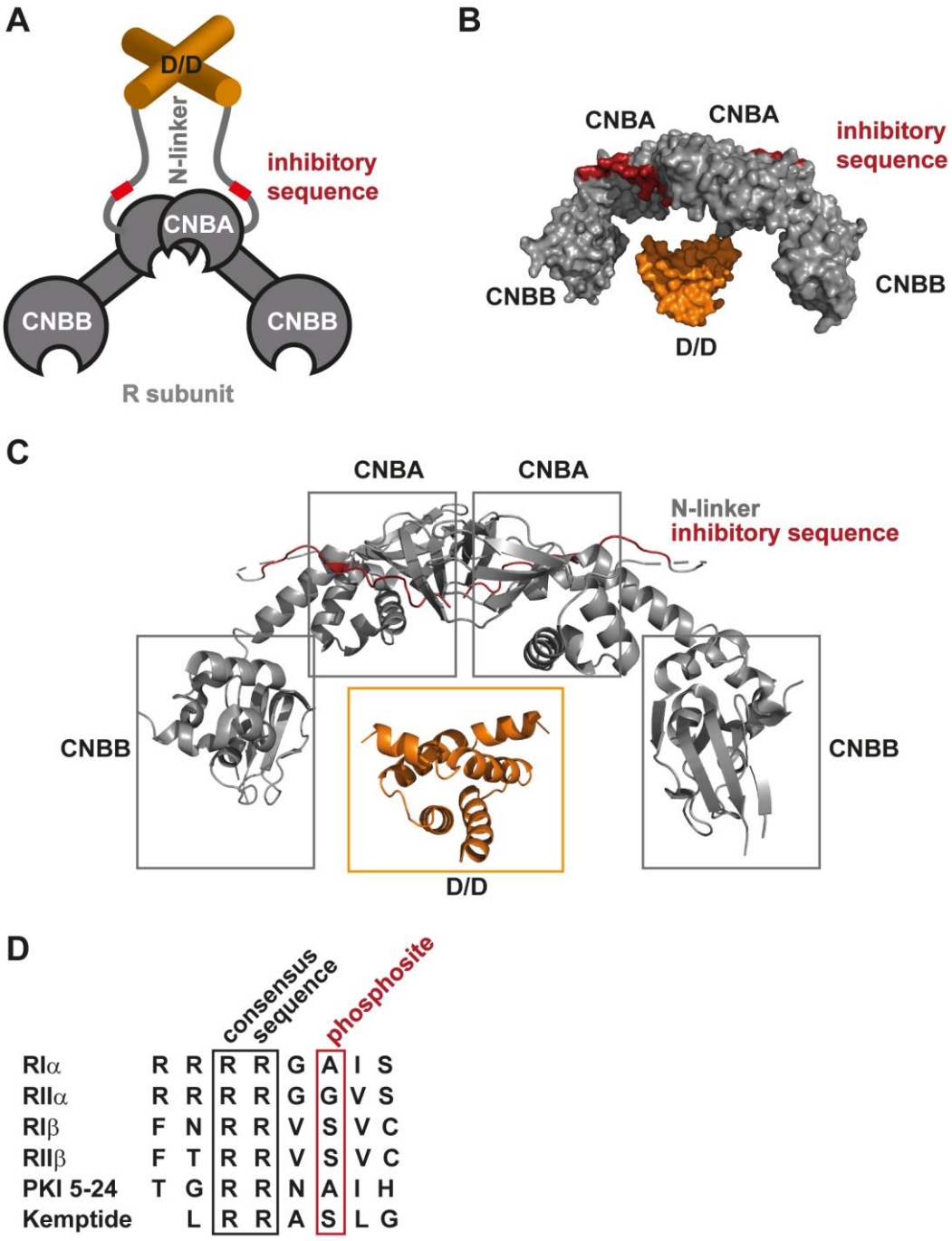

Figure 6: Protein kinase A regulatory subunit. Shown are the functional parts of the RIIβ-dimer in a schematic depiction (A), a structural depiction including the surface of the protein (B) and a structural depiction showing the different structural motifs (C). Highlighted are the cyclic nucleotide binding domains (CNBA, CNBB) in grey, the dimerization/docking domain (D/D) in orange and the inhibitory sequence in red (A-C). The sequences of the inhibitory sequences of the different R subunit isozymes, the heat stable protein kinase inhibitor peptide (PKI 5-24) and the artificial substrate kemptide are compared in D. For the structure, PDB entry 3TNP is used for the holoenzyme, the D/D domain is taken from PDB entry 3IM4 and oriented as predicted by Zhang *et al.*[101].

1.2.2 Structure of the catalytic subunit

1.2.2.1 Overall structure

The catalytic subunit of PKA is a serine/threonine kinase and responsible for most of the effects of cAMP signaling[97]. It is a bilobal enzyme built of two major subdomains that are conserved throughout the protein kinase family[104] (Figure 7A). Several conserved sequence motifs have been identified in the protein kinase family[119, 120] (Figure 7B). At the N-terminus, the structure harbors a disordered myristylation motif[117] followed by a non-conserved long A-helix which spans the two lobes[117]. This is followed by the small lobe (residues 41-120) which consists of a five stranded antiparallel β-sheet and a single conserved helix, the C-helix[117] (Figure 7B, dark blue). The small lobe also constitutes the nucleotide binding domain of the kinase[117]. An essential part for catalysis in the small lobe is the glycine-rich loop (residues 50-58, Figure 7B, cyan) which lies between β-strands 1 and 2[103]. The small and large (residues 129-301) lobe of the C subunit are only joined by a single linker strand (Figure 7B, black)[117]. The large lobe is mostly comprised of helices but also contains a single small β-sheet which is positioned at the active site cleft[117]. The joining β-strands 6 and 7 in this β-sheet contain the catalytic loop (Figure 7B, red), which is formed by six highly conserved residues (Asp-Leu-Lys-Pro-Glu-Asn; residues 167-172)[103]. The linker between β-strands 8 and 9 is called magnesium positioning loop (Asp-Phe-Gly-Phe; residues 185-188, Figure 7B, orange)[103]. The β-strand 9 is followed directly by the activation loop (Thr-Trp-Thr; residues 196-198, Figure 7B, pink) and the peptide positioning loop (Leu-Gly-Thr-Pro-Glu-Tyr-Leu; residues 199-206, Figure 7B, purple)[103]. The surface of the large lobe also builds the docking site for the peptide and protein substrates[103]. The C-terminus (residues 301-351) is not conserved among kinases[119] and positioned at the surface of both lobes[117].

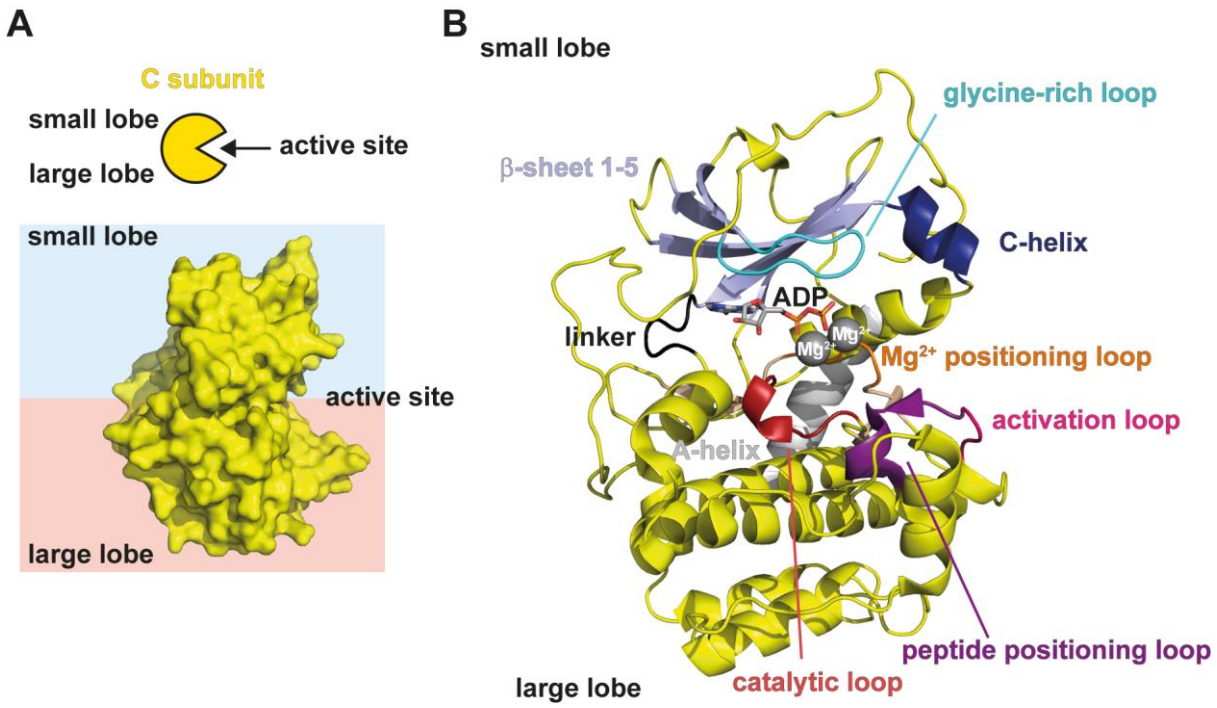

Figure 7: Structure of the protein kinase A catalytic subunit. Shown is the overall structure including a schematic and a structural view (A) and the important structural motifs of the C-subunit (B). Structures are based on the PDB structure of the RIIβ:Cα heterodimer (3TNQ)[101].

As shown in figure 7, a deep, hydrophobic pocket is formed between the two lobes[103]. This pocket constitutes the active site[117] and the binding site for the adenine ring of ATP which also mediates most of the interaction between the small and large lobe[103] (Figure 8B). This pocket is surrounded by the glycine-rich loop and the C-helix in the small lobe and the β-sheet in the large lobe[103] (Figure 8A, B). The C subunit also has two magnesium binding sites[121, 122]. The magnesium ions are essential for catalysis of phosphoryl transfer[121]. To coordinate the first Mg^{2+} ion (Mg1), the β- and γ-phosphates of ATP, aspartic acid 185 and two water molecules are needed[121]. Coordination of the second Mg^{2+} ion (Mg2) is mediated by asparagine 172, one oxygen atom of aspartic acid 185, the α- and γ-phosphates of ATP and one water molecule (Figure 8C)[121].

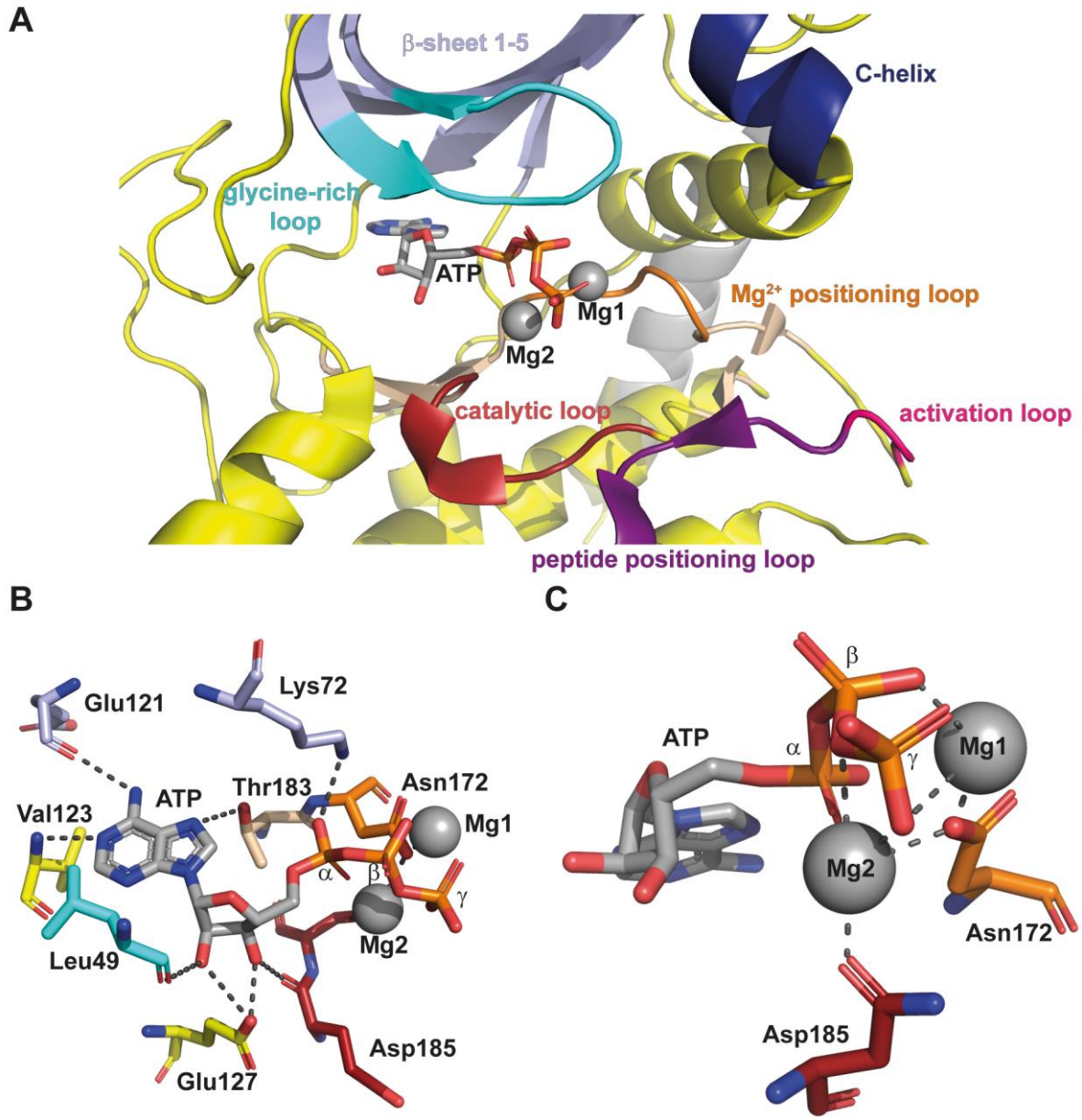

Figure 8: ATP binding pocket of the protein kinase A catalytic subunit. Shown is an overview of the surrounding structural motifs (A), the interactions of ATP with different residues of the C subunit (B) and the coordination of the two magnesium ions by ATP, aspartate 185 and asparagine 172 (C). Structural depictions are based on a Cα subunit structure bound to Mg-ATP and a substrate peptide (3X2U)[123].

1.2.2.2 Phosphorylation sites

Due to the fact that the C subunit is autophosphorylated when expressed in *Escherichia coli* (*E.coli*)[124], the structure of the inactive, nonphosphorylated enzyme is unknown[117]. Four phosphosites have been identified in the C subunit of PKA: serine 11, serine 140, threonine 198 and serine 339[124]. Threonine 198[124, 125] and serine 339[124, 125] are autophosphorylated also in *E.coli* expressed recombinant proteins[124]. Autophosphorylation on serine 11 is mainly observed for the Cα subunit[126]. Until recently, just threonine 198 and serine 339 were known to be phosphorylated in the mammalian enzyme[125]. New advancements in mass spectrometry have suggested phosphorylation at serine 11 and 140 and at threonine 196[127]. Whereas phosphorylation of serine 339 stabilizes a turn near the C-terminus and is therefore important for stabilization of the C subunit, it was shown that phosphorylation of threonine 198 in the activation loop is essential for catalytic activity[128]. Phosphorylation of serine 11 seems to play a role in organization of the N-terminus of the C subunit. If phosphorylation at this site is absent, the unordered N-terminus can be organized[129].

1.2.2.3 Conformational dynamics in PKA Cα

There are several structures of the Cα subunit available, including crystallized active conformations in the presence and absence of both substrates and inhibitors. These structures reveal the flexibility of the Cα subunit which is an essential part of catalysis [117]. The opening and closing of the active site cleft is mainly mediated by the small lobe[103] (Figure 9). As a marker of the current conformation, the distance between histidine 88 in the small lobe (C-helix) and threonine 198 in the large lobe (activation loop) can be used[117]. The interaction between those two residues is the only direct ionic interaction between the small and the large lobe and it only appears in the closed conformation of the enzyme[103]. The closed conformation of the enzyme positions the glycine-rich loop over the phosphates of ATP so that the backbone amide of serine 54 can form a hydrogen bond to the γ-phosphate of ATP[117] (Figure 9B). The most open conformation of the Cα subunit, where the distance between small and large lobe is maximal, was shown for the apo C-subunit[122]. This structure is based on an inhibitor peptide (IP20) bound to the C subunit[104]. It was shown that most of the active site is already preformed in this conformation[130]. Intermediate conformations between open and closed have also been described[103].

When the C subunit is a part of the holoenzyme, its conformation depends on the type of R subunit[97]. For the RIIβ holoenzyme, a closed conformation has been reported[97]. In contrast,

the RIIα-C heterodimer presents an open conformation[97]. Interestingly, both RII holoenzymes do not need ATP to be formed[97, 131]. Contrary, the RI subunits need ATP and two magnesium ions to form a tight heterodimer[131, 132]. This induces a closed conformation[97].

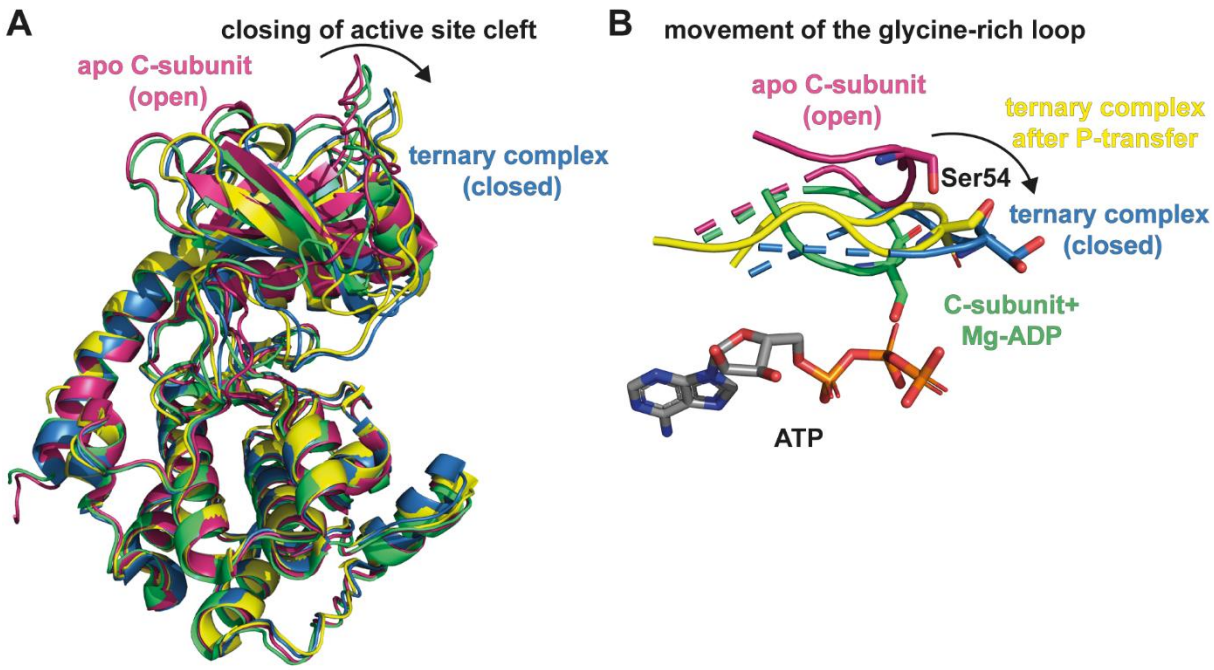

Figure 9: Dynamics of the Cα subunit. Shown are the conformational changes in the whole Cα subunit (A) and for the glycine-rich loop with serine 54 shown in sticks (B). The following PDB entries were used: Conformations of the C subunit in the apo C subunit (open conformation) without any bound ligands (pink, PDB: 4NTS); of the ternary complex (closed) ready for phosphoryl-transfer with bound ATP, two Mg^{2+} ions and substrate (blue, PDB: 3X2W); of the ternary complex after phosphoryl-transfer with bound ADP, two Mg^{2+} ions and phospho-substrate (yellow, PDB: 3TNQ); and of the C subunit after release of the phospho-substrate and one Mg^{2+} (limegreen, PDB: 4NTT).

1.2.2.4 Mechanism of phosphoryl transfer in the PKA Cα subunit

Even though the detailed catalytic mechanism of PKA is still unknown, several studies gave insight into the phosphoryl transfer mechanism.

Contrary to previous suggestions that Mg2 initially binds the active site[121, 133], crystal structures showed that Mg1 together with ATP binds first to the active site[123]. Binding of ATP, as described in 1.2.2.1, links the small and large lobe of the C subunit. This leads to pre-organization of the active site[134]. It is not clear yet whether this is followed by the second Mg^{2+} ion or the substrate binding[121]. Binding of the above components to the C subunit induce conformation changes in the kinase, which mainly occur in the small lobe[123] (Figure 9). In particular, in the glycine-rich loop[121, 123](Figure 9B), which adapts its position depending on the phospho-site residue in the substrate[121].

It was discussed whether the phosphoryl transfer is performed by a concerted[135, 136] or dissociative[121, 137, 138, 139] mechanism. The concerted (S_N2) mechanism includes a trigonal bipyramidal transition state with a -3 charge[121]. Bond formation of the γ-phosphate of ATP with the phospho-site serine of the substrate would then begin before the bond break between the β- and γ- phosphate is complete[121].In contrast, the dissociative (S_N1) mechanism[121, 137, 138, 139] involves a break of the bond with the γ-phosphate leading to a metaphosphate with a -1 charge[121]. Whereas most studies suggested the dissociative mechanism[121, 137, 138, 139], recent studies on the structure of the Michaelis complex show formation of an in-line configuration[123, 135] and thus suggest a S_N2 mechanism[123, 136]. This potential mechanism is depicted in figure 10. In the Michaelis complex, the side chain of the phospho-site amino acid (serine/ threonine) forms a hydrogen bond with aspartate 167[136]. The hydroxyl group of the phospho-site amino acid of the substrate then performs a nucleophilic attack on the γ-phosphate of ATP[136]. Simultaneously, the hydroxyl group is dephosphorylated by aspartate 167, acting as a catalytic base[136, 138]. The reaction proceeds via a concerted S_N2 mechanism via a trigonal bipyramidal transition state[136] (Figure 10).

After phosphoryl transfer, the phospho-substrate is the first component to leave the ternary complex[136]. This leads to a lower coordination of Mg1, which just keeps bonds with the β-phosphate of ADP and aspartate 185[136]. Thereafter, Mg1 leaves the active site (moves away from aspartic acid 185) allowing ADP release[121, 140, 141], which is the rate limiting step of the product turnover[142]. Mg2 recruits a new water molecule to maintain an octahedral geometry following transfer of the γ-phosphate[121]. This might also help to stabilize the transition state[121].

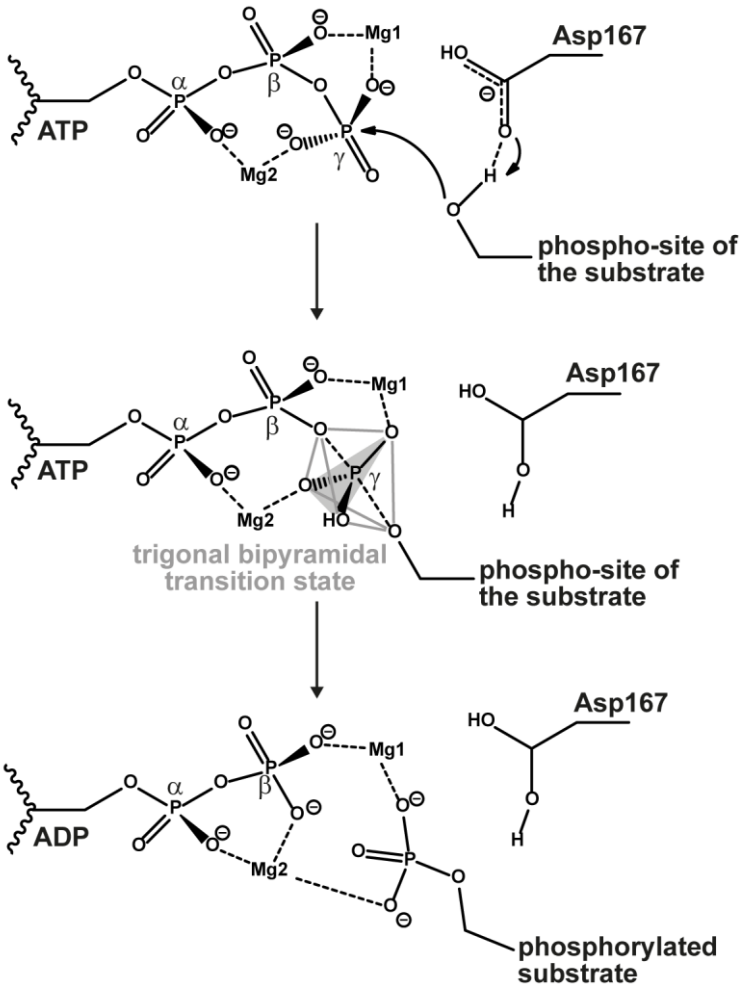

Figure 10: Possible phosphoryl transfer reaction of the catalytic subunit. The Phospho-site amino acid (serine/ threonine) of the substrate forms a hydrogen bond with aspartate 167. The hydroxyl group of the phospho-site amino acid of the substrate then performs a nucleophilic attack on the γ-phosphate of ATP. Simultaneously, the hydroxyl group is dephosphorylated by aspartate 167. The reaction proceeds via a concerted S_N2 mechanism via a trigonal bipyramidal transition state.

1.2.2.5 Substrate recognition

The main docking region for substrate peptides is provided by the large lobe, which therefore controls the affinity of R subunit or substrate binding [117]. For substrate binding, two peripheral recognition sites (PRS1/2) have been identified[143].For PKI binding, PRS1 was shown to be important[143]. It involves the residues arginine 134, tyrosine 236 and glutamate 204. PRS2 is a basic region with histidine 88, tryptophan 197 and the phosphorylated threonine 198 in the center[143]. PRS2 forms a node for the binding of the regulatory subunit[143].

1.2.3 Mutations in PKA catalytic subunit

The first mutations in the gene coding for the Cα subunit of PKA (*PRKACA*) were identified by our group in CPAs, which were found to be responsible for Cushing's syndrome[89]. These initial findings were supported by further studies of our collaborators[93, 94] and other groups[90, 91, 92]. Additionally, mutations in genes encoding for PKA catalytic subunits have been found in other, more rare conditions. In particular, a genomic deletion leading to a fusion of DNAJB1 and PKA Cα was identified in FL-HCC[95]. Additionally, a mutation in *PRKACA* was found in aldosterone-producing adenomas (APAs)[144] and a mutation in the gene encoding for the catalytic β (Cβ) subunit of PKA (*PRKACB*) was identified in a patient having overt Cushing's syndrome[145]. The effects of these mutations on the PKA C subunit are discussed here.

1.2.3.1 *PRKACA* mutations in cortisol-producing adenomas

Several mutations have to date been identified in CPAs of Cushing's patients. Most of these mutations lie in a hot-spot region around the active site cleft of the Cα subunit (Figure 11) and are linked to overt Cushing's syndrome[89, 90, 91, 92, 93, 94].

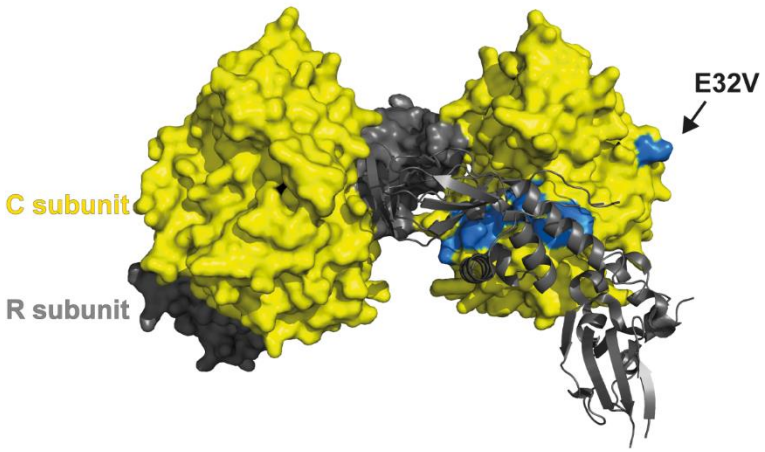

Figure 11: Positions of mutations in the PKA holoenzyme. Positions of mutations identified in CPAs are highlighted in blue. The structure of the holoenzyme is based on the structure of the Cα:RIIβ holoenzyme (PDB: 3TNP).

As mentioned in 1.1.4, the first identified and by far most frequent mutation is a substitution of leucine 206 with arginine (L206R), which is found in about 30-60% of the cases, typically in the ones associated with overt Cushing's Syndrome[89, 90, 91, 92, 93]. Leucine 206 is located in the

active site cleft of the Cα subunit and interacts with both substrates and the inhibitory sequence of the R subunit[89, 101]. Based on this information derived from the crystal structure of the RIIβ holoenzyme[101], it was hypothesized that the substituted arginine, a bulky and positively charged amino acid, would clash with valine 115 and tyrosine 228 in the R subunit, and thus interfere with the interaction between R and C subunits[89, 146]. A study by our group verified this by a detailed functional characterization using a set of biochemical and optical methods which is described in more detail in the results section (4)[146]. Also, the solved crystal structure by Cheung *et al.* illustrates this finding[147](Figure 12). More recently, Lubner *et al.* suggested based on a study in *E. coli* that this mutation might also cause a change in substrate specificity of the PKA Cα subunit[148]. Therefore, *E. coli*, which lack PKA, were transformed with a plasmid encoding for the wild-type or the L206R mutated *PRKACA* to look at *E. coli* surrogate substrates[148]. Even though this setup is far from physiological conditions and substrates, this gave useful insights into the substrate specificity of the L206R mutated PKA Cα subunit. As a result, the study reported a loss of hydrophobic preference (except for leucine) at the +1 position of the substrate[148]. Moreover, they showed a preference for an acidic amino acid (aspartate, glutamate) in the +2 position of the substrate[148]. They speculate that this increased enrichment for acidic residues is due to an electrostatic interaction of this position in the substrate with the positively charged guanidinium group of arginine 206 in the Cα mutant[148]. This change in substrate specificity was also suspected by other studies showing reduced specificity – probably due to a reduced interaction – of the L206R mutant to the artificial substrate kemptide[149] and a reduced activity with the Förster resonance energy transfer (FRET) based A kinase activity reporter AKAR4[150]. A recent study by the group of Prof. Fassnacht also linked the down-regulation of RIIβ[151, 152] and RIα in CPAs with the presence of the L206R mutation[153]. This down-regulation appears post-transcriptionally and was suggested to be linked to changes in the subcellular localization of PKA subunits[153]. Even though, this mutation was studied in detail, no direct proof that *PRKACA* L206R mutation causes a change in substrate specificity leading to hypo- or hyperphosphorylation of PKA substrates in CPAs existed.

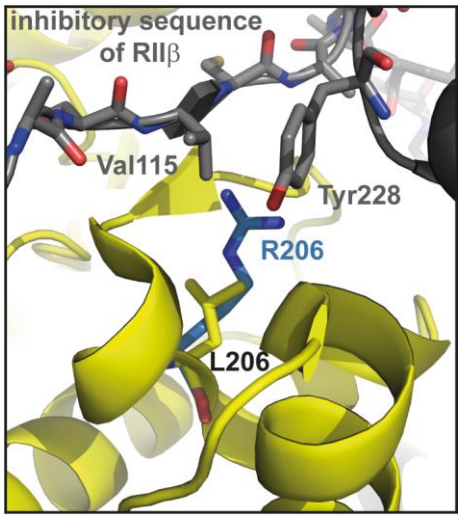

Figure 12: Structure of the PKA Cα L206R mutant. Structure of the PKA Cα (yellow): RIIβ (grey) holoenzyme (PDB: 3TNP) in an overlay with the Cα L206R mutant (blue, PDB:4WB6).

In parallel to this initial L206R mutation, a second mutation causing an insertion of an additional tryptophan between residues leucine 199 and cysteine 200 (199_200insW, Figure 13), was found in one patient[89]. These amino acids are located next to threonine 198 in the so-called activation loop[89, 103](Figure 7). Threonine 198 is phosphorylated during the synthesis of the Cα subunit, which is required for PKA activity [97]. This region of the C subunit is oriented parallel to the inhibitory sequence of the R subunit [154]. Importantly, residues glycine 201 and leucine 199 are involved in main-chain hydrogen bonding interactions with residues valine 115 and alanine 117 of the RIIβ subunit [146]. Thus, it was predicted that an insertion of an additional amino acid at this position might also interfere with the interaction with the R subunit[146]. This mutation is not studied as well as the L206R mutant, but it was also included in our study investigating functional consequences using a set of biochemical and optical methods showing the interference with the formation of a stable holoenzyme. These results are described in more detail in the results section (4)[146].

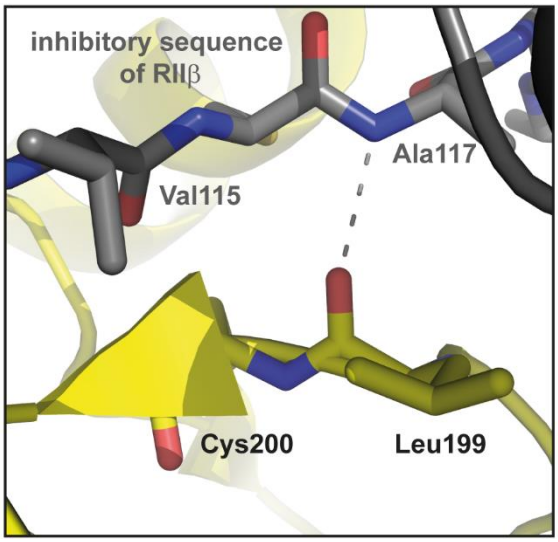

Figure 13: Structure of the PKA Cα 199_200insW mutant. Structure of the PKA Cα (yellow):RIIβ (grey) holoenzyme (PDB: 3TNP). The mutation would cause an insertion between the two highlighted residues cysteine 200 and leucine 199.

After identification of these two initial mutations (L206R, 199_200insW), our group screened a large set of patients with cortisol-secreting adrenocortical adenomas for additional *PRKACA* mutations[93, 94]. The most frequent of these novel mutations is the insertion of a valine between positions 200 and 201 (200_201insV) (Figure 14), which was found in three patients[93]. The mechanism of action of this mutation is probably similar to the 199_200insW mutant[93].

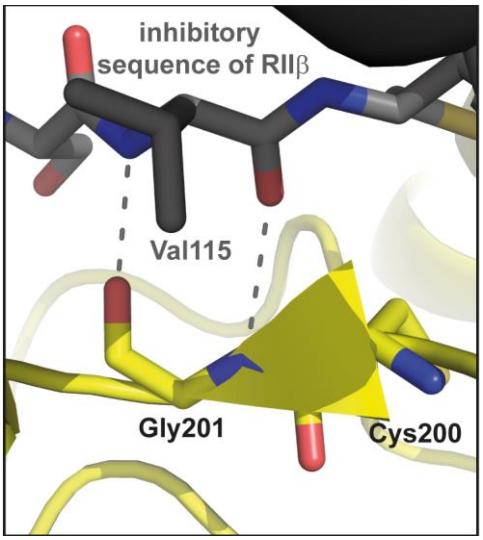

Figure 14: Structure of the PKA Cα 200_201insV mutant. Structure of the PKA Cα (yellow): RIIβ (grey) holoenzyme (PDB: 3TNP). The mutation would cause an insertion between the two highlighted residues cysteine 200 and glycine 201.

The next mutation is complex and consisting of a substitution and an insertion of four amino acids (Ile-Ile-Leu-Arg) between position 212 and 214 (S213R+insIILR). This mutation was found in one patient[93]. Residues 212-214 are part of one of the interaction sites for the R subunit that are located outside the active site cleft[130, 143]. This region forms a tip-like structure that protrudes into the R subunit [93](Figure 15). The insertion of several residues at this position likely leads to an enlargement of the tip which probably impairs the association between C and R subunits [93].

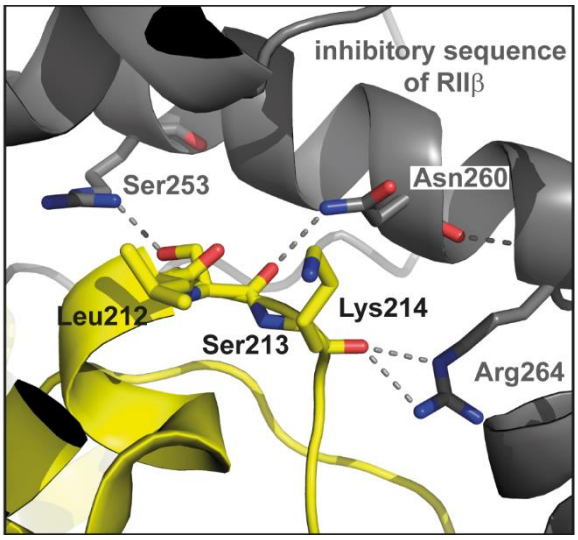

Figure 15: Structure of the PKA Cα S213R+insIILR mutant. Structure of the PKA Cα (yellow): RIIβ (grey) holoenzyme (PDB: 3TNP). The mutation would cause a substitution of the highlighted serine 213 with arginine and an insertion between the two highlighted residues leucine 212 and lysine 214.

Another identified mutation is a substitution of the hydrophobic tryptophan 197 to the positively charged, hydrophilic arginine (W197R, Figure 16)[94]. This mutation is positioned directly beside the phospho-threonine 198 in the activation loop [103]. Phospho-threonine 198 is important for the assembly of the active conformation of the small lobe [103]. The mutation described was found to affect the binding of the C subunit to the R subunit for RI and RII isoforms [155]. Conversely, full length PKI was still able to inhibit the activity of the mutant [156]. Later on it was shown that this mutant is still able to bind to a R subunit that is stripped from cAMP [143]. Interestingly, this mutation, as the L206R, was also linked to down-regulation of RIIβ subunit in CPAs[153].

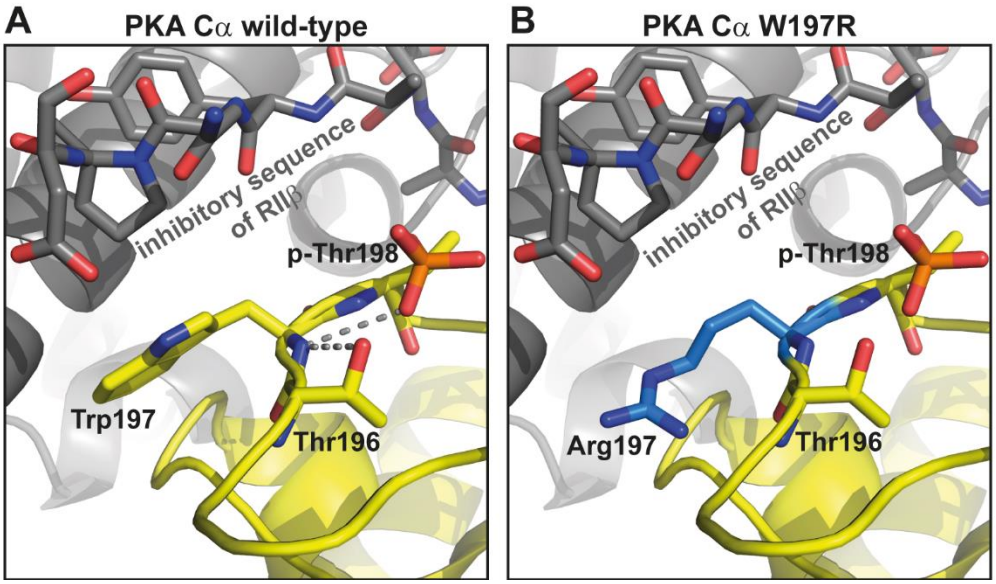

Figure 16: Structure of the PKA Cα W197R mutant. Structure of the PKA Cα (yellow): RIIβ (grey) holoenzyme (PDB: 3TNP). Depicted are the wild-type enzyme (A) and a prediction of the structure of the W197R mutated protein (B).

Also, a deletion of the amino acids 244 to 248 combined with a substitution of glutamic acid 249 with a glutamine (d244-248+E249Q) has been identified[94]. This deletion of four amino acids is also located at the interface with the regulatory subunit (Figure 17). But due to the nature of the mutation, it is hard to predict how this mutation will affect the tertiary structure of the C subunit. Interestingly, this mutation was detected additionally to the reported overt Cushing's syndrome patient[93] in a patient with subclinical Cushing's syndrome[153]. The d244-248+E249Q mutation, contrary to the L206R, was shown to have no effect on the expression of RIIβ subunit in CPAs[153].

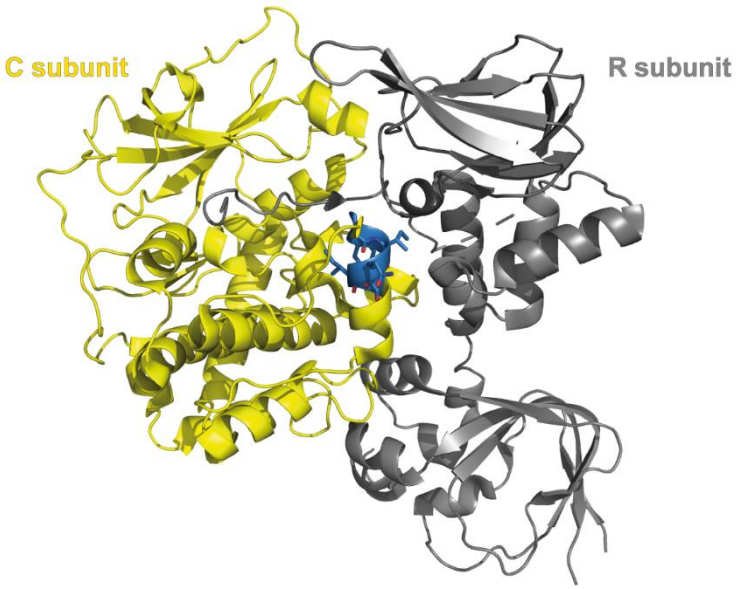

Figure 17: Structure of the PKA Cα d244-248+E249Q mutant. Structure of the PKA Cα (yellow): RIIβ (grey) holoenzyme (PDB: 3TNP). The mutation would cause deletion of the highlighted residues (blue) and a substitution of glutamate 249 with glutamine also at the highlighted position (blue).

The last identified mutation is a substitution of glutamic acid 32 with a valine (E32V)[94]. Glutamic acid 32 is a solvent exposed residue and seems not to be involved in R binding or catalysis (Figure 11). The structure does not indicate any effects on the C subunit. Therefore, it is not surprising that levels of RIIβ subunit in E32V mutated CPAs were comparable to *PRKACA* wild-type tumors[153].

However, the mechanism of action of the *PRKACA* mutations remained largely unknown, even though the data on the L206R mutant gave some insights. Therefore, the aim of this work was to investigate the mechanism of action of the *PRKACA* mutations. All *PRKACA* mutations identified so far in CPAs of patients with overt adrenal Cushing's syndrome and investigated in this work are summarized in Table 1. Tumor sizes were varying, but overall, the mutated tumors were smaller than the wild-type CPAs[93, 157]. The mutations were often linked to a more severe autonomous cortisol secretion[93, 157].

Table 1: Summary of *PRKACA* mutations identified so far in patients with overt adrenal Cushing's syndrome.

Mutation	Number of patients (frequency)	Reference
199_200insW	1 (2%)	Beuschlein *et al.*[89]
L206R	21 (36%)	Beuschlein *et al.*[89]
	34 (52%)	Sato *et al.*[92]
	84 (67%)	Cao *et al.*[90]
	13 (35%)	Goh *et al.*[91]
	3 (23%)	Nakajima *et al.*[158]
	18 (28%)	Di Dalmazi *et al.*[93]
	12 (23%)	Thiel *et al.*[157]
200_201insV	3 (5%)	Di Dalmazi *et al.*[93]
S213R+insIILR	1 (2%)	Di Dalmazi *et al.*[93]
W197R	1 (3%)	Ronchi *et al.*[94]
d244-248+E249Q	1 (3%)	Ronchi *et al.*[94]
E32V	1 (3%)	Ronchi *et al.*[94]

Additionally to *PRKACA* mutations found frequently in CPAs responsible for Cushing's syndrome[89, 90, 91, 92, 93, 94, 157, 158], mutations in genes encoding for PKA C subunits have been identified in other, more rare conditions.

1.2.3.2 *DNAJB1-PRKACA* chimera in fibrolamellar hepatocellular carcinoma

FL-HCC is a rare liver tumor[159] which does not respond well to chemotherapy[160]. Therefore, the main therapy is surgical resection which just reaches a survival of 30 to 40% at 5 years[159]. In 2014, Honeyman *et al.* reported a 400 kbp deletion on chromosome 19 causing a fusion of exon 1 of *DNAJB1* gene, coding for a member of the heat shock 40 protein family, and exons 2 to 10 of *PRKACA* in patients with FL-HCC[95]. The resulting fusion protein (Figure 18) was linked to an increase in expression of *PRKACA*, because of higher transcription of *PRKACA* due to the junction to the *DNAJB1* promoter[95]. Interestingly, the transcription and expression of *DNAJB1* was decreased. Additionally, a second chimera, just found in two patients, was also identified[95]. It links the middle of exon 2 of *DNAJB1* to exon 2 to 10 of *PRKACA*[95]. Both chimeras were identified to appear heterozygous[95]. The missing exon 1 of *PRKACA* codes for a domain that is implicated in binding of the R subunit[95]. Therefore, binding to the R subunit could be hindered which would render the *DNAJB1-PRKACA* fusion protein constitutively active. This was disproved by surface plasmon resonance, gel filtration analysis and structural modeling, which showed normal binding of the chimeric protein to RI and RII subunits[147]. Therefore, it was concluded that the enhanced cAMP/PKA signaling is caused by the higher expression of the chimeric protein compared to wild-type PKA Cα[147]. To show the implication of the chimeric protein on tumorigenesis, Engelholm *et al.* used clustered regularly interspaced short palindromic repeats (CRISPR) associated proteins (CRISPR/Cas9) to delete a complementary region on chromosome 8 in mice, causing a *DNAJB1-PRKACA* fusion protein[161]. Interestingly, 80% of mice treated for *DNAJB1-PRKACA* fusion developed neoplasms. These neoplasms contained the chimeric protein and presented histologic and cytologic features of human FL-HCCs[161]. Therefore, it was concluded that the induction of *DNAJB1-PRKACA* fusion protein is sufficient to cause tumors[161].

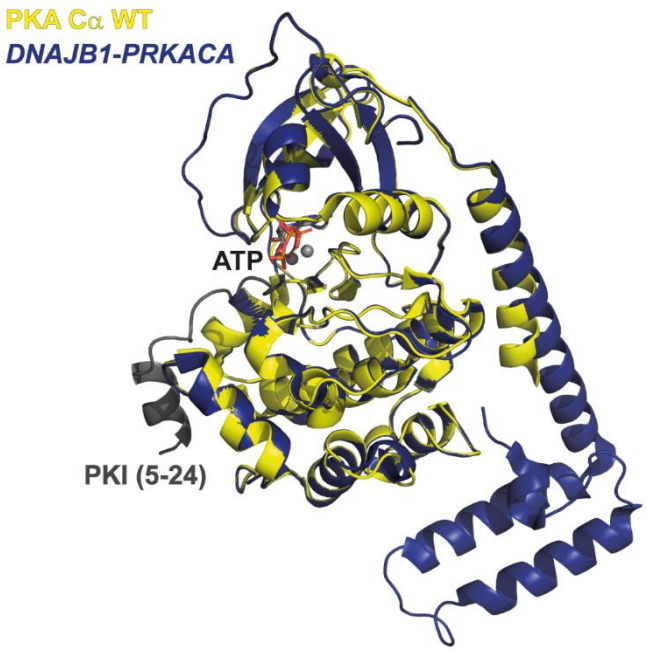

Figure 18: Structure of the *DNAJB1-PRKACA* fusion protein. Shown is the structure of the wild-type (WT) PKA Cα (yellow, PDB:4WB5) in an overlay with the *DNAJB1-PRKACA* fusion protein (blue, PDB:4WB7). ATP is depicted in red.

1.2.3.3 *PRKACA* somatic mutations in aldosterone-producing adenomas

Recently, the first somatic mutation in *PRKACA* was found in APAs[144]. APAs are one of the prevalent causes for primary aldosteronism (Conn's syndrome)[162, 163], which is the predominant cause for secondary hypertension[164]. Two patients were identified to harbor mutations in *PRKACA*[144]. The first mutation was the L206R mutation also identified in Cushing's syndrome and discussed in more detail in 1.2.3.1[144]. The second mutation causes a substitution of histidine 88 with an aspartate (H88D)[144] (Figure 19). As discussed in 1.2.2.3, histidine 88 is positioned at the beginning of the C-helix in the small lobe and forms the only direct ionic interaction between the small and large lobe, which is present only in the closed conformation of the Cα subunit[117]. It was already reported earlier, that this mutation interferes with the binding of RI subunits, due to the fact that this would need a closed conformation[165]. Additionally it was reported that this mutant is deficient in phosphorylating some peptide substrates[165]. A study by Rhayem *et al.* revealed that the substitution of histidine 88 with an aspartate results in a significantly reduced activity of the PKA Cα subunit[144]. Interestingly, the expression of the steroidogenic enzyme CYP11B1 was low, which could be explained by the decrease in cAMP signaling [144].

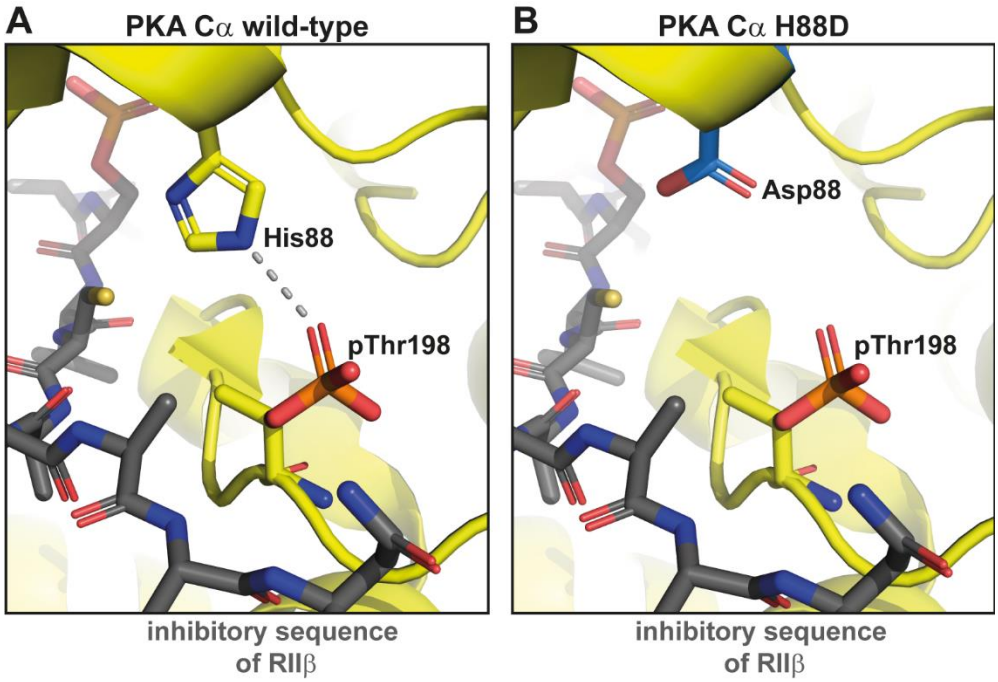

Figure 19: Structure of Cα H88D mutant found in APAs. PKA Cα subunit is shown in yellow and RIIβ subunit in grey. Prediction of structure of the Cα H88D mutant is based on the wild-type holoenzyme structure (PDB: 3TNQ).

1.2.3.4 *PRKACB* somatic mutation in cortisol-producing adenomas

Until recently, only mutations in *PRKACA* have been identified in CPAs. Very recently, also mutations in another C subunit, the gene encoding the PKA Cβ subunit (*PRKACB*), have been found in a patient having overt Cushing's syndrome[145]. The identified mutation codes for a substitution of serine 54 with leucine (S54L)[145] (Figure 20). This serine is conserved in Cα, Cβ and Cγ subunits[145]. As described in 1.2.2.3, serine 54 forms a hydrogen bond with the γ-phosphate of ATP in the closed conformation of the enzyme[117] (Figure 9B). Espiard *et al.* have reported that the mutation of serine 54 to leucine causes a decreased stability for RI but not RII holoenzymes, due to weaker interactions[145]. Additionally, it was found that the Cβ S54L-RI holoenzymes have increased cAMP sensitivity leading to dissociation of the holoenzymes at already low cAMP levels[145]. Interestingly, under basal conditions, the Cβ S54L mutant shows higher phosphotransferase activity than wild-type Cβ[145]. However, the maximal activity of the enzyme was reduced[145].

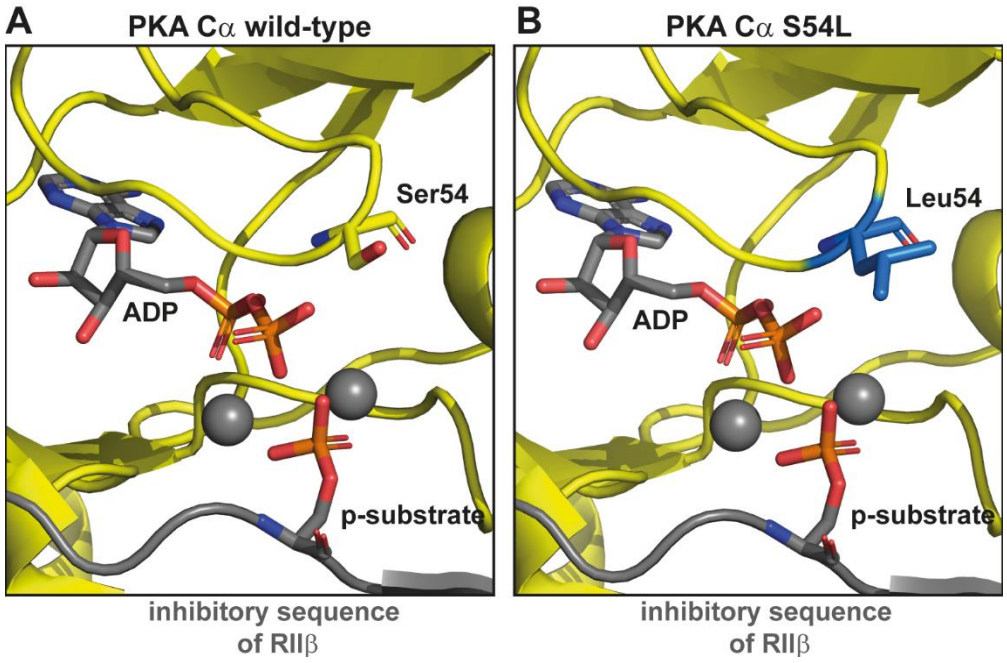

Figure 20: Structure of Cβ S54L mutant identified in CPA. PKA Cα subunit is shown in yellow and RIIβ subunit in grey. Prediction of structure of the Cβ S54L mutant (B) is based on the wild-type (A) holoenzyme structure (PDB: 3TNQ).

2 Aim and strategy of the study

The aim of this project was to investigate the mechanisms and functional consequences of the mutations in the gene encoding the PKA Cα subunit (*PRKACA*), which were recently identified in cortisol-producing adrenocortical adenomas (CPAs) responsible for Cushing´s syndrome.

The newly identified PKA Cα mutants, identified in Cushing's syndrome and investigated in this study were: 200_201insV, S213R+insIILR, W197R, d244-248+E249Q and E32V (1.2.3.1). For comparison, I included the two initially identified and well characterized mutants L206R and 199_200insW. To study the mechanism of action of these mutants, I used optical methods and biochemical techniques, including phosphoproteomics, which allowed me to investigate holoenzyme formation, activity, subcellular localization and substrate specificity of the PKA Cα mutants. In addition, I used the CRISPR/Cas9 system to generate a cell line harboring the most frequent and best studied L206R mutation. This cell line was used to investigate the subcellular localization of the PKA subunits and provides a highly valuable model for future investigations of the mechanisms and impact of *PRKACA* mutations.

3 Materials and Methods

3.1 Materials

3.1.1 Cell lines

Escherichia coli (E. coli) Top10	C404010, Thermo Fisher Scientific
Mouse hepatoma Hepa1-6 cells	CRL-1830, ATCC
Human Embryonic Kidney (HEK)-293 A cells	R70507, Thermo Fisher Scientific
Human Embryonic Kidney (HEK)-293 T cells	CRL-3216, ATCC
Human adrenal gland carcinoma NCI-H295R cells	CRL-2128, ATCC

3.1.2 Cell culture media and supplements

100x GlutaMAX	35050-061, Thermo Fisher Scientific
Ammoniumhydrogencarbonate	40867, Fluka
Arginine 0	A5131, Sigma-Aldrich
Arginine 10	CNLM-539-H-PK, Cambridge Isotope Laboratories
Dialyzed fetal bovine serum (FBS)	26400044, Thermo Fisher Scientific
DMEM with phenol red	P04-03600, PAN Biotech
DMEM/ F-12 without Phenol red	11039-021, Gibco
DMEM/ F-12, Hepes	11330-032, Life technologies
Dulbecco's modified Eagle's medium (DMEM) without Arginine and Lysine	A14431-01, Gibco
Dulbecco's phosphate buffered saline (DPBS) without Ca^{2+} and Mg^{2+}	14190-094, Gibco
Fetal bovine serum (FBS)	S0115, Biochrom AG
Insulin-Transferrin-Selenium-Sodium Pyruvate (ITS)	41400-045, Gibco
L-Proline	P5607, Sigma-Aldrich
Lysine 0	L5626, Sigma-Aldrich
Lysine 8	CNLM-291-H-PK, Cambridge Isotope Laboratories
Nu-serum	355100, BD Biosciences
OptiMEM	11058-201, Gibco
Penicillin/Streptomycin	P4333, Sigma-Aldrich

Sodium selenite	S5261-10G, Sigma
Trypsin/Ethylenediaminetetraacetic acid (EDTA) solution	P10-023100, PAN Biotech

3.1.3 Chemicals/reagents

Aqueous buffers were prepared in ultrapure water (Barnstead smart2pure water purification system or Thermo Scientific or OmniaTap12 UV/UF, 18200103, Stakpure). Double distilled pyrogen-free, mycoplasma-free, endotoxin-free injection grade water (ddH2O) (B. Braun) was used for molecular cloning. Solutions for mouse zygote injections were prepared with water for embryo transfer, which is sterile-filtered, BioXtra, suitable for mouse embryo (W1503, Sigma-Aldrich). DNA primers and guides were purchased from Eurofins (MWG). RNA for ribonuclear protein complex formation and long DNA oligos were purchased from Integrated DNA Technologies (IDT).

1 kb DNA ladder	N3232L, New England Biolabs (NEB)
100 bp DNA ladder	323-1, NEB
10x *Pfu* reaction buffer	M776A, Promega
4-(2-hydroxyethyl)-1-piperazineethanesulfonic acid (HEPES)	A3724, Applichem
5‘ ATTO AltR –CRISP Cas9 tracrRNA	1075934, IDT
Acetonitrile	34967, Fluka
Agar	A0949, Applichem
Agarose	peqGold Universal Agarose 35-1020, peqlab
Ammonium peroxodisulfate (APS)	1012001000, Merck
Aprotinin	10236624001, Roche Diagnostics
BbsI	R0539S, NEB
Benzonase	RPN2236, Sigma-Aldrich
Bovine serum albumin, fraction V (BSA)	A1391, AppliChem
Bromphenolblue	A2331,0025, Applichem
BssHII	R0199S, NEB
C18 material	Empore Disk C18 (2215) 3M, Sigma-Aldrich
Calcium chloride dihydrate ($CaCl_2(H_2O)_2$)	C7902, Sigma-Aldrich
cOmplete MINI protease inhibitor cocktail tablets	04693120001, Roche Diagnostics
cOmplete MINI protease inhibitor cocktail tablets, EDTA free	04693159001, Roche Diagnostics
Cutsmart buffer	B7204S, NEB

Cyclic-adenosine monophosphate (cAMP)	102296, Boehringer Mannheim
Diluent B	B80025, NEB
Dimethyl sulfoxide (DMSO)	A1391, AppliChem
Dithiothreitol (DTT) (NuPAGE Sample Reducing Agent 10x)	NP0009, lifetech (novex)
ECL Prime Western Blotting Detection Reagent	RPN2236 Amersham, GE Healthcare
Ethanol	32205-2.5L-M, Sigma-Aldrich
Ethidium bromide	A1152.0025, Applichem
Ethylene glycol-bis(β-aminoethyl ether)-N,N,N',N'-tetraacetic acid (EGTA)	A0878, Applichem
Ethylenediaminetetraacetic acid (EDTA)	A5097, Applichem
Forskolin	1099, Tocris
Fuji Medical X-Ray Films 18x24	RF22, Hartenstein
Glycerol	49783, Fluka
Glycine	A1067, Sigma
Goat serum	G9023-10mL, Sigma-Aldrich
Immobilon-P PVDF membrane	IPVH00010, Merck
Iodoacetamide	I1149, Sigma-Aldrich
Leupeptin	11017101001, Roche Diagnostics
Lysyl Endopeptidase (LysC)	129-02541, Wako
Magnesium chloride hexahydrate ($MgCl_2(H_2O)_6$)	3618, Applichem
Manganese(II) chloride tetrahydrate ($MnCl_2(H_2O)_4$)	221279, Sigma
Methanol	322130,2.5L-M, Sigma-Aldrich
Neb2 buffer	B7002S, NEB
Nonfat dried milk powder	A0830, Applichem
Nonidet P 40 Substitute (NP-40)	74385-1L, Sigma-Aldrich
Orange G DNA loading dye	3756, Sigma-Aldrich
PAGE-blue	24620, Thermo Fisher Scientific
Paraformaldehyde (PFA)	P6148, Sigma-Aldrich
Peptone from Casein	1298Gr500, BioFox
Pfu DNA Polymerase	M7741, Promega
phenylmethylsulphonyl fluoride (PMSF)	P7626, Sigma-Aldrich
Phosphatase inhibitor cocktail	04906837001, Roche Diagnostics
Phostag-AAL-107	304-93521, Wako Chemicals GmbH
PKI 6-22 amide	P6062-5mg, Sigma-Aldrich

Potassium chloride (KCl)	A3582, Applichem
Protein A sepharose	17-5280-01, GE Healthcare
Protein Marker III	PEQL27-1110, peqlab
Proteinase K	A3830, Applichem
Quick Extract DNA Extraction Solution	QE09050, Epicentre (Lucigen)
Quick-Load 50 bp DNA Ladder	N0473, NEB
Rotiphorese gel 30	3029.1, Roth
Round glass coverslips Ø 24 mm	41001124, Assistent
Sep-Pak C18	WAT051910, Waters Corporation
Sodium chloride (NaCl)	A1149, AppliChem
Sodium dodecyl sulfate (SDS)	A1502, Applichem
Sodium orthovanadate	S6508, Sigma-Aldrich
Sodium pyrophosphate	S9515, Sigma-Aldrich
Spectra Multicolor Broad range Marker	26634, Thermo Fisher Scientific
Tetramethylethylenediamine (TEMED)	UN2372, Applichem
Thiazolyl Blue Tetrazolium Bromide (MTT)	M2128-100mg, Sigma-Aldrich
Triflouracetic acid (TFA)	T6508, Sigma-Aldrich
Tris	A2264, AppliChem
Triton X-100	A4975,050, Applichem
Trypsin Gold	V5280, Promega
Tween 20	A4974, Applichem
Urea	U2709, Sigma-Aldrich
Whatman filter paper	GB46, Hartenstein
Yeast extract	A1552, Applichem
β-glycerophosphate disodiumsalt hydrate	G5422-25G, Sigma-Aldrich

3.1.4 Antibodies

Primary Antibodies

Mouse monoclonal anti PKA RIα	610609, BD Transduction Lab.
Mouse monoclonal anti α-Tubulin	T9026, Sigma-Aldrich
Mouse monoclonal anti-PKA Cα	610980, BD Transduction Lab.
Mouse monoclonal anti-PKA RIIβ	610625, BD Biosciences
Mouse monoclonal anti-TOMM34	LS-C173137, LS Bio
Mouse monoclonal anti-FLAG M2	F3165, Sigma-Aldrich

Mouse polyclonal anti-CRIK	611377, BD Transduction Lab.
Rabbit monoclonal anti-H1.2	ab181977, Abcam
Rabbit monoclonal anti-phospho-CREB	4276, Cell Signaling
Rabbit polyclonal anti-phospho -GSK-3α/β(Ser21/9)	9331, Cell Signaling
Rabbit polyclonal anti-phospho β-catenin (Ser33/37/Thr41)	9561, Cell Signaling
Rabbit polyclonal anti-Phospho-(Ser/Thr) PKA substrate	9621, Cell Signaling
Rabbit polyclonal anti-CIT	ab86782, Abcam
Rabbit polyclonal anti-FLAG	F7425, Sigma-Aldrich
Rabbit polyclonal anti-GOLPH4	ab28049, Abcam
Rabbit polyclonal anti-histone H1.4 antibody	PA5-31908, Thermo Fisher Scientific
Rabbit polyclonal anti-phospho Histone H1.4(Ser35)	PA5-31907, Thermo Fisher Scientific
Rabbit polyclonal anti-PKA Cα	4782, Cell Signaling
Rabbit polyclonal anti-PKA RIα	29250002-0.1mg, Novus Biologicals
Rabbit polyclonal anti-PKA RIIβ	HPA008421, Sigma-Aldrich
Rabbit polyclonal anti-TOMM34 antibody	ab103585, Abcam

Secondary antibodies

Goat anti-mouse horseradish peroxidase conjugate	115-035-003, Jackson ImmunoResearch
Goat anti-rabbit horseradish peroxidase conjugate	111-035-144, Jackson ImmunoResearch
Goat anti-mouse Cy2-conjuaged polyclonal	115-225-062, Jackson ImmunoResearch
Goat anti-rabbit IgG Alexa Fluor 594 conjugate	A-11037, Thermo Fischer Scientific
Goat anti-mouse IgG Alexa Fluor 647 conjugate	A-21237, Thermo Fischer Scientific

3.1.5 Commercially available kits

Alt-R Mouse Control Kit CRISPR-Cas9	1072555, IDT
BCA Protein Assay Kit	23225, Pierce (Thermo Fischer Scientific)
Effectene Transfection Reagent	301425, QIAGEN
EN Gen Mutation Detection Kit	E3321S, NEB
GenElute Mammalian	G1N70, Sigma-Aldrich

Lipofectamin CRISP MAX RNP	CMAX 00003, Thermo Fisher Scientific
PepTag non-radioactive cAMP-dependent protein kinase assay	V5340, Promega
PTMScan Phospho-PKA Substrate Motif (RRXS/T) Kit	5565, Cell Signaling
QIAGEN MIDI plus DNA extraction kit	12945, QIAGEN
Surveyor Mutation Detection Kit	706020, IDT

3.1.6 Laboratory equipment/apparatus

Agarose gel system	Agaget Standard, Whatman Biometra
Blotting chamber	Criterion Blotter, BioRad
Bottletop-filter, 0.2 μM aPES	595-4520, Thermo Fisher Scientific
Centrifuge 1	Centrifuge 5810R, Eppendorf
Centrifuge 2	Rotanta 48R, Hettich
Confocal microscope	TCS SP5 confocal microscope, Leica Microsystems
Cycler 1	GeneAmp PCR System 9700, Applied Biosystems
Cycler 2	Mastercycler epgradient, Eppendorf
Electrophoresis Power Supply	EPS 301, Amersham Biosciences
Electrophoresis Unit	SE600 Series, Hoefer
Eppendorf LoBind, Protein low binding tubes	0030108116, Eppendorf
Fluorescence activated cell sorting (FACS) instrument	Aria III , BD biosciences
FRET microscope	Zeiss Axiovert 200
Gel-imaging system	UVT-28ME-HC, Herolab
Imaging chamber (Attofluor)	A7816, Thermo Fisher Scientific
Lyophilizer	Alüha 1-2 LDplus, 101521, Martin Christ Gefriertrocknungsanlagen GmbH
Mass spectrometer	Orbitrap Fusion, EASY-Spray Ion Source Thermo Fisher Scientific
NanoDrop 2000c spectrophotometer	Peqlab
Plate reader	SPECTRAmax Plus, Molecular Devices
Scanner	1660, Epson
Shaker 1	Duomax 1030, Heidolph
Shaker 2	WT12, Biometra
Sonicator Tip	Sonopuls HD206, Bandelin

Speedvac	Concentrator plus, Eppendorf
Syringe filter 0.2 μm	Filtropur S 0.2, 83.1826.001, Sarstedt
Table top centrifuge 1	EBA12R V2.02, Hettich
Table top centrifuge 2	5424, Eppendorf Centrifuge
Ultracentrifuge	Optima TLX Ultracentrifuge, Beckmann
Ultrasonic bath	Sonorex Super Rk255H, Bandelin
Ultraturrax	T8, IKA Labortechnik

3.2 Methods

3.2.1 Plasmids

3.2.1.1 Plasmid origins and cloning

The plasmids encoding for human PKA Cα (RC210332, Origene), RIIβ (RC209900, Origene) and RIα (RC203828, Origene) wild-type were purchased from Origene. Mutations in the sequence coding for the Cα subunit were introduced by polymerase chain reaction (PCR) as described before[13]. For generating plasmids encoding the FLAG-tagged RIα and RIIβ subunits, fragments containing the entire coding sequence of the human RIIβ and RIα subunit was amplified by PCR with a forward primer containing the FLAG tag (amino-acid sequence DYKDDDDA) and KpnI (for RIIβ) or HindIII (for RIα) restriction site at the 5' and a reverse primer containing a NotI restriction site at the 3'. This fragment was subsequently inserted between the KpnI or the HindIII and NotI sites in pcDNA3. Plasmids encoding for cyan fluorescent protein (CFP)-tagged mouse RIIβ and RIα subunits or the yellow fluorescent protein (YFP)-tagged Cα subunit[166] were available in the Institute of Pharmacology (University of Würzburg). Plasmids encoding YFP-tagged human PKA Cα were generated by replacing the sequence of the mouse Cα subunit with the sequence of the wild-type human PKA Cα subunit between the NotI and ClaI sites. The mutated sequences were then inserted between the XhoI and SbfI (L206R, 199_200insW, W197R, d244-248+E249Q, S213R+insIILR, 200_201insV) or NotI and XhoI (E32V) site of the Cα(WT)-YFP plasmid. The CFP-tagged human RIIβ and RIα subunits were generated by replacing the mouse with human PKA subunits. Specifically, fragments containing the entire PKA subunit coding sequences without stop codons were amplified by PCR using primers containing a NotI (RIIβ) or HindIII (RIα) site at the 5' and a ClaI (RIIβ) or XbaI (RIα) site at the 3' and used to replace the mouse subunits contained between a NotI site and a ClaI site (RIIβ) or the HindIII and XbaI site (RIα) in the original constructs. Cloning of all the above R and C subunit expression constructs was done by Dr. Ulrike Zabel (Institute of Pharmacology, University of Würzburg).

The plasmid encoding for the GFP-tagged SpCas9 and the sgRNA was purchased from Addgene (42230, Addgene). The guide sequence (MWG, Eurofins) was inserted into the expression cassette between the BbsI sites as described by Ran *et al.*[167]

3.2.1.2 Transformation of chemically competent *Escherichia coli* (Top10)

5x KCM: 500 mM KCl, 150 mM $CaCl_2$, 250 mM $MgCl_2$
Lysogeny broth (LB) medium: 1% peptone, 0.5% yeast extract. 1% NaCl
Nutrient Agar plates (LB supplemented with 1.5% agar)

To amplify plasmids, chemically competent *E. coli* (Top10) were used. For each plasmid transformation, the reaction was comprised of 80 μL ddH_2O, 20 μL 5xKCM and 0.5 to 1 μg DNA, followed by 100 μL of competent *E. coli* (Top10). This mixture was incubated 20 min on ice followed by 10 min at room temperature (RT). Afterwards, 1 mL of pre-warmed LB medium was added. The mix was incubated for 50 min at 37°C under horizontal shaking. The bacteria were spun down by centrifugation at 5,000 rpm for 2 min (EBA12R, Hettich). The bacterial pellet was resuspended in 100 μL LB medium and 10-100 μL of this suspension was plated on nutrient agar plates containing ampicillin (0.1 mg/ml) or kanamycin (0.04 mg/ml) as per the antibiotic resistance of the vector backbone. The plates were incubated overnight at 37°C. On the next day, a single isolated colony was picked and was used to inoculate LB medium for further plasmid amplification and extraction.

3.2.1.3 Plasmid DNA extraction

To extract plasmid DNA from bacteria, the Qiagen MIDI plus kit was used.

Midiprep

Briefly, 2 mL LB medium containing ampicillin (0.1 mg/ml) or kanamycin (0.04 mg/ml) was inoculated with a single isolated colony of transformed *E.coli* (Top10) as described above or with a stab from a glycerol stock of transformed bacteria. This pre-culture was incubated for 8 h at 37°C with horizontal circular shaking at 180 rpm. From this pre-culture, 50 μL were used to inoculate 50 mL LB medium containing ampicillin (0.1 mg/ml) or kanamycin (0.04 mg/ml) and incubated overnight for 15 hours at 37°C and horizontal circular shaking at 180 rpm. On the next day, bacteria were harvested by centrifuging the culture at 4,000 rpm (Rotanta 48 R, Hettich) at 4°C for 15 min in a 50 ml tube. The supernatant was discarded, and the pellet was resuspended in 4 ml buffer P1 containing LyseBlue (mixed to a ratio of 1:1,000) by pippeting it up and down. To this suspension, 4 ml of P2 buffer were added followed by mixing the contents by inverting the tube 4-6 times so that mix was uniformly blue in color (because of LyseBlue). This was followed by an incubation time of 4 minutes so that all the cells were lysed. The lysis was stopped by adding 4 ml S3 buffer and mixed by inverting the tube till the blue

solution was colorless. Then, the mixture was centrifuged at RT for 5 min at 4,000 rpm (5810R, Eppendorf). The clear supernatant containing the lysate and the plasmid DNA was decanted into the QIAfilter cartridge and incubated further for 5 min. The lysate was then filtered through the QIAfilter cartridge in a new 15 ml tube followed by addition of 2 ml BB buffer. Using the provided vacuum pump assembly, the lysate was then filtered through the provided column to bind the DNA. The column was washed with 700 µL ETR-buffer by centrifuging it for 10,000x*g* for 1 min (EBA12R, Hettich). This was followed by a wash with 700 µL PE-buffer containing ethanol at 10,000x*g* for 1 min (EBA12R, Hettich). The column was further centrifuged without any solution for 10,000x*g* for 1 min (EBA12R, Hettich) to remove any trace amounts of salts or ethanol. The plasmid DNA was eluted in 100 µL PCR grade water by incubation for 1 min, followed by centrifugation at 10,000x*g* for 1 min. Plasmid DNA was quantified using a Nanodrop 2000c spectrometer. On average, the yield from one 50 ml culture was around 500 to 600 µg. After quantification, the plasmid DNA was diluted to a stock concentration of 1 µg/µl and stored at -20°C. Ratios of absorbance at 260 nm and 280 nm and at 260 nm and 230 nm were used to assess the purity of DNA. A ratio of 1.8 (260/280) and 2.0 to 2.2 (260-230) were considered as pure and DNA was stored for further use.

Miniprep

For a mini purification, a nutrient agar plate containing freshly transformed bacteria or a glycerol stock were used for inoculations. Briefly, one isolated colony from a plate culture or a stab from a glycerol stock was used to inoculate 2ml LB containing ampicillin (0.1 mg/ml) or kanamycin (0.04 mg/ml) and incubated at 37°C for 8 hours on the rotary shaker set at 180 rpm. From this mini culture, 1.5 mL were used for plasmid isolation and 0.5 mL were stored at 4°C. Bacteria were harvested by centrifugation at 5,000 rpm (EBA12R, Hettich) for 2 min. The pellet was resuspended in 300 µL P1 buffer containing LyseBlue (mixed to a ratio of 1:1,000), followed by 300 µL P2 buffer. After mixing, 300 µL S3-buffer was added and mixed gently until the solution was colorless. The mixture was incubated 5 min on ice and then centrifuged at 14,000 rpm (EBA12R, Hettich) for 2 min. 800 µL of the supernatant was transferred to a new tube and 400 µL isopropanol was added followed by incubation for 5 min on ice. The mixture was centrifuged at 14,000 rpm (EBA12R, Hettich) for 3 min. The supernatant was discarded, and the pellet was washed by centrifuging in 150 µL 70% ethanol followed by air drying the pellet till all the ethanol was evaporated. The pellet was then dissolved in 50 µL ddH_2O. Plasmid DNA was then sent for sequencing (MWG Eurofins). If the sequence was correct, the stored 0.5 mL of the initial culture were used to start a Midiprep.

3.2.1.4 Ribonuclear protein (RNP) complex formation

$T_{10}E_{0.1}$ buffer: 10 mM Tris, 0.1 mM EDTA in water for embryo transfer, pH 7.4
Diluent B: 300 mM NaCl, 10 mM Tris-HCl, 1 mM DTT, 0.1 mM EDTA, 500 μg/ml BSA, 50% Glycerol, pH 7.4

Equimolar amounts (72 pmol) of target specific guide RNA (20 μM stock in $T_{10}E_{0.1}$ buffer) and trans-activating crRNA (tracrRNA) (20 μM stock in $T_{10}E_{0.1}$ buffer) were mixed and incubated at 95°C for 5 min. Then the mixture was slowly cooled down to form an RNA complex. The complex was then diluted with $T_{10}E_{0.1}$ buffer to a total volume of 100 μl and final concentration of 0.72 μM. To check for transfection efficiency, a fluorescently labelled Atto550-tracrRNA was used. Then, to 17 μl of the RNA complex, the repair template was added to a final concentration of 50 ng/μl (stock: 1 μg/μl). Afterwards, 1 μg Cas9 protein (1 μg/μL stock in diluent B) was added to a final concentration of 50 ng/μl, followed by incubation at RT for 5 min to form a ribonuclear protein (RNP) complex. The resulting RNP complex is stable when stored at -80°C for up to 6 months.

3.2.2 Cell culture and transfection

HEK293 A, HEK293T and Hepa1-6 cells were cultured in Dulbecco's modified Eagle's medium (DMEM) containing 10% fetal bovine serum (FBS), 1% penicillin-streptomycin and maintained at 37ºC and 5% CO_2. NCI-H295R cells were cultured in DMEM/F-12, Hepes supplemented with 3% Nu-serum and 1% Insulin-Transferrin-Selenium-Sodium Pyruvate (ITS).

3.2.2.1 SILAC labeling

Light medium: DMEM without Arginine and Lysine supplemented with 0.2 mg/ml L-Proline, and light amino acids: 146 μg/ml Lys0, 84 μg/ml Arg0. Sterile filtered medium was further supplemented with 10% dialyzed FBS, 1% 100x GlutaMAX and 1% penicillin-streptomycin.
Heavy medium: DMEM without Arginine and Lysine supplemented with 0.2 mg/ml L-Proline, and heavy amino acids: 152.35 μg/ml Lys8, 87.96 μg/ml Arg10. Sterile filtered medium was further supplemented with 10% dialyzed FBS, 1% 100x GlutaMAX and 1% penicillin-streptomycin.

5-10 cell doublings are typically sufficient for a complete stable isotope labeling by amino acids in cell culture (SILAC). In practice, I observed complete incorporation in 6 subcultures of HEK293A cells. When using Trypsin for detaching cells between subcultures, cells were spun down and the supernatant was removed before resuspending the cells in fresh growth medium. The cells were counted during every passaging procedure to ensure equal number of cells in light and heavy cultures. For phosphoproteomics experiments, the Cα wild-type samples were labeled with light amino acids and the Cα mutants (L206R, d244-248+E249Q, 200_201insV) with heavy amino acids. For each experiment, two 15 cm plates transfected with Cα mutants (L206R, d244-248+E249Q, 200_201insV) and cultured in heavy medium and two 15 cm plates transfected with Cα wild-type and cultured in light medium were used.

3.2.2.2 Transfection of cells with Effectene

HEK293A of HEK293T cells were seeded at a density of 250,000 cells, $1.2x10^6$ cells or $3.5x10^6$ cells in a 6-well, 10 cm or 15 cm plate respectively on the day before transfection. On the next day, cells were transfected using the Effectene Transfection Reagent. Briefly, for one well in a 6-well plate, 150 µL EC-Buffer was mixed with 1 µg DNA and incubated for 2 min. This was followed by 4 µL Enhancer and the mixture was incubated for further 2 min. Finally, 12 µL

Effectene was added followed by incubation for 20 min. Then 150 µL of this mixture was added to the cells. For 10 cm plates, all the above amounts were multiplied by a factor of 5.6 and for 15 cm plates, by a factor of 14. For co-transfection of R and C PKA subunits a ratio of 1:8 was optimal. Meaning that for each well in a 6-well plate, 0.1 µg of C-subunit and 0.8 µg of R subunit were used. For co-transfection of SpCas9-plasmid and repair template, equal amounts of both were used. After transfection, cells were incubated at 37°C for 48 hours.

3.2.2.3 Transfection of Hepa1-6 cells with Lipofectamin CRISPRMAX

Transfections of Hepa1-6 cells using Lipofectamin CRISPRMAX was done by Bianca Klüpfel (AG Calebiro, Institute for Pharmacology, University of Würzburg) with my guidance. The reverse transfection of Hepa1-6 cells with the RNP complex was done using Lipofectamin CRISPRMAX. 1.5 µl of the previously generated RNP complex (1 µM) was mixed with 0.6 µL CRISPR plus reagent, 1.2 µL CRISPR MAX and 46.7 µL of OptiMEM. The mixture was incubated for 10 min at RT. 50 µL of this mixture was then added to an empty 96-well plate and 100 µL cells (300 cells/µL normal culture medium) were added. After transfection, cells were incubated at 37°C for 48 hours.

3.2.2.4 Stimulation

For western blot, histone extraction, phosphoproteomics, nuclear translocation and Immunofluorescence experiments, cells were stimulated with a saturating concentration of forskolin (10 µM) for 30 min at 37°C, to ensure full activity of PKA. This was followed by cell lysis as required for the respective protocol.

For stimulation, forskolin (FSK) was used at a final concentration of 10 µM in cell culture medium. The cells were incubated at 37°C for 30 min in this stimulation medium.

3.2.3 Cell lysis

3.2.3.1 Membrane-free lysates

5/2 buffer: (5 mM Tris, 2 mM EDTA, pH 7.4)

Membrane-free lysates were used to asses PKA activity using the PepTag non-radioactive cAMP-dependent protein kinase assay. HEK293A cells were co-transfected with either RIα or RIIβ and the wild-type or mutant Cα subunit. Cells were washed twice with DDPBS at RT 48 hours after transfection this was followed by lysing the cells in 300 µL 5/2 buffer per well of a 6-well plate and the cells were detached using a scraper. The suspension was transferred to a 2 mL reaction tube. The cells were lysed using an ultraturrax for 20 s. The resulting lysate was centrifuged at 50,000 rpm (Ultracentrifuge, Rotor TLA120.2) for 30 min at 4°C. The supernatant was transferred to a new 2 ml tube and used for PKA activity measurements.

3.2.3.2 Total lysates

Lysis buffer: 20 mM HEPES pH 8.0, 8 M urea, 1 mM sodium vanadate, 2.5 mM pyrophosphate, 1 mM β-glycerophosphate, 1 cOmplete MINI protease inhibitor cocktail tablet per 10 mL lysis buffer

Total lysates were used to investigate PKA substrate phosphorylation in western blot and phosphoproteomics experiments. HEK293A cells were co-transfected with either RIα or RIIβ and the wild-type or mutant Cα subunit. 48 hours after transfection, cells were lysed under basal or stimulated condition. Therefore, cells were washed once with DPBS. Then, lysis buffer (300 µl/well for a 6-well plate or 2 ml/15cm plate) was added and the cells were scratched into the buffer and transferred to a 2 ml or 15 ml reaction tube. For Phosphoproteomics, the heavy and light cell suspensions were combined before lysis. Cells were lysed on ice using a sonicator tip (3 pulses for 15 s each). The lysate was cleared by centrifugation at 4000 rpm at 15°C for 1 hour (Centrifuge 5810R, Eppendorf). The supernatant was transferred to a new tube. Lysate was further used for phosphoproteomics experiments or prepared for western blot.

3.2.3.3 Histone extraction

Hypotonic lysis buffer: 150 mM Tris-HCl, 1 mM KCl, 1.5 mM $MgCl_2$ 1 mM DTT, pH 8.0, 0.5 μg/ml leupeptin, 2 μg/ml aprotinin, 0.1 mM phenylmethylsulphonyl fluoride (PMSF), cOmplete MINI protease inhibitor cocktail, phosphatase inhibitor cocktail 1 tablet per 10 mL

HEK293A cells were co-transfected with either RIα or RIIβ and the wild-type or mutant Cα subunit. 48 hours after transfection, cells were lysed under basal or stimulated condition. Histones were then acid extracted from cells and CPA tissues as described by Shechter et al[168]. Briefly, harvested cells or tissue samples were lysed in a hypotonic lysis buffer by homogenizing in a douncer. The cytosolic fraction was removed by centrifugation at 10,000x*g* at 4°C for 10 min (EBA12R, Hettich). The pellet containing the nuclear proteins was then acid-extracted with 0.2 M H_2SO_4 for 30 min. This results in precipitation of nuclear proteins, except histones. After separation of the soluble nuclear fraction from the insoluble fraction by centrifugation for 10 min at 4°c at 16,000x*g* (EBA12R, Hettich), the histones were precipitated for 30 min by adding 100% trichloroacetic acid to a final concentration of 33%. The pellet was washed twice with 1 mL ice-cold acetone, dried for 20 min at RT and resuspended in dd$H_2$0.

3.2.4 Biochemical techniques

3.2.4.1 Estimation of protein amount by bicinchoninic acid assay

To estimate the protein amount in cell lysates and histone extracts, a bicinchoninic acid (BCA) assay kit was used. All samples and calibration curves were measured in triplicates or duplicates respectively. For the calibration curve, BSA in DPBS was used in 9 different concentrations (2 mg/mL, 1.5 mg/mL, 1 mg/mL, 0.75 mg/mL, 0.5 mg/mL, 0.25 mg/mL, 0.125 mg/mL, 0.025 mg/mL, 0 mg/mL). For the BCA mixture 50 parts of solution A and 1 part of solution B were mixed. Then 25 µL of each sample and 200µL of the BCA mixture was mixed in a 96-well plate. The reaction was incubated at 37°C for 30 min, followed by measuring the absorption at 562 nm using a plate reader.

3.2.4.2 SDS-PAGE analysis

5% stacking gel (recipe sufficient for two 14x9 cm gels): 1.5 ml Rotiphorese 30, 2.5 ml 4x Tris/SDS pH 6.8 (500 mM Tris, 0.4% SDS), 7.5 ml H_2O, 240 µl 10% APS, 22.5 µl TEMED.
7.5% separating gel (recipe sufficient for two 14x9 cm gels): 5.7 ml Rotiphorese 30, 5.6 ml 4xTris/SDS pH 8.8 (1.5 M Tris, 0.4% SDS), 11.25 ml H_2O, 300 µl 10% APS, 22.5 µl TEMED.
10% separating gel (recipe sufficient for two 14x9 cm gels): 7.2 ml Rotiphorese 30, 5.6 ml 4xTris/SDS pH 8.8 (1.5 M Tris, 0.4% SDS), 9.75 ml H_2O, 300 µl 10% APS, 22.5 µl TEMED.
15% separating gel (recipe sufficient for two 14x9 cm gels): 15.14 ml Rotiphorese 30, 7.87 ml 4xTris/SDS pH 8.8 (1.5 M Tris, 0.4% SDS), 8.5 ml H_2O, 300 µl 10% APS, 22.5 µl TEMED.
5x SDS loading buffer: 300 mM Tris pH 6.8, 5% SDS, 50% glycerol, 0.1% bromophenol blue, 10 mM DTT
SDS running buffer: 25 mM Tris, 190 mM glycine, 0.1% SDS, pH 8.3.

Proteins were separated according to their size using sodium dodecyl sulfate polyacrylamide gel electrophoresis (SDS-PAGE). Generally, histone samples were analyzed on a 15% separating gel, CIT was analyzed on a 7.5% separating gel and all other proteins on a 10% separating gel. Samples were mixed with 5x SDS loading buffer and boiled at 99°C for 3 min to denaturate the proteins. 14x9 cm SDS-PAGE gels were prepared in advance and were stored at 4°C if needed. Samples and protein ladder were loaded and run in an electrophoresis unit filled with SDS running buffer at a constant voltage of 80 V, which was changed to 150 V when the bromophenol blue front reached the separating gel. Before the front ran out of the

separating gel, the unit was switched off and disassembled. The stacking gel was discarded, and the separating gel was either used further for western blot transfer or PAGE-blue staining.

To check for complete digestion of proteins, proteins or peptides in the separation gel were stained using PAGE-blue. For this, the gel was washed in water three times for 10 min at RT to remove the SDS. Then, 10 mL of PAGE-blue was added, and staining was done for 30 min at RT. The staining was followed by destaining using water till the protein-bands were clearly visible against a clear background on the gel.

3.2.4.3 Phos-tag gels

5% stacking gel (recipe sufficient for one 14x9 cm gel): 1.5 ml Rotiphorese 30, 3 ml 4x Tris/SDS pH 6.8 (500 mM Tris, 0.4% SDS), 7.5 ml H_2O, 240 µl 10% APS, 24 µl TEMED.
10% separating gel, 100 µM Phos-tag (recipe sufficient for one 14x9 cm gel): 3.33 ml Rotiphorese 30, 2.5 ml 4xTris/SDS pH 8.8 (1.5 M Tris, 0.4% SDS), 3.71 ml H_2O, 0.2 ml 10 mM $MnCl_2$, 0.2 ml 3% Phos-tag AAL-107, 150 µl 10% APS, 11.25 µl TEMED.
Transfer buffer: 25 mM Tris, 150 mM glycine, 10% methanol
Transfer buffer with SDS: 25 mM Tris, 150 mM glycine, 0.1% SDS, 10% methanol

Phos-tag is a functional molecule which is able to capture several phosphorylated residues[169]. Therefore, in addition to their size, Phos-tag in SDS-PAGE analysis separates the proteins according to their degree of phosphorylation. Samples were mixed with 5x SDS loading buffer and boiled at 99°C for 3 min to denature the proteins. SDS and polyacrylamide were copolymerized with 100 mM Phos-tag and the final 14 x 9 cm gels were used on the same say. Samples and protein ladder were loaded and run in an electrophoresis unit filled with SDS running buffer at a constant current of 50 mA. The stacking gel was discarded, and the separating gel was washed twice, 10 min each, with transfer buffer with SDS supplemented with 4 mM EDTA to remove the Mn^{2+}-ions and twice, 10 min each, with transfer buffer to equilibrate for transfer.

3.2.4.4 Western blot analysis

TBS-T: 10 mM Tris pH 7.4, 100 mM NaCl, 0.1% Tween20
Blocking solution: 5% BSA or milk powder in TBS-T buffer.
Transfer buffer: 25 mM Tris, 150 mM glycine, 10% methanol
Transfer buffer with SDS: 25 mM Tris, 150 mM glycine, 0.1% SDS, 10% methanol
Wash buffer: 50 mM Tris pH 7.4, 150 mM NaCl, 0.2% BSA, 0.2% NP-40
Stripping buffer: 100 mM glycine, 0.1% SDS, pH 2.5

After SDS-PAGE separation of the proteins, they were transferred to a Polyvinylidene difluoride (PVDF) membrane for western blot analysis. The PVDF membrane was first activated in methanol for 10 min at RT. The blot assembly consisted of three pre-wet Whatman filter papers (9x16 cm), the separating gel, the activated PVDF membrane (5.5x15 cm) and again three pre-wet Whatman filter papers (9x16 cm). For the transfer of large proteins (like CIT) or for Phos-tag gels, the transfer buffer with SDS was used. The proteins are negatively charged and therefore will run in the direction of the anode. Therefore, the blot assembly was placed in the blotting chamber in a way that the PVDF membrane was positioned between the separating gel and the anode. The proteins were then transferred to the PVDF membrane by blotting at 100V for 50 min (90 min for Phos-tag gels). For large proteins (e.g. CIT) the following blotting program was used: 20 min 200 mA, 20 min 300 mA, 20 min 400 mA, 1h 440 mA. Afterwards, the PVDF membrane was blocked for 1 h at RT in blocking solution to prevent unspecific binding. For blocking, 5% BSA or milk-powder in TBS-T was used depending on the requirements of the respective primary antibody solutions. Incubation with the primary antibody was carried out at 4°C overnight using gentle shaking.

Table 2: Dilutions and incubation times of primary antibodies for western blot

Antibody	Dilution	Incubation
Rabbit polyclonal anti-PKA Cα	1:7,000 in 5% milk in TBS-T	4°C, overnight
Rabbit monoclonal anti-FLAG	1:4,000 in 5% milk in TBS-T	4°C, overnight
Mouse monoclonal anti-PKA RIα	1:1,000 in 5% milk in TBS-T	4°C, overnight
Mouse monoclonal anti-PKA RIIβ	1:2,000 in 5% milk in TBS-T	4°C, overnight
Rabbit polyclonal anti-phospho-(Ser/Thr) PKA substrate	1:1,000 in 5% BSA in TBS-T	4°C, overnight
Mouse monoclonal anti α-Tubulin clone DM1A	1:40,000 in 5% BSA in TBS-T	RT, 1 hour (was done after the overnight incubation with above prim Ab followed by washing as described below)
Mouse monoclonal anti-TOMM34	1:1000 in 5% BSA in TBS-T	4°C, overnight
Mouse polyclonal anti-CRIK	1:2000 in 5% BSA in TBS-T	4°C, overnight

On the next day, the PVDF membrane was washed three times, 10 min each, with wash buffer and gentle shaking followed by incubation with an appropriate horseradish peroxidase-conjugated (HRP) secondary antibody (1:10,000 in wash buffer) for 1 hour at RT. After removal of the secondary antibody solution and three washing steps with wash buffer (each 10 min) the membrane was treated with the ECL prime western blotting detection reagent, a substrate of HRP for 1 min. Images of various exposure times (3 s- 1 h) were acquired on Fuji Medical X-Ray Films which were then scanned (at 1,200 dpi) and densiometric analysis of the signals was performed using ImageJ (http://rsbweb.nih.gov/ij).

To detect other proteins of similar size on the same membrane, the membrane was stripped to wash away bound antibodies. For this, the membrane was washed once with H_2O for 10 min at RT and then incubated with stripping buffer for 2 h at RT and gentle shaking. The membrane was then washed twice with H_2O and processed further to blocking.

3.2.4.5 Agarose gel analysis

TAE buffer: 2 M Tris, 50 mM EDTA, 5.7% acetic acid, pH 8.3

Agarose gel electrophoresis was used to analyze deoxyribonucleic acid (DNA) or kemptide phosphorylation.

For DNA analysis, 1 or 2% agarose gels were used depending on the expected size of the DNA fraction. For gel preparation, 1 or 2 g of agarose was dissolved in 100 mL of TAE buffer by boiling the suspension. After the solution was cooled to 60°C ethidium bromide was added to a final concentration of 0.005%. Samples were mixed in a 1:9 ratio with Orange G DNA loading dye and loaded on the gel. As a reference, a 1 kbp or 100 bp DNA ladder was used. Electrophoresis was done at a constant voltage of 100 V for 45 min. Images of the gels were acquired with a gel documentation system and analyzed using ImageJ (http://rsbweb.nih.gov/ij).

For kemptide phosphorylation analysis, 0.8% agarose gels in 50 mM Tris/HCl pH 8.0 was used. Samples were mixed with 1-2 μl of 80% glycerol and loaded on cavities in the middle of the 0.8% agarose gel. Kemptide has different net charge if phosphorylated compared to unphosphorylated. Therefore, the sample is separated by electrophoresis in these two fractions. Electrophoresis was carried out at a constant voltage of 100 V for 20 min. Images of the gels were acquired with a gel documentation system and analyzed using ImageJ (http://rsbweb.nih.gov/ij).

3.2.5 Functional assays

3.2.5.1 MTT assay

MTT solution: 5mg/ml in DPBS
Solubilization solution: 50% DMSO, 50% ethanol

For analysis of relative growth using thiazolyl blue tetrazolium bromide (MTT), 4,000 cells/well in 96-well plates containing a final volume of 100 µl/well were seeded and incubated for 24, 48 or 72 hours. As blank, a well containing 100 µl medium only was used. On the day of experiment, 10 µl MTT solution was added to each well (to reach a final concentration of 0.45 mg/ml). Cells were incubated at 37°C for 3 hours, during which time they convert the water soluble MTT into insoluble formazan. Afterwards, medium was removed and 100 µl of solubilization solution was added to each well to dissolve the formazan crystals. To allow complete solubilization an incubation for 10 min at 37°C was done. Then absorbance of the formazan was recorded at 550 nm.

$$relative\ growth\ (\%) = 100 * \frac{OD_{550\,nm}\ (sample)}{OD_{550\,nm}\ (control)}$$

Equation 1: Calculation of relative growth. Where $OD_{550\,nm}$ (sample) is the absorbance of the mutant PKA Cα expressing cells at 550 nm and $OD_{550\,nm}$ (control) is the absorbance of the wild-type PKA Cα expressing cells at 550 nm

3.2.5.2 PKA activity assay

PKA activity assay mix for 20 samples: 100 µl of 5x PepTag PKA React, 100 µl PepTag A1, 10 µl Peptide Protect, 100 µl ddH_2O

PKA catalytic activity was measured using the PepTag non-radioactive cAMP-dependent protein kinase assay, which uses fluorescent kemptide as a substrate. Briefly, membrane-free cell lysates were prepared (section 3.2.3.1) and analyzed by western blot (section 3.2.4) to adjust for similar expression of PKA R and C subunits in the different samples. Depending on the expression level of the C subunit, 1-9 µl lysate was used to measure PKA activity. The pure lysate was used to check the basal activity while addition of 40 µM cAMP was used to analyze the activity of PKA under stimulation and 15 µM PKI 5-24 (a specific inhibitor for PKA) for analysis upon inhibition of PKA activity. To the lysate with stimulators or inhibitors, 15 µl PKA activity assay mix was added. The reaction was incubated at RT for 30 min in the dark.

In this time, the kemptide is phosphorylated by PKA. Phosphorylation of the kemptide changes its net charge from +1 to -1. This allows distinguishing between unphosphorylated and phosphorylated kemptide by agarose electrophoresis. The phosphorylation reaction was stopped by heating the sample at 95°C for 10 min. Then 1-2 µl of 80% glycerol was added and the samples were analyzed on a 0.8% agarose gel (see section 3.2.4.5).

3.2.5.3 Co-Immunoprecipitation

Lysis buffer: 20 mM Tris pH 7.5, 150 mM NaCl, 1mM EDTA, 1mM EGTA, 1 tablet of cOmplete MINI protease inhibitor cocktail for every 10 ml of lysis buffer
Lysis buffer with cAMP: above lysis buffer supplemented with 200 µM cAMP.

Co-immunoprecipitation was used to investigate the association of the R and C subunits of PKA under basal or stimulated conditions. Antibody-coupled Protein A sepharose beads were prepared in advance. For this, for one sample, 12 µl of protein A slurry were washed three times with 500 µl DPBS each by centrifuging at 800x*g* for 30 s (EBA12R, Hettich). Then 500 µl of lysis buffer and 0.5 µl of anti-FLAG M2 mouse was added to the beads. The suspension was incubated over night at 4°C with vertical circular rotation. Finally, the beads were washed once with lysis buffer (for basal activity) or lysis buffer with cAMP (for stimulated condition).

For co-immunoprecipitation (Co-IP), confluent HEK293A 10 cm plates, transfected with FLAG-tagged R subunit and C subunit for 48 hours were used. The medium was aspirated from the plate and 1 ml of ice cold lysis buffer or lysis buffer with cAMP was added to the cells. The lysis was carried out at 4°C for 10 min. The suspension was then transferred to a reaction tube and centrifuged at 14,000 rpm at 4°C for 10 min (Centrifuge 5810R, Eppendorf). From the supernatant, 80 µl was taken out as an input control and mixed with 20 µl of 5x SDS loading buffer, boiled at 95°C for 5 min and stored at -20°C or -80°C. The remaining supernatant was used for the co-immunoprecipitation. To this remaining lysate, the prepared antibody-coupled Protein A sepharose beads were added. This mixture was incubated at 4°C for 2 hours under vertical circular rotation to enable proper mixing of the contents and binding of the FLAG-tagged R subunit to the antibody. The beads were then washed 5 times with 500 µl lysis buffer or lysis buffer with cAMP to remove unspecific bound proteins. To elute the proteins from the beads, 30 µl of 1x SDS loading buffer were added to the beads and boiled at 99°C for 3 min. Then the sample was centrifuged at 800x*g* for 30 s (EBA12R, Hettich). The supernatant was then analyzed by immunoblotting.

3.2.5.4 Immunoprecipitation of TOMM34 and CIT

Lysis buffer: 50 mM Tris-HCl pH 7.5, 150 mM NaCl, 0.5% NP-40, 1 mM EDTA, 0.5 μg/ml leupeptin, 2 μg/ml aprotinin, 0.1 mM phenylmethylsulphonyl fluoride (PMSF), cOmplete Mini protease inhibitor cocktail, phosphatase inhibitor cocktail 1 tablet per 10 mL
Binding buffer: 50 mM Tris-HCl pH 7.5, 150 mM NaCl, 0.05% NP-40, 1 mM EDTA, 0.5 μg/ml leupeptin, 2 μg/ml aprotinin, 0.1 mM phenylmethylsulphonyl fluoride (PMSF), cOmplete Mini protease inhibitor cocktail, phosphatase inhibitor cocktail 1 tablet per 10 mL

Immunoprecipitation (IP) was used to isolate TOMM34 and CIT to analyze the phosphorylation status under basal or stimulated (10 μM forskolin for 30 min) condition of PKA. Antibody-coupled Protein A sepharose beads were prepared in advance. For this, for one sample, 12 μl of protein A slurry were washed three times with 500 μl DPBS each by centrifuging at 800x*g* for 30 s (EBA12R, Hettich). Then 500 μl of lysis buffer and 2.5 μl of anti-CIT rabbit antibody or anti-TOMM34 rabbit antibody was added to the beads. The suspension was incubated over night at 4°C with vertical circular rotation. Finally, the beads were washed once with lysis buffer (for basal activity) or lysis buffer with cAMP (for stimulation condition). For immunoprecipitation, confluent 15 cm plates of HEK293A cells co-transfected with RIIβ and the wild-type or mutant Cα subunit were used. 48 hours after transfection, cells were lysed under basal or stimulated condition. Cells were washed twice with ice-cold DPBS, then 1 ml of lysis buffer was added, and the cells were incubated for 10 min at 4°C. Then the lysate was transferred into a 1.5 ml reaction tube and centrifuged 14,000 rpm at 4°C for 15 min (EBA12R, Hettich). The cytosolic fraction, which is the supernatant, was transferred into a new tube. As an input control, 80 μl was taken out from this lysate and mixed with 20 μl of 5x SDS loading buffer, boiled at 95°C for 5 min and stored at -20°C or -80°C. The remaining lysate was used for the immunoprecipitation. To this remaining lysate, the prepared antibody-coupled Protein A sepharose beads were added. This mixture was incubated at 4°C over night under vertical circular rotation to enable proper mixing of the contents and binding of the proteins to the antibody. The beads were then washed 5 times with 500 μl binding buffer to remove unspecific bound proteins. To elute the proteins from the beads, 45 μl of 1x SDS loading buffer were added to the beads and boiled at 99°C for 3 min. Then the sample was centrifuged at 800x*g* for 30 s (EBA12R, Hettich). The supernatant was then analyzed by immunoblotting.

3.2.5.5 Immunofluorescence

Fixing solution: 4% paraformaldehyde in DPBS
Permeabilization solution: 0.1 % in DPBS triton X-100:
Blocking solution: 5 % goat serum in DPBS

Cells were seeded on 24 mm round glass coverslips placed in 6-well plates followed by transfection with PKA R and C subunits. 48 h post transfection, cells were used under basal and stimulated (section 3.2.2.) condition.

Cells were washed twice with 1 ml DPBS and fixed for 15 min with 4 % paraformaldehyde at RT. After four washing steps each for 5 min with 1 ml DPBS, cells were permeabilized using 1 ml 0.1 % Triton-X100 for 3 min at RT. Three washes, each for 5 min with 1ml DPBS, were followed by blocking with 1 ml 5% goat serum for 1 hour at RT. The permeabilized cells were then incubated with the primary antibody in 5% goat serum overnight at 4°C in a humidifying chamber. On the next day, the coverslips were washed three times with DPBS followed by incubation with secondary antibody in 5% goat serum for 2 hours at RT in a humidifying chamber. Finally, the coverslips were washed three times with DPBS. To preserve the samples, the coverslips were mounted in glycerol on glass slides.

Table 3: Antibodies used for Immunofluorescence.

Antibody	Dilution
Mouse monoclonal anti-PKA Cα	1:200
Rabbit polyclonal anti-GOLPH4	1:200
Mouse monoclonal anti-PKA RIIβ	1:100
Goat anti-rabbit IgG Alexa Fluor 594 conjugate	1:2,000
Goat polyclonal anti-mouse Cy2 conjugate	1:400

3.2.6 Genome modifying using CRISPR/Cas9

The CRISPR/Cas9 system was discovered in 1987[170] and was hypothesized to be the immune system of bacteria and archaea in 2005[171, 172, 173]. It was then developed as an efficient tool to modify the genome of cells[174, 175]. Here, a type II CRISPR/Cas9 system of *Streptococcus pyogenes*, which is the most widely CRISPR system[176], was used. This system includes three main components: the Cas9 endonuclease, trans-activating CRISPR RNA (tracrRNA), and CRISPR RNAs (crRNA)[167]. The guide sequence that is complementary to the nucleic acid target is included in the crRNA[177]. After recruitment into the Cas9 complex by tracrRNA, this complementary sequence guides Cas9 to the target site. For Cas9, to successfully bind the target, a sequence termed a protospacer adjacent motif (PAM), which originally is used to differentiate foreign DNA from the host genome, must be present just downstream of the target sequence[174]. If present, Cas9 cleaves the DNA element just upstream of the PAM[174]. The PAM required for Cas9 recognition in *Streptococcus pyogenes* (Sp) is 5'-NGG, though the sequence varies for other CRISPR systems[167, 174]. For the purposes of genome editing, this system has been simplified by combining the tracrRNA and crRNA into a single guide RNA (sgRNA)[174].

3.2.6.1 Design of guide sequence

A guide sequence can be every 20 nucleotide sequence which is followed by a PAM sequence at the 3' end in the genome. The PAM sequence is specific for the CRISPR system used[167]. Here, I have used a system derived from Sp which requires an NGG-motif[167]. The Sp CRISPR-associated proteins (SpCas9) induces a double strand break approximately 3 bp upstream of the PAM. To select a suitable guide sequence, the web-tool (http://crispr.mit.edu/)[167] was used. This tool predicts the off-targets for all possible guide sequences in a target region. Based on this prediction, the tool scores the possible guide sequences. From the top 10 in this list, two guides were chosen and tested. Using these two guides, it was checked whether the most likely off-targets are located in a coding or non-coding region of the genome. Off-targets located in non-coding regions were preferred.

Table 4: Selected guides and their nucleotide sequences.

Guide	Sequence
Guide 1 *PRKACA*	5'- GTGCGGCACCCCTGAGTACC -3'
Guide 2 *PRKACA*	5'-GGGAGGCTCCTACTTTGCTC-3'
Guide 1 *GRM4*	5'-TCCCGGACATTTCGGAAAGG-3'
Guide 2 *GRM4*	5'-GCCTCCCTTCCCGGACATTT-3'

3.2.6.2 Design of repair template

To introduce specific mutations or to insert base pairs for a tag in the genome, homology directed repair is used. For this, a DNA template is needed to repair the DNA in the specified manner. As a repair template, a single stranded oligonucleotide sequence was used for small insertions and a plasmid for big insertions. In general, a repair template consists of the desired sequence of the target site flanked on each side by a homology arm which is identical to the region around the target site. It is important, that the used guide sequence is not included in the repair template; otherwise the SpCas9 would also cut the repair template[167]. To prevent cleavage of the repair template, silent mutations were inserted to remove the guide sequence.

Repair template for *PRKACA*

The mutation to introduce in *PRKACA* is just a small substitution of two base pairs, therefore the approach using a single stranded oligonucleotide sequence was used. 90 base pairs of the genomic sequence directly following or preceding the target site were used as homology arms. To prevent cutting of the repair template by SpCas9, the PAM sequence was removed from the repair template by introducing silent mutations. This silent mutation was designed in such a way that a BssHII cutting site was formed. This cutting site can be used to control for insertion of the repair template.

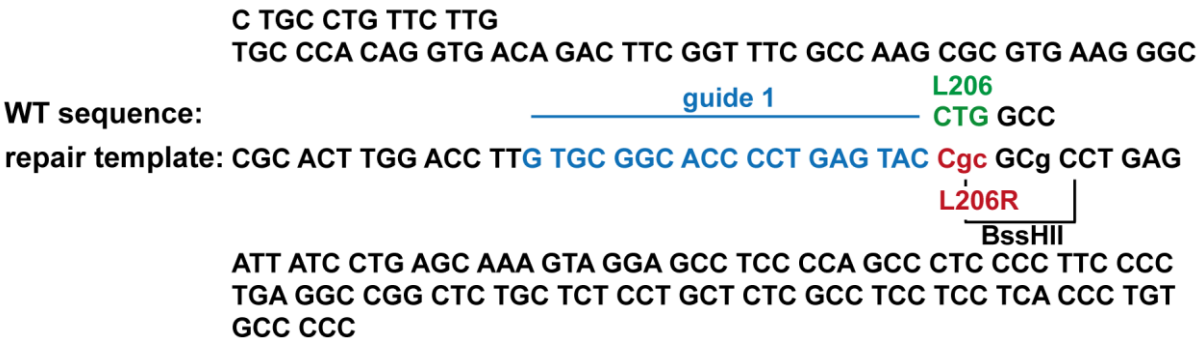

Figure 21: Sequence of repair template for guide 1. Mutated base pairs are lower cases and corresponding wild-type (WT) sequence is written above. The guide sequence (blue), the leucine at position 206 (green) and the introduced L206R mutation (red) are also represented. The introduced cutting site for the enzyme BssHII is also marked.

Repair template for *GRM4*

The design of the repair template for the GRM4 locus was done with the help of Sana Siddig (AG Calebiro, Institute for Pharmacology, University of Würzburg), who decided on the position of the tags and the appropriate signal peptide. The insertion planned for the *GRM4* locus consists of a new signal peptide, a HA-tag and a SNAPf tag. In total this counts for 648 base pairs. Therefore, it was too big to be done by single stranded oligonucleotides and the plasmid-based method was used. Due to the bigger insertion, longer homology arms were required. We used homology arms of 1100 bp on the 5' and 1260 bp on the 3'. The guide sequence was automatically deleted from the repair template since the endogenous signal peptide of *GRM4* was replaced by the signal peptide of mGlu5. As a backbone, the pcDNA3.0 plasmid was used. The cloning of the repair template was done by Bianca Klüpfel (Institute for Pharmacology, University of Würzburg).

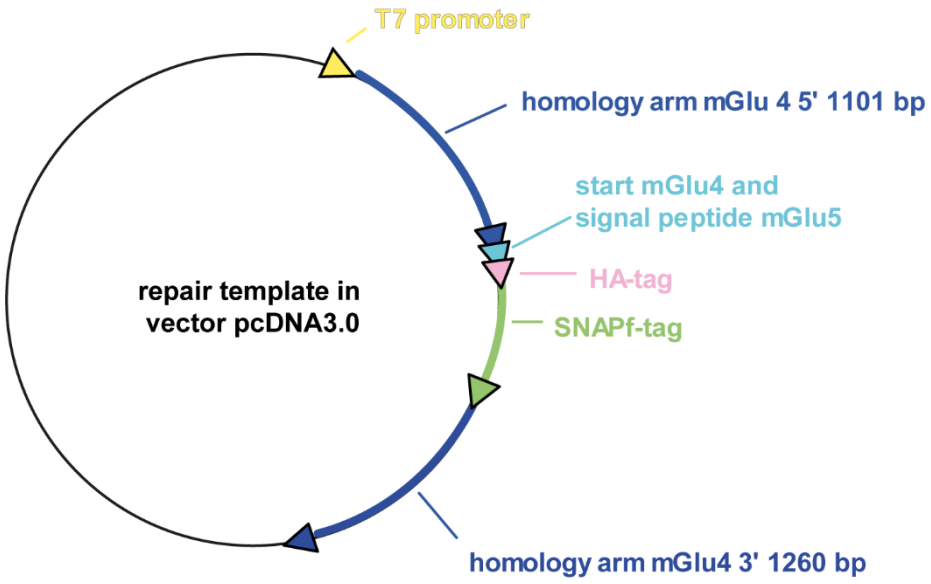

Figure 22: Circular map of the repair template used to insert HA- and SNAPf-tag into the mGlu4 mouse gene.

3.2.6.3 Fluorescence-activated cell sorting (FACS)

Conditioned medium: Remove the medium from a confluent 10 cm plate and sterilize it by filtering (0.2 µm syringe filter). Then mix in a 1:1 ratio with fresh medium.

Fluorescence-activated cell sorting (FACS) was performed with the help of Christian Linden (Institute of Virology and Immunobiology, University of Würzburg). FACS was used to get transfected single cells. For this purpose, the cells were detached from the plate using Trypsin 48 h after transfection and sorted using a FACS machine (BD biosciences) in groups of 1 or 5 cells into a 96 well plate containing conditioned medium. On the next day, the wells were checked and were marked if they contained just one single cell. These single cell clones were then maintained.

3.2.6.4 Extraction of genomic DNA

QuickExtract DNA Extraction Solution was used to extract the genomic DNA of the sorted single cell clones in a 96 well format. After aspiration of the medium, 10 µl of the QuickExtract DNA Extraction Solution was added to each well of a 96-well plate. The cells were detached by pipetting up and down and transferred to a 0.2 µl reaction tube. The suspension was vortexed for 15 s and then incubated at 65°C for 6 min. After vortexing for 15 s the suspension

was incubated at 98°C for 2 min. The resulting DNA was used for PCR without any further clean-up.

To extract DNA from 10 cm culture plates, the GenElute Mammalian kit was used. The cells were detached by trypsinization and pelleted by centrifugation at 800 rpm for 3 min (Rotanta 96R, Hettich). The supernatant was discarded, and the cell pellet was resuspended in 200 µl resuspension buffer and 20 µl RNAse A solution. After incubation at RT for 2 min, 20 µl PKK solution and 200 µl lysis buffer C were added to the cell suspension. The resulting mixture was vortexed and incubated at 70°C for 10 min. In these 10 min, the column was prepared by adding 500 µl column prep solution to the preassembled column and centrifugation at 12,000x*g* for 1 min (EBA12R, Hettich).Then 200 µl 100% ethanol was added to the cell suspension and mixed by pipetting the solution up and down. The solution was transferred to a column and spun at 6,500x*g* for 1 min (EBA12R, Hettich). Then the column was washed with 500 µl wash buffer and centrifuged at 6500x*g* for 1 min (EBA12R, Hettich). The wash was repeated with 500 µl wash buffer and centrifugation at 15,500x*g* for 3 min (EBA12R, Hettich). To dry the column, it was centrifuged at 15,500x*g* for 1 min (EBA12R, Hettich). The DNA was eluted by adding 15 µl ddH_2O into the middle of the column followed by a short incubation for 5 min at RT and centrifugation at 6,500x*g* for 1 min (EBA12R, Hettich). This elution step was repeated. The DNA was incubated at RT for 30 min before determining the concentration by Nanodrop.

3.2.6.5 Polymerase chain reaction (PCR)

10xPfu buffer: 200 mM Tris pH 8.8, 100 mM KCl, 100 mM $(CH_4)_2SO_4$, 20 mM $MgSO_4$, 1% Triton X-100, 1 mg/mL BSA

PCR was used to amplify DNA for sequencing. A PCR comprises three major steps: denaturation, annealing and elongation. The first step, denaturation, is needed to form single-stranded DNA templates out of the double-stranded DNA template. This is followed by a decrease in temperature to allow the complimentary oligonucleotides (referred to as primers) to anneal to the single-stranded DNA template. Finally, elongation of the primers by DNA polymerase to produce the complimentary sequence. These three steps are repeated 28-35 times for sequence amplification. Here, the PCR reaction mixture contained 0.5 Units Pfu polymerase, 0.25 pmol/µl forward primer (stock 10 pmol/µl), 0.25 pmol/µl reverse primer (stock 10 pmol/µl), 0.2 mM deoxyribonucleotide triphosphates mix (dNTPs) (stock 10 mM) and 150 ng DNA in 50 µl 1x Pfu reaction buffer. The reaction was run on a thermocycler (GeneAmp PCR system 9700, AB Applied Biosystems) with the program specified in table 5. The standard

annealing temperature was adapted to the melting temperature of the oligonucleotides (Table 6) and the elongation time depended on the length of the desired PCR product (Pfu polymerase elongates 1 kbp in 2 min). To check for specificity of the PCR primers and the efficiency of the PCR, 2 µl of the completed PCR reaction were analyzed on a 1% Agarose gel.

Table 5: PCR program used for reaction with Pfu polymerase.

Step	Temperature	Time
initial denaturation	94°C	5 min
35 cycles	94°C	30 sec
	55°C	30 sec
	72°C	90 sec
final extension	72°C	5 min
hold	4°C	∞

Table 6: Primer sequences and sizes of resulting PCR templates.

Primer name	Sequence	Melting temperature	Size of product
PRKACA fwd	CACCTGCTGGACCATTTTGG	62°C	713 bp
PRKACA rev	GGCCTGACTTAAGGAACTTC	60°C	
Human chr14 fwd	GGTCCTGGTTGTAGAAGGGC	64°C	567 bp
Human chr14rev	CGTGTGTTCTCCGAGGACCG	66°C	
Human chr2 fwd	CAGAGGGAGGCAGGACCATG	66°C	583 bp
Human chr2 rev	CCTTTGCCCCAGGTGTTTCC	64°C	
Human chr9 fwd	GGCGATCCAGCTGGTTGTGG	66°C	558 bp
Human chr9 rev	GTGATGGAGTACGTGCCGGG	66°C	
Mouse *GRM4* fwd	CAGGACACAGGGACAAGGAT	62°C	870 bp
Mouse *GRM4* rev	CTGCCCCATTCTCAAACACT	60°C	

The PCR to control for indels by T7E1 assay was done by Bianca Klüpfel (Institute for Pharmacology, University of Würzburg) under my co-supervision. For usage in the T7E1 assay (3.2.6.8), the PCR was done using the polymerase included in the kit. Briefly, 5 µl DNA template was mixed with 15.5 µl Q5 hotstart high fidelity master mix, 1.25 µl of each primer (10 µM) and 5 µl ddH_2O. The PCR program listed in Table 7 was used.

Table 7: PCR program used for T7E1 assay.

Step	Temperature	Time
initial denaturation	98°C	30 sec
35 cycles	98°C	5 sec
	60°C	10 sec
	72°C	20 sec
final extension	72°C	2 min
hold	4°C	∞

3.2.6.6 *In vitro* testing of CRISPR/Cas9 guides

1x Cas9 nuclease reaction buffer: 20 mM HEPES, 100 mM NaCl, 5 mM $MgCl_2$, 0.1 mM EDTA, pH 6.5 at 25°C

The *in vitro* testing of guides was performed by Bianca Klüpfel (Institute for Pharmacology, University of Würzburg) under my co-supervision. Testing of guides can be done *in vitro* using a PCR template. Therefore, 10 nmol RNP (stock 100 nM) and 1 nmol of the PCR template (stock 10 nM) were mixed in 10 µl Cas9 nuclease reaction buffer. The digestion mix was incubated for 60 min at 37°C. Finally, 1 µl proteinase K (20 mg/mL) was added and incubated for 10 min at 56°C to release the bound template from Cas9. The mixture was analyzed for cutting by SpCas9 on a 1% Agarose gel.

3.2.6.7 Determination of cutting efficiency by Surveyor

10x Taq PCR buffer: 100 mM Tris, 500 mM KCl, 15 mM $MgCl_2$, pH 8.3

The cutting efficiency of the guide was determined using the Surveyor mutation detection kit. This assay is used to detect random insertion or deletions (indels) caused by cutting of the genomic DNA by SpCas9 in HEK293T cells. Therefore, 180 ng of a PCR product of the target locus of wild-type cells was mixed with 180 ng of a PCR product of potentially modified cells in 1x Taq PCR buffer to a final volume of 20 μL. The PCR products are then denatured and re-annealed using the program described in table 8. This results in heteroduplexes of PCR products from wild-type and potentially modified cells.

Table 8: Program used for denaturation and annealing of PCR products.

Step	Temperature	Time or ramp speed
denaturation	95°C	10 min
annealing	95-85°C	-2°C/sec
	85-75°C	-0.3°C/sec
	25-4°C	-0.3°C/sec
hold	4°C	∞

Then the aligned PCR products were digested using the surveyor mismatch nuclease S. This enzyme detects mismatches of base pairs which is a marker for indels. Therefore, to the annealed PCR product, 2 ml $MgCl_2$ (150 mM), 1 ml ddH_2O, 1 ml surveyor nuclease S and 1 ml surveyor enhancer S was added, and the mixture was incubated at 42°C for 1 hour. Then the reaction was stopped by adding 2 ml of stop solution and analyzed on a 2% agarose gel. The percentage of indels was calculated using equation 2. To control if the assay was performed correctly a positive control plasmid DNA was included in the surveyor kit. The two control plasmids (C and G) differ in a single base pair. These plasmids were treated like the samples. After running the PCR, the PCR products were either annealed with itself (*e.g.* C with C) to form homoduplexes as a negative control or with the other control (*e.g.* C with G) to form heteroduplexes as a positive control.

$$indel\ (\%) = 100 \times \left(1 - \sqrt{1 - \frac{b + c}{a + b + c}}\right)$$

Equation 2: Calculation of indel-efficiency. Where a is the integrated intensity of the undigested PCR product and b and c are the integrated intensities of each cleavage product.

3.2.6.8 Determination of cutting efficiency by T7E1

1xNeb2 buffer: 50 mM NaCl, 10 mM Tris-HCl, 10 mM $MgCl_2$, 1 mM DTT pH 7.9

The determination of cutting efficiency by T7E1 was conducted by Bianca Klüpfel (Institute for Pharmacology, University of Würzburg) under my supervision.

The EnGen Mutation Detection kit was used to determine cutting efficiency of RNP complexes in Hepa 1-6 cells. For heteroduplex formation, 5 µl of the PCR mix was mixed with 10x Neb2 buffer and 5 µl of ddH_2O. To form heteroduplexes, the following program depicted in table 9 was used. 1 µl of T7E1 enzyme was added to the annealed product and the reaction was incubated at 37°C for 30 min. To release the DNA template from the enzyme, 1 µl proteinase K was added, and the mixture was incubated further 5 min at 37°C. The product was analyzed on a 2% agarose gel.

Table 9: Program used for heteroduplex formation of PCR products for the T7E1 assay.

Step	Temperature	Time or ramp speed
denaturation	95°C	5 min
re-annealing	95-85°C 85-25°C	-2°C/sec -0.1°C/sec

3.2.6.9 Determination of HDR efficiency by BssHII digestion

1xCutSmart buffer: 50 mM potassium acetate, 20 mM Tris-acetate, 10 mM magnesium acetate, 0.1 mg/ml BSA, pH 7.9

To detect whether the repair template was inserted in the *PRKACA* gene of the cells, the homology directed repair (HDR) efficiency was analyzed. Therefore, the repair template was designed with an inserted BssHII restriction site, which was not present in the wild-type *PRKACA*. To detect insertion of the repair template, the PCR product of the *PRKACA* gene was digested using BssHII. For this, 5 µl of the PCR product was mixed with 0.5 µl BssHII in CutSmart buffer in a final volume of 10 µl and incubated at 50°C for 1 hour. Then, the mixture was analyzed on a 2% agarose gel and HDR efficiency was determined using equation 3.

$$HDR\ efficiency\ (\%) = \frac{b+c}{a+b+c}$$

Equation 3: Calculation of HDR efficiency. Where *a* is the integrated intensity for the undigested HDR PCR product and *b* and *c* are the integrated intensities for the BssHII-cut fragments.

3.2.6.10 Mouse zygote injection and breeding

The genome modification of mice was done in collaboration with Prof. Bösl (Zentrum für Experimentelle Molekulare Medizin, University of Würzburg). The injection of mouse zygotes with the RNP complex, including the breeding and pairing of mice was conducted by Daniela Östreich (Zentrum für Experimentelle Molekulare Medizin, University of Würzburg). All animal experiments were performed according to institutional and governmental guidelines of Germany.

3.2.7 Microscopy techniques using SP5

Experiments were performed on a TCS SP5 confocal microscope (Leica Microsystems) using a 63x oil-immersion objective (HCX PL APO Lambda blue 63x/1.4 oil UV).

3.2.7.1 Imaging of Immunofluorescence

Alexa 594 was excited using the 594 nm line of a HeNe594 laser and emission was detected with a GaAsP hybrid detector (HyD) in a range from 608-647 nm. Cy2 was excited using a 488 line of a 65 mW argon-ion laser set at 13% and detected using a HyD detector in a range from 509-533 nm. Analysis of images was done using ImageJ (http://rsbweb.nih.gov/ij) by measuring the mean grey value of the nucleus and the cytosol of cells.

3.2.7.2 Acceptor photobleaching

FRET-buffer: 137 mM NaCl, 5 mM KCl, 2 mM $CaCl_2$, 1 mM $MgCl_2$, 10 mM HEPES, pH 7.3

Cells were grown on 24 mm round glass coverslips and transfected with RIIβ subunit in combination with wild-type or mutant Cα subunit. 48 h after transfection, coverslips were mounted in an imaging chamber (Attofluor). To prevent the cells from drying FRET buffer was added. Pictures of the basal state and stimulated state (10 μM forskolin for 30 min) were taken in the donor (CFP) channel before and after bleaching of the FRET-acceptor (YFP). CFP excitation was performed using the 488-nm line of a 65 mW argon-ion laser set at 15% and emission was detected with a HyD in a range from 465 to 490 nm. YFP bleaching was done using the 514-nm line of the same laser set at 50%. Images were taken in basal state and after stimulating for 30 min using 10 μM forskolin before and after bleaching of YFP. Analysis of images was done using ImageJ (http://rsbweb.nih.gov/ij) by measuring the mean grey value of the nucleus and the cytosol of cells. After subtracting the background, FRET efficiency (E) was calculated from these images using equation 4.

$$E = 1 - \frac{I_0}{I_{bl}}$$

Equation 4: Calculation of FRET efficiency (E). Where I_0 is the CFP intensity before and I_{bl} is the corresponding value after photobleaching.

3.2.7.3 PKA nuclear translocation

FRET-buffer: 137 mM NaCl, 5 mM KCl, 2 mM $CaCl_2$, 1 mM $MgCl_2$, 10 mM HEPES, pH 7.3

Cells were grown on 24 mm round glass coverslips and transfected with the R subunit in combination with wild-type or mutant Cα subunit. 48 h after transfection the coverslips were mounted in an imaging chamber. To prevent the cells from drying FRET buffer was added. CFP was excited using the 488-nm line of a 65 mW argon-ion laser set at 15%. CFP emission was detected with a HyD detector in a range from 440-481 nm. YFP was excited using a 405 Diode and detected using a HyD detector in a range from 579-621 nm. Images were taken in basal state and after stimulating for 30 min using 10 μM forskolin. Analysis of images was done using ImageJ (http://rsbweb.nih.gov/ij) by measuring the mean grey value of the nucleus and the cytosol of cells. After subtracting the background, the ratio of the amount of Cα subunit in the nucleus and cytosol was calculated.

3.2.8 Functional test of SNAPf-mGlu4 using FRET

HBSS/BSA buffer: 150 mM NaCl, 2.5 KCl, 2.5 mM $MgCL_2$, 4 mM $CaCl_2$, 10 mM HEPES, 10 mM Glucose, % BSA, pH 7.4

The functionality test of the SNAPf-mGlu4 construct by Förster resonance energy transfer (FRET) was done by Dr. Marie-Lise Jobin (AG Calebiro, Institute of Pharmacology, University of Würzburg).

Briefly, HEK293A cells were seeded on poly-L-Lysine coated 24mm round glass cover slips at a density of 200,000. After 24 hours, cells were co-transfected with a plasmid coding for the CFP-Epac-YFP sensor [178] (0.5 μg/well), one for glutamate transporter EAAC1 (0.25 μg/well) and either the mGlu4 wild-type or the SNAPf-mGlu4 construct (0.25 μg/well) using effectene (protocol described in 3.2.2.2). After 24 hours of transfection, cells were starved using DMEM with 1% 100x GlutaMAX and 1% penicillin-streptomycin. One hour before the experiment, 6.25 μg/ml glutamate-pyruvate transaminase (10 mg/mL stock in HBSS/BSA buffer) and 2 mM pyruvate (100 mM stock in HBSS/BSA buffer) were added to the cells to remove residual glutamine. FRET traces were then obtained on an imaging setup composed of a standard inverted microscope (Zeiss Axiovert 200), equipped with a 63x/1.25 NA oil-immersion objective (Zeiss, Jena, Germany) and a wheel to switch excitation filter cube (436/20 excitation filter plus a 455LP dichroic mirrors). A Monochromator-based light source was used (Polychrome V), which contained a 150 W xenon lamp (TILL photonics, Gräfelfing, Germany). The emission

light was splitted into donor and acceptor channels using a Dual View beam splitter (Photometrics), which uses a 505LP dichroic mirror and two emission filters: 480/15 for CFP and 535/20 for YFP. Images in the two channels were simultaneously collected with an electron multiplying charge-coupled device (EMCCD) camera (iXon ultra, Visitron System) and monitored online using the MetaFlour software (Molecular Devices/TILL photonics). The ratiometric traces were corrected for bleed-through using equation 5.

$$FRET_{corr} = (YFP_{436} - A * CFP_{436} - B + YFP_{500})/CFP_{436}$$

Equation 5: Correction of FRET ratio for bleed-through. YFP_{436} is the fluorescence intensity of the acceptor at 436 nm excitation (CFP), CFP_{436} is the fluorescence intensity of the donor at 436 nm excitation (CFP) and YFP_{500} is the fluorescence intensity of the acceptor at 500 nm excitation (YFP). A and B represent correction factors which are microscope specific (A = 0.57, B = 0.07) and calculated previously for this setup.

3.2.9 Structural analysis of mutations

Structural images were prepared using the PyMOL software (www.pymol.org). The structure of the mouse full-length tetrameric RIIβ(2):Cα(2) holoenzyme[19] (PDB: 3TNP) was used to display the PKA catalytic (Cα) and regulatory (RIIβ) subunit structures. For the D/D domain, the PDB entry 3IM4[179] was used. Additionally, structures of the apo C subunit without any bound ligands (PDB: 4NTS)[122]; of the ternary complex with bound ATP, two Mg^{2+} ions and substrate (PDB: 3X2W)[123]; of the ternary complex with bound ADP, two Mg^{2+} ions and phospho-substrate (PDB: 3TNQ)[19]; and of the C subunit with ADP and one Mg^{2+} (PDB: 4NTT) [122] were used. For depictions of the C subunit with Mg-ATP and a substrate peptide (PDB: 3X2U) [123] was used. For the structure of the DNAJB1-PRKACA fusion protein in comparison with PKA Cα wild-type PDB entries 4WB5[147] and 4WB7[147] were used respectively. For the structure of the PKA Cα L206R mutant the structure published by Cheung *et al.* was used (PDB: 4WB6)[147].

3.2.10 Substrate specificity of PKA Cα mutants *in silico*

The prediction of changes in substrate specificity was done by Dr. Steven Pelech (Kinexus) using the Kinase Substrate Prediction v 2.0 algorithm[180]. This algorithm predicts the substrate specificity of a given kinase based on the primary amino acid. Therefore, a database of sequences of more than 488 human protein kinase catalytic domains and 10,000 known kinase-substrate phospho-site pairs is used. The algorithm then generates a specificity matrix for the wild-type and mutant Cα kinases, where values indicate the relative preference for each amino acid at each position around the phoshoacceptor site.

3.2.11 Phosphoproteomics

The substrate specificity was assessed using the PTMScan Phospho-PKA Substrate Motif (RRXS*/T*) Kit following the manufacturer´s instructions. Mutant samples were heavy labelled and wild-type samples were light labelled. Before preparing total cell lysates, the cells were stimulated with 10 μM forskolin for 30 min at 37°C to achieve fully activated PKA. Protein concentration of the total cell lysates was determined using the BCA assay. For the Phosphoproteomics experiments, not more than 20 mg protein were used.

3.2.11.1 Reduction and Alkylation of proteins

The total protein lysate from each condition was reduced with dithiothreitol (DTT) at a final concentration of 10 mM at 55°C for 30 min. After cooling down to RT, iodoacetamide was added to a final concentration of 25 mM and the alkylation was done in the dark for 15 min at RT.

3.2.11.2 LysC digestion

The alkylated proteins were diluted with 20 mM HEPES pH 8.0 to reduce the amount of urea in the buffer to a of 3.5 M. For digestion, the protease Lys-C (5 µg/mg protein) was added. Digestion was performed overnight in the dark at RT. A sample of the digested proteins was analyzed by SDS-PAGE to check for total digestion.

3.2.11.3 Sep-Pak C18 purification

Solution A: 2% acetonitrile, 0.1% Trifluoroacetic acid
Solution B: 40% acetonitrile, 0.1% Trifluoroacetic acid

To precipitate the fatty acids, 1/20 volume 20% TFA was added to the digestion solution. The pH should be lower than 3. This solution was incubated for 15 min on ice. Then the solution was centrifuged at 1,780x*g* for 15 min at RT (5810R, Eppendorf) to clear the lysate. The supernatant was decanted into a new tube and a sample was taken for SDS-PAGE analysis.

A Sep-Pak C18 column was used for purification of the lysate. For this, the column was pre-wet with acetonitrile and equilibrated with 0.1% Trifluoroacetic acid (TFA). After loading of the lysate, the column was washed twice with 0.1% TFA and then with solution A. The peptides were eluted using solution B. The eluate was lyophilized overnight.

3.2.11.4 Immunoaffinity purification

IP buffer: 50 mM MOPS, pH 7.2, 10 mM sodium phosphate, 50 mM NaCl

The lyophilized peptides were centrifuged at 4,000 rpm for 1 min at RT (5810R, Eppendorf). The peptides were resuspended in 1.4 ml of IP buffer by vortexing for 5 min. The remaining precipitate was removed by centrifuging at 4,000 rpm for 5 min at RT (5810R, Eppendorf). The solution was transferred in a low binding 2 mL tube and centrifuged again at 16x*g* for 5 min at RT (5424, Eppendorf). The supernatant was transferred to a new tube. The pH of the peptide solution was controlled so that it remains at pH 7.0. Then the phospho-PKA substrate antibody beads were washed three times with DPBS and added to the peptide solution and incubated for 2 hours at 4 °C under vertical circular rotation. The mixture was centrifuged at 2,000x*g* for 30s at 4°C (5424, Eppendorf). The supernatant was transferred to a new tube and stored at -20°C for later use. The beads were washed 3 times with 1 ml IP buffer and three times with 1 ml H_2O, at 4 °C. Peptides were eluted by the addition of 55µl 0.15% TFA for 10 min at RT. This was repeated with 50µl 0,15% TFA. Eluates were combined.

3.2.11.5 Stage Tip

Solution C: 80% acetonitrile, 0.3% TFA
Solution D: 2% acetonitrile and 0.3% TFA
Solution E: 40% acetonitrile and 0.3% TFA

The immunoprecipitated peptides were purified using Stage Tips. Stage Tips were prepared using 200 ml pipet tips and four discs of C18 material. The C18 material discs were positioned in the tip by putting soft pressure. The sample was acidified by adding TFA to a final concentration of 1%. The Stage Tip was first equilibrated in three steps: methanol, solution C and twice 0.3% TFA. After loading of the protein on the Stage Tip, the column was washed twice with solution D. Then the peptides were eluted using solution E. The eluate was dried in a speedvac (Eppendorf).

3.2.11.6 Digestion with Trypsin

The peptides were dissolved in 50 mM ammonium bicarbonate, resulting in a basic solution (pH higher than 8). 0.1 µg Trypsin was added to the peptides and incubated at 37°C overnight. The digest was followed by a Stage Tip purification (section 3.2.11.3)

3.2.11.7 NanoLC-MS/MS analysis

Solution F: 2% acetonitrile and 0.1% formic acid

The nanoscale liquid chromatography coupled to tandem mass spectrometry (nanoLC-MS/MS) measurements were performed by Dr. Jens T. Vanselow (AG Schlosser, Rudolf-Virchow Zentrum Würzburg, University of Würzburg). Measurements were performed on an Orbitrap Fusion (Thermo Fisher Scientific) equipped with an EASY-Spray Ion Source, coupled to an EASY-nLC 1000 (Thermo Fisher Scientific). Peptides were resuspended in solution F and loaded on a trapping column (2 cm x 75 µm ID, PepMap C18, 3 µm particles, 100 Å pore size). Separation was done on an EASY-Spray column (50 cm x 75 µm ID, PepMap C18, 2 µm particles, 100 Å pore size) with a 140-minute linear gradient from 3% to 45% acetonitrile and 0.1 % formic acid.

An Orbitrap analyzer with a resolution of 60,000 for mass spectrometry (MS) scans and 15,000 for tandem mass spectrometry (MS/MS) scans was used for both, MS and MS/MS scans.

Higher-energy collisional dissociation (HCD) fragmentation with 35 % normalized collision energy was applied. Additionally, a Top Speed data-dependent MS/MS method with a fixed cycle time of 3 seconds was used. Dynamic exclusion with a repeat count of 1 and exclusion duration of 60 seconds was utilized. Singly charged precursors were excluded from selection. The minimum signal threshold for precursor selection was set to 5e4. Predictive automatic gain control (AGC) was used with AGC at target value of 2e5 for MS scans and 5e4 for MS/MS scans. For internal calibration EASY-IC was used.

3.2.11.8 Raw data processing and database search

The raw data processing and data base search was done by Dr. Jens T. Vanselow, (AG Schlosser, Rudolf-Virchow Zentrum Würzburg, University of Würzburg). MaxQuant version 1.5.6.5 (MaxPlanck Institute of Biochemistry) [181] was used for raw-data processing, database searches and SILAC quantification. The human UniProt reference proteome database (http://www.uniprot.org/proteomes/UP000005640, download date: 2016-12-09), a small database containing known immunoglobulin chains and a database containing common contaminants (included in MaxQuant) was used for peptide identification. The search was performed with tryptic cleavage specificity and 3 allowed miscleavages. A false-discovery rate (FDR) of <1% was applied for protein identification on peptide and phosphosite level. Additionally, for modified peptides a minimum score of 40 and a minimum delta score of 6 was used. In addition to default settings carbamidomethyl (C) was set as fixed modification and protein N-terminal acetylation, glutamine to pyro-glutamate formation (N-term. Q), oxidation (M) and phosphorylation (STY) were included as variable modifications. For SILAC quantification, light (Arg0/Lys0) and heavy (Arg10/Lys8) labeling were used, with a maximum allowance of four labeled amino acids per peptide. Matching between runs was disabled. For further data analysis in R (Free Software Foundation's GNU project), the MaxQuant "Phospho (STY)Sites" table was processed. Only phosphosites with a localization probability greater than 0.75 and a posterior error probability (PEP) lower than 0.05 have been included. Normalization of the distribution of log2-transformed SILAC ratios heavy/light to the first mode of the distribution was done for each experiment. Then, data from replicate experiments were combined, and student´s t-test as well as limma p-values were calculated and corrected for multiple-hypothesis testing (Benjamini-Hochberg algorithm, FDR). Additionally, boxplot outliers were considered as significant or highly significant if values were outside of the 1.5x and/or the 3x interquartile range (IQR) of the 1st or 3rd quartile (Q1 or Q3) and if a replicate notch (1.58*IQR / sqrt(number of experiments)) was not overlapping with the median of all such notches.

3.2.12 Tumor tissue samples

All samples were collected at the University Hospital of Würzburg and provided by Prof. Martin Fassnacht. Patients have given their informed, written consent and the research complies with the Declaration of Helsinki (http://www.wma.net/en/30publications/10policies/b3/index.html). In total, 8 snap-frozen tumor specimens from CPAs of individual patients were investigated. Seven of these samples have been included in previous reports from our group (three in Ronchi *et al.*[94], three in Beuschlein *et al.*[89] and one in Weigand *et al.*[153]). Previously available sequencing data revealed that four of these CPA samples were affected by somatic *PRKACA* mutations. Three samples presented the L206R substitution and resulted in overt Cushing's syndrome and one sample presented a d244-248+E249Q mutation resulting in a mild Cushing's syndrome. The four remaining tumor samples presented wild-type *PRKACA* and were associated with overt Cushing (two samples) and mild Cushing syndrome (two samples).

3.2.13 Statistical analysis

The Prism 6 software (GraphPad) was used for statistical analysis. If not otherwise indicated, values are depicted as mean ± s.e.m. Differences between two groups were evaluated by two-tailed student's t-test. In case of three or more groups, differences were assessed by two-way analysis of variance (ANOVA), followed by Bonferroni's post hoc test. Differences were considered significant for P values < 0.05.

4 Results

When I joined the lab of Prof. Davide Calebiro, I had the great chance to contribute to finishing a study on the mechanism of action of the two initially discovered *PRKACA* mutations L206R and 199_200insW[89, 146]. This study used a set of biochemical and optical methods to investigate the association of the PKA Cα mutants with the RIIβ subunit[146]. These assays included co-immunoprecipitation (Co-IP) experiments, Förster resonance transfer (FRET) measurements between the catalytic and regulatory subunit in cell lysates and living cells and acceptor photobleaching in living cells[146]. The study revealed that, contrary to the wild-type Cα, where we observed a robust Co-IP and FRET response, we could not observe this for the L206R and the 199_200insW mutants[146]. Therefore, the data showed that the mutation hinders the binding to the RIIβ subunit, rendering the C subunit constitutively active[146].

This was the starting point of my main PhD project where I studied the five most recently discovered somatic PKA Cα subunit mutants identified by our collaborators Di Dalmazi *et al.* (200_201insV, S213R+insIILR)[93] and Ronchi *et al.* (W197R, d244-248+E249Q, E32V)[94] in unilateral CPAs of patients having overt Cushing's syndrome. As comparison, the two previously studied mutants L206R and 199_200insW were included. A summary of the *PRKACA* mutations found in CPAs and investigated here is given in Table 1.

As mentioned before, we could show in a previous study that the L206R and the 199_200 insW mutation interfere with the formation of a stable holoenzyme[146]. Therefore, I started the characterization of the abovementioned mutants by investigating the binding to R subunits. Additionally, I investigated the activity of the PKA Cα mutants using different assays, which also suggested changes in substrate specificity of the PKA Cα mutants. Therefore, I used an algorithm predicting relevant changes in the substrate specificity of kinases. The mutants predicted to have the major effect on substrate specificity were investigated in more detail using phosphoproteomics. This approach was able to directly compare the substrate repertoire of the wild-type and the mutated PKA Cα subunit in cells. This revealed several substrates that were hypo- or hyperphosphorylated by the mutants. Those results were then verified by phospho-specific western blot analysis of transfected HEK293A cells and tumor tissue of Cushing's patients. In parallel, I used the CRISPR/Cas9 system in HEK293T cells to generate a cellular model for L206R mutated tumors. Those cells were used to assess the question of altered subcellular localization of PKA subunits by immunofluorescence.

4.1 Binding of PKA Cα mutants to R subunit

Using a FRET-based approach our group has previously shown that the increased basal PKA activity in L206R and 199_200 insW mutated samples was due to a deficient binding of the Cα mutant to the R subunit. [146]. So, as a first step, I performed co-immunoprecipitation (Co-IP) experiments to investigate the interaction between the different PKA Cα mutants and R subunits. For this purpose, I transfected HEK293A cells with FLAG-tagged RIIβ or RIα and either wild-type or mutant Cα subunits at comparable expression levels. Using anti-FLAG antibody coupled protein A beads, FLAG-tagged R-subunit was then immunoprecipitated from lysates of these transfected cells and analyzed for interaction with Cα subunits by western blot analysis using an antibody directed against Cα. To control for specificity of the Co-IP, experiments with antibody-free protein A beads and without co-transfection of FLAG-tagged R subunit were also performed as negative controls (Figure 23). As expected, only co-transfection with FLAG-tagged R subunit followed by immunoprecipitation using an antibody conjugated protein A beads resulted in a robust Co-IP.

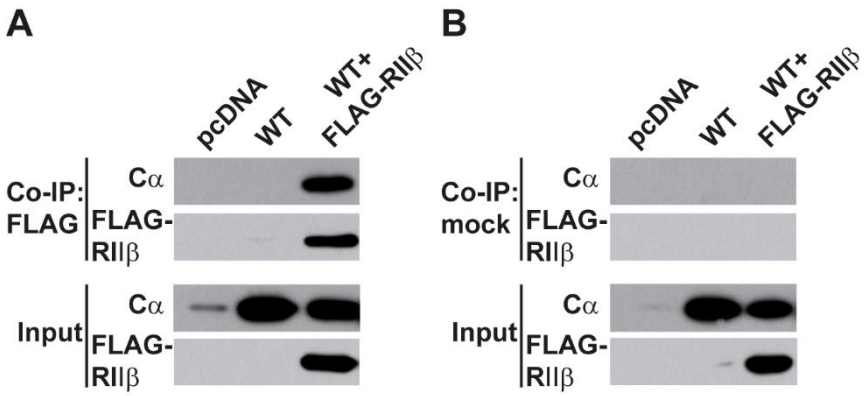

Figure 23: Setup of co-immunoprecipitation (Co-IP) experiment. HEK293A cells were transfected with empty vector (pcDNA), wild-type (WT) Cα subunit or FLAG-tagged RIIβ and wild-type (WT) Cα subunit. The association between Cα and R subunits was investigated by Co-IP using an anti-FLAG antibody followed by detection of the co-precipitated Cα subunits using antibodies specific against the Cα subunit. Controls for specific Co-IP using mock transfection (empty vector pcDNA and a sample without FLAG-RIIβ) (A) and a mock Co-IP (using beads without bound antibody) (B). Modified from Calebiro *et al.*[146].

This demonstrated the specificity of this experimental setup, which was also used for the study on the mechanism of action of the L206R and 199_200insW mutants[146]. When performed with the exogenously expressed wild-type Cα subunit, I observed a robust Co-IP under basal conditions. This interaction was lost upon PKA stimulation via cAMP addition. In contrast, only

faint signals were detected for most of the Cα mutants under basal conditions, suggesting a much weaker interaction (Figure 24A-B). Except the two mutants, W197R and E32V, all mutants showed a deficiency in binding to at least one of the R subunits. The deletion mutant d244-248+E249Q was unique because it showed a normal binding to RIIβ but a complete lack of binding to RIα (Figure 24A-B). Post cAMP stimulation, the formed holoenzymes were able to dissociate in nearly all cases. Only, the S213R+insIILR mutant which showed under basal conditions an interaction to RIIβ of 50% of the wild-type Cα did not dissociate from the holoenzyme after cAMP stimulation.

These experiments showed that formation of a stable holoenzyme is impaired for most of the mutants, but not for all. Additionally, this impairment can be specific for one R subunit, as shown by the d244-248+E249Q mutant, where just the binding to RIα is disrupted.

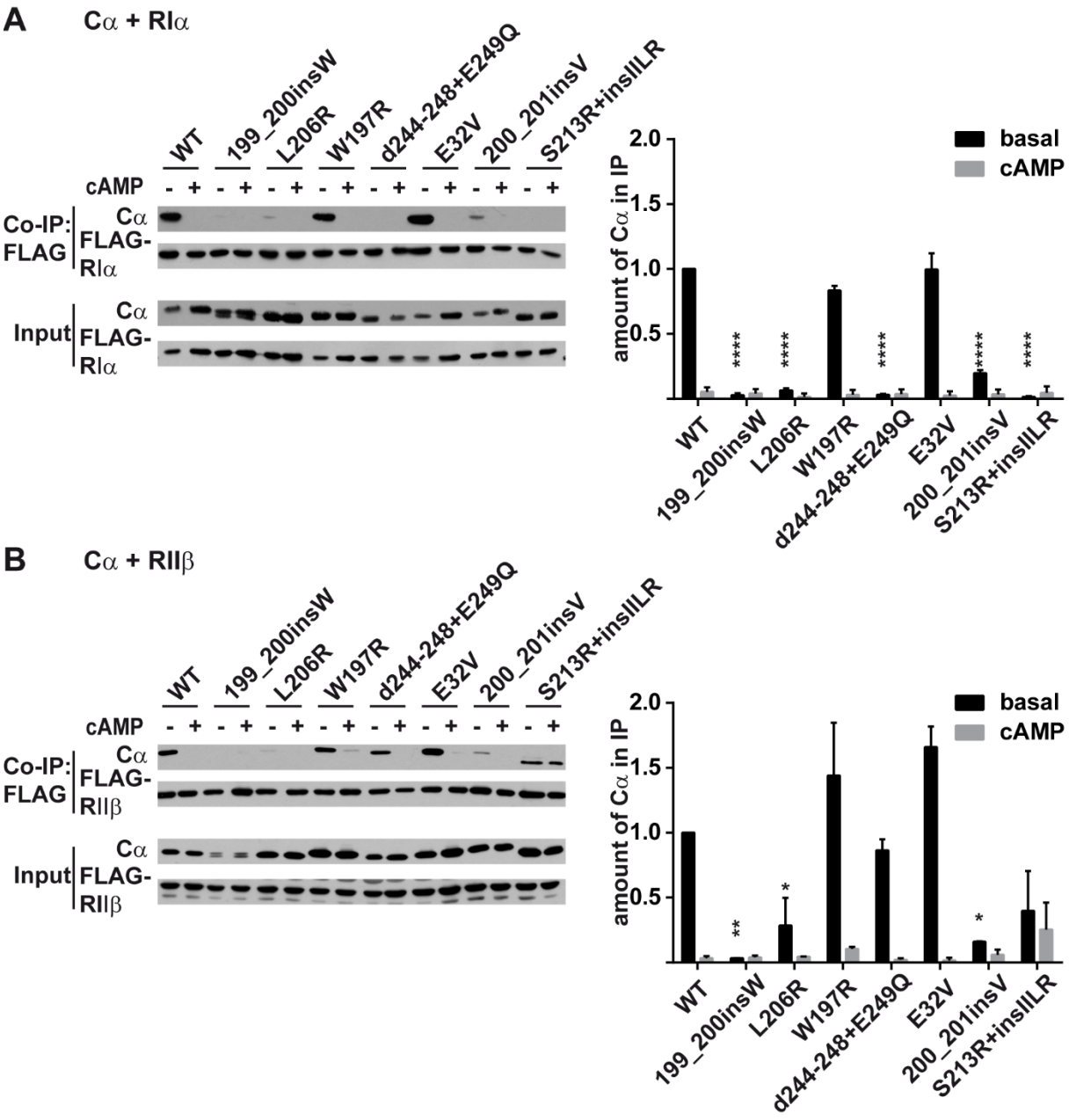

Figure 24: Effect of *PRKACA* mutations on the association between Cα with R subunits. HEK293A cells were co-transfected with FLAG-tagged RIα (A) or RIIβ (B) and either wild-type (WT) or mutant Cα subunits. The association between Cα and R subunits was investigated by Co-IP, with and without addition of 200 μM cAMP, using an anti-FLAG antibody followed by detection of the co-precipitated Cα subunits using antibody specific against the Cα subunit. Shown are Representative western blots (left) and quantitative analysis of three independent experiments (right). Therefore, intensities of Cα bands in Co-IP western blots were quantified and normalized to the wild-type sample. Data are mean ± s.e.m. of three independent experiments. Differences are statistically significant by two-way ANOVA. *P<0.05, **P<0.01 and ****P<0.0001 vs. WT basal by Bonferroni´s post hoc test.

4.2 Activity of PKA Cα mutants

Next, I investigated the activity of the PKA Cα mutants using a kemptide assay. This assay measures the phosphorylation of an artificial PKA substrate (kemptide) to analyze the activity of the PKA Cα subunit[182]. For this, I co-transfected HEK293A cells with RIIβ or RIα and either wild-type or mutant Cα subunit. Then I prepared membrane-free cell lysates and used them directly in the kemptide assay to investigate the activity of the Cα subunits (Figure 25) under basal and stimulated (in the presence of 40 μM cAMP) condition. The activity of the wild-type and mutant Cα subunits in combination with RIα showed a higher basal level than in combination with RIIβ. Besides this, the results showed that the Cα mutants can be divided in three groups. Most of the mutants were activating and showed partial to full constitutive activity (199_200insW, L206R, W197R, d244-248+E249Q, S213R+insIILR), one mutant behaved like the wild-type C subunit (E32V) and one mutant comprised an inactivating mutation (200_201insV).

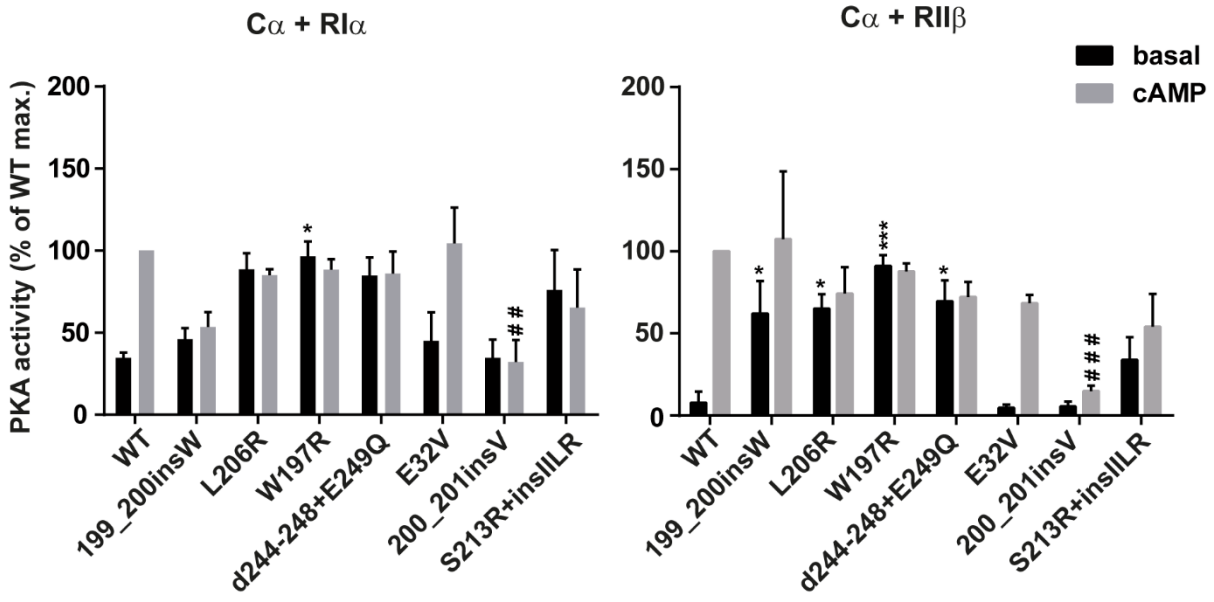

Figure 25: Effect of *PRKACA* mutations on PKA activity on the artificial substrate kemptide. HEK293A cells were co-transfected with RIα or RIIβ and either wild-type (WT) or mutant Cα subunits. PKA activity in cell lysates was then measured by kemptide assay with or without addition of 40 μM cAMP. Data are mean ± s.e.m. of three independent experiments. Data are statistically significant by two-way ANOVA. *P<0.05, ***P<0.001 vs. WT basal and ##P<0.01, ###P<0.001 vs. WT stimulated by Bonferroni´s post hoc test. Endogenous activity was subtracted from the values.

Due to the interference with the binding of the R subunit of some mutations (section 4.1), I tested whether a peptide, designed from the endogenous PKA inhibitor PKI, is capable to inhibit PKA activity. As shown in figure 26, the mutants are still inhibited by the peptide. Even though the S213R+insIILR retains some activity.

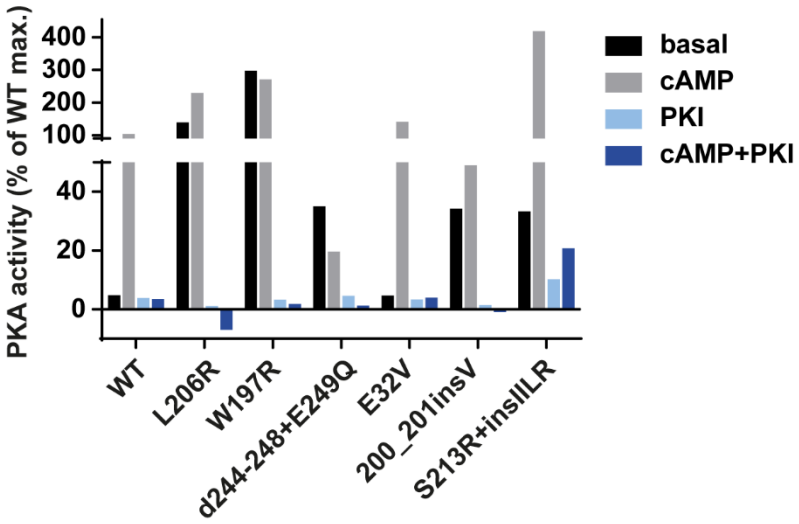

Figure 26: Inhibition of PKA Cα mutants by PKI (6-22 amide). HEK293A cells were co-transfected with RIIβ and either wild-type (WT) or mutant Cα subunits. PKA activity in cell lysates was then measured by kemptide assay with or without addition of 40 μM cAMP and/or 15 μM PKI. Data are of one single experiment.

In addition to the artificial substrate, I also investigated the effect of the mutation on endogenous PKA substrates. Therefore, I transfected HEK293A cells, as described, for the kemptide assay and prepared total cell lysates of these cells under basal and stimulated (cells were stimulated with 10 μM forskolin for 30 min before lysis) condition. The phosphorylated PKA substrates were then analyzed using western blot analysis with an anti-phospho-PKA substrate antibody (Figure 27). As for the kemptide assay, RIα was not capable to efficiently inhibit the activity of exogenous wild-type or mutant Cα subunits, which is reflected by the high basal level of the wild-type Cα activity. Also, in this assay not all the mutants showed constitutive activity. The highest basal activity was observed for the 199_200insW, L206R and d244-248+E249Q mutants. The remaining mutants showed a variable, but mainly low degree of increased basal activity compared to wild-type Cα. The results also showed that, contrary to the kemptide assay, the 200_201insV mutant could be stimulated. Additionally, the S213R+insIILR mutant is inactive in respect to endogenous substrates, whereas it showed constitutive activity in the kemptide assay.

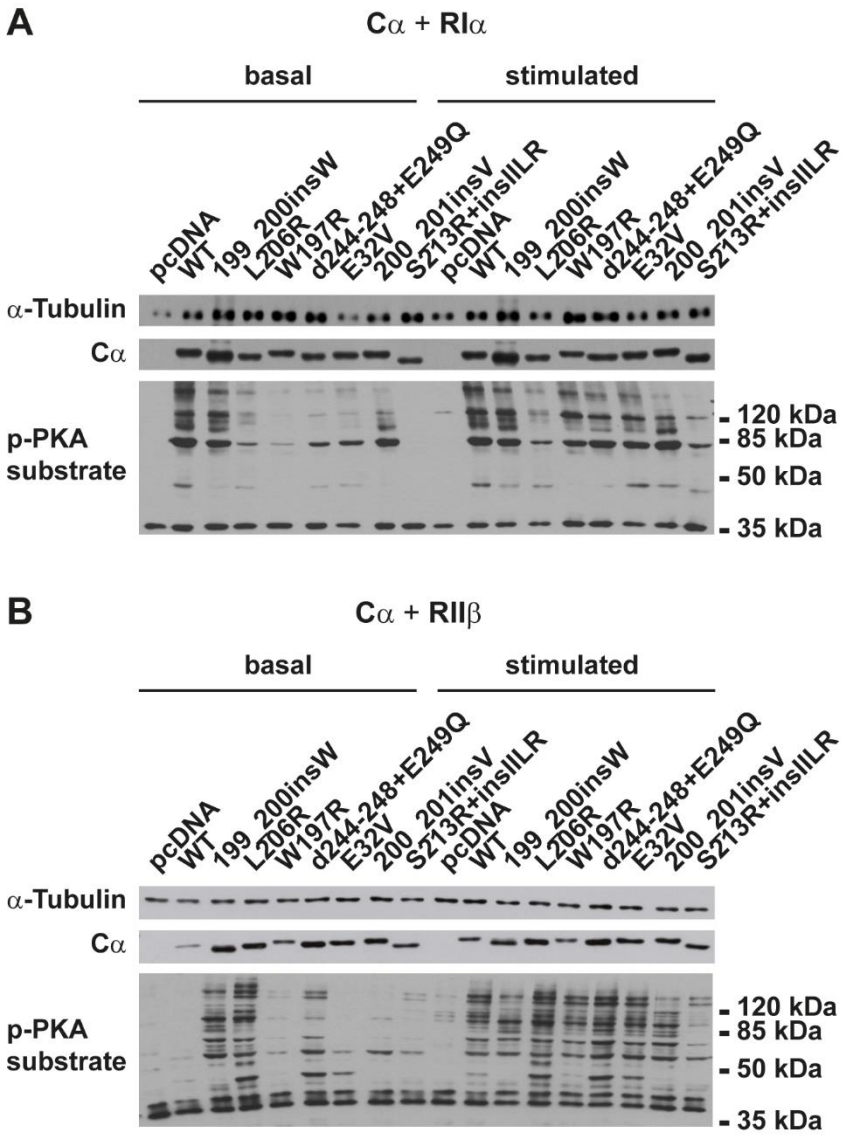

Figure 27: Effect of *PRKACA* mutations on PKA activity on endogenous PKA substrates. HEK293A cells were co-transfected with RIα (A) or RIIβ (B) and either wild-type (WT) or mutant Cα subunits. Representative western blots showing PKA activity based an antibody detecting phosphorylated PKA substrates under basal and stimulated (10 μM forskolin, 30min) condition.

These experiments revealed that not all mutants cause constitutive activity of PKA. Interestingly there were also discrepancies between the results of the two assays used (phosphorylation of kemptide and of endogenous PKA substrates) suggesting also a change in substrate specificity of the PKA Cα mutants.

4.3 Substrate specificity of PKA Cα mutants

While analyzing PKA activity (see 4.2), I discovered differences in the phosphorylation patterns generated by the PKA Cα mutants in HEK293A cells. An expanded view of figure 27A revealing these differences is shown in figure 28. Compared to the wild-type PKA Cα, the Cα mutants showed differences in phosphorylation patterns of phosphorylated PKA substrates. This indicated that the substrate specificity of the PKA Cα mutants could be changed due to the location of the mutations near the active site of the kinase.

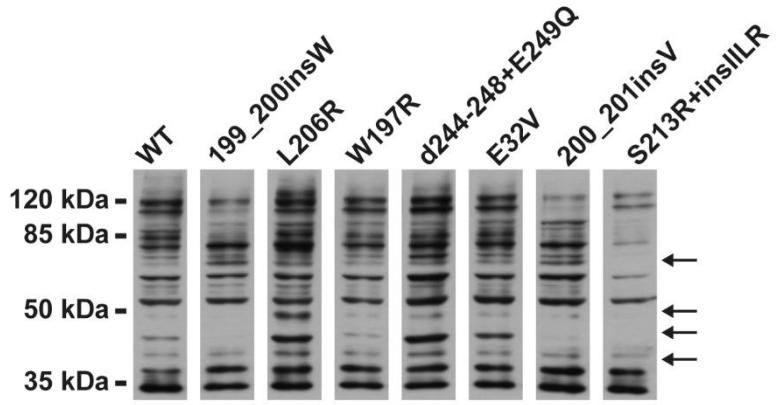

Figure 28: Differences in phosphorylation patterns among PKA Cα mutants. Shown is an expanded view of the corresponding lanes from figure 27B upon stimulation. Arrows indicate bands of phosphorylated PKA substrates with different intensities in the different samples.

To further characterize this phenomenon, I first analyzed two known PKA substrates and one downstream effector for their phosphorylation by PKA Cα mutants by western blot analysis. The β-catenin pathway is a major pathway involved in adrenal tumorigenesis[183, 184, 185] and was shown to have an important role in many malignancies[186]. Therefore, this pathway was of particular interest and I decided to test the PKA substrates CREB (phosphorylated by PKA at serine 133) [17] and glycogen synthase kinase 3 alpha (phosphorylated by PKA at serine 21) and beta (phosphorylated by PKA at serine 9) (α/β-GSK)[187]. As down-stream effector, I chose β-catenin, which is phosphorylated (at threonine 41, serine 37 and serine 33) by α/β-GSK[188]. Just minor differences could be detected in the phosphorylation of α and β-GSK by the PKA Cα mutants under basal and stimulated condition. For the other tested substrates virtually no differences were detected (Figure 29).

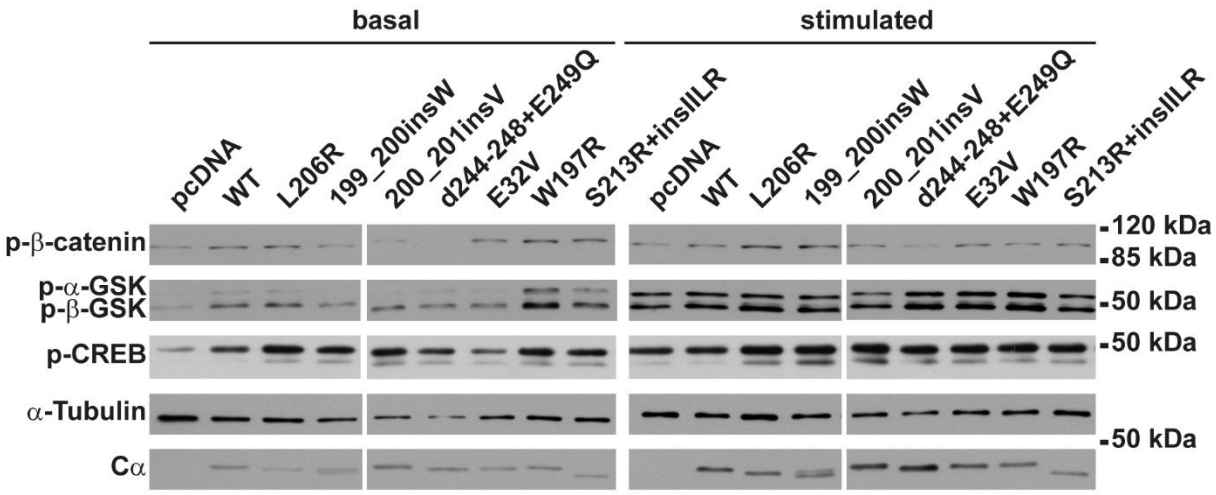

Figure 29: Effect of *PRKACA* mutations on phosphorylation of known PKA substrates. HEK293A cells were co-transfected with RIIβ and either wild-type (WT) or mutant Cα subunits. Lysates were analyzed by western blot for phosphorylation of substrates under basal and stimulated (10 μM forskolin for 30min) conditions. Representative western blots (of two experiments) showing phosphorylated CREB, β-catenin and α/β-GSK.

4.3.1 *In silico* prediction of substrate specificity

To investigate the substrate specificity in more detail, I did an *in silico* prediction of substrate specificity (Figure 30) using the Kinase Substrate Prediction v 2.0 algorithm (Kinexus)[180]. This algorithm predicts the substrate specificity of the PKA Cα wild-type and mutants based on their primary amino acid sequence by comparison to known human protein kinase catalytic domains and kinase–substrate phosphosite pairs. The algorithm compares computed specificity matrices for the wild-type and mutant PKA Cα, where values indicate the relative preference for each amino acid at each position around the phosphoacceptor site of the substrate. This algorithm predicted that the strongest effect on substrate specificity is expected for the d244-248+E249Q mutant. According to the prediction, the requirement for the amino acid residues of the consensus sequence of PKA (RRXS/T) was reduced for this mutant. In addition, the recognition of substrates that feature proline, serine or glutamic acid around the phosphoacceptor site (position 0) was increased.

The L206R mutant was predicted to just have an effect on the preference for amino acids in the +1 position of the substrate. The algorithm anticipated a reduced requirement for a hydrophobic amino acid and an increased preference for a proline residue at the +1 position of the substrate peptide.

The two insertion mutants (199_200insW, 200_201insV) gave similar results. Both were predicted to increase the recognition of phenylalanine at the -6 position. Additionally, they were predicted to increase the requirement for a valine and in turn decrease the requirement for a phenylalanine at position +1. Additionally, to the serine and threonine residues phosphorylated by wild-type PKA Cα, these mutants interestingly may be able to recognize tyrosine residue at the phosphoacceptor site.

For the S213R+insIILR mutant the algorithm predicted relatively little effects on the substrate specificity and for the two remaining mutants (E32W, W197R) no changes were predicted.

The prediction highlighted relevant changes in substrate specificity for four mutants (199_200insW, L206R, d244-248+E249Q and 200_201insV), a minor effect on substrate specificity for the S213R+insIILR mutant and no effect on substrate specificity for two mutants (W197R and E32V).

L206R

Position	Amino Acid	WT	L206R	Change
1	F	30.4	25.9	-4.5
1	L	21.5	15.9	-5.7
1	P	-4.1	8.7	12.8

199_200insW

Position	Amino Acid	WT	199_200 insW	Change
-6	F	0.6	5.9	5.3
-5	L	5.5	12.3	6.8
-5	R	56.9	41.0	-15.9
-3	R	109.3	90.7	-18.6
-2	D	-5.2	0.0	5.2
-2	R	76.3	56.7	-19.6
0	S	165.4	148.7	-16.7
0	Y	0.5	8.6	8.2
1	F	30.4	20.1	-10.3
1	L	21.5	14.5	-7.0
1	V	6.6	20.2	13.6

200_201insV

Position	Amino Acid	WT	200_201 insV	Change
-6	F	0.6	5.9	5.3
-5	L	5.5	12.3	6.8
-5	R	56.9	41.0	-15.9
-3	R	109.3	91.6	-17.6
-2	D	-5.2	0.0	5.2
-2	R	76.3	57.6	-18.7
0	S	165.4	149.9	-15.4
0	Y	0.5	8.6	8.1
1	F	30.4	20.1	-10.3
1	L	21.5	14.5	-7.0
1	V	6.6	20.2	13.6

S213R+insIILR

Position	Amino Acid	WT	S213R +insIILR	Change
-4	P	-5.9	-2.7	3.1
5	P	5.2	2.0	-3.2

d244-248+E249Q

Position	Amino Acid	WT	d244-248 +E249Q	Change
-6	E	-4.3	4.6	8.9
-6	S	5.3	13.7	8.5
-5	E	-8.0	2.3	10.4
-5	P	-4.5	4.6	9.1
-5	R	56.9	36.2	-20.8
-5	S	-11.1	4.1	15.2
-4	E	0.8	9.9	9.2
-4	P	-5.9	3.8	9.6
-3	E	-9.1	1.8	10.8
-3	L	-6.6	2.6	9.2
-3	P	-8.0	2.5	10.5
-3	R	109.3	56.9	-52.4
-3	S	-10.7	4.5	15.2
-2	E	-6.6	2.0	8.7
-2	P	-8.6	2.2	10.8
-2	R	76.3	44.0	-32.3
-2	S	1.3	13.6	12.2
-1	E	-3.9	5.0	8.9
-1	P	-4.0	5.0	9.0
-1	S	-0.1	11.6	11.7
0	S	165.4	82.3	-83.1
1	E	-6.7	3.1	9.9
1	F	30.4	21.5	-8.8
1	S	-4.2	8.3	12.5
2	E	-3.8	5.4	9.2
3	S	7.0	17.1	10.1
4	E	-5.2	4.1	9.3
4	P	-5.2	4.2	9.4
5	E	-1.7	7.5	9.2
6	E	-4.7	4.4	9.1
6	P	-4.8	4.5	9.2
6	S	6.3	16.3	10.0
7	E	-7.8	2.5	10.3
7	P	-6.9	3.8	10.8
7	S	2.2	13.9	11.7

decreased requirement | no change | increased requirement

Figure 30: *In silico* prediction of substrate specificity changes caused by *PRKACA* mutations. Shown are only relevant changes with respect to wild-type PKA Cα. The prediction was done using the Kinase Substrate Prediction v 2.0 algorithm (Kinexus)[180].

4.3.2 In vitro investigation of substrate specificity by phosphoproteomics

To prove if the *in silico* predictions were correct I performed phosphoproteomics experiments for some mutants. For this experiment I chose the most frequent L206R mutant, the d244-248+E249Q mutant which was predicted to have the strongest effect on substrate specificity and the 200_201insV mutant which was predicted to have similar effects like the 199_200insW mutant. The 200_201insV was of more interest than the 199_200insW due to the fact that there was a significant difference between the results of the kemptide activity assay (Figure 25), where it was found to be inactive, and the immunoblot analysis, showing an increase in phosphorylation upon stimulation (Figure 27).

For the phosphoproteomics experiment, HEK293A cells were SILAC labeled. To check for complete incorporation of the heavy and light amino acids, a sample of untransfected cells was lysed after 6 passages in the SILAC medium and analyzed by mass spectrometry. This showed that incorporation was complete. Cells were then co-transfected with RIIβ and either wild-type or mutant Cα subunits for 48 h and lysed after stimulation (10 μM forskolin for 30 min) to reach maximal PKA activity. Proteins were then proteolytically digested and peptides were purified and analyzed by nanoLC-MS/MS. This experiment was done in biological triplicates. The results (Figure 31) showed that all three tested mutations influence substrate specificity. This included 62, 116 and 75 substrates that were either hypo- or hyperphosphorylated by the L206R, d244-248+E249Q and 200_201insV mutant, respectively. Clear differences were visible between the mutants. Just four substrates were hyperphosphorylated compared to wild-type by all three mutants: citron rho-interacting kinase (CIT) at serine 480, mitochondrial import receptor subunit TOM34 at serine 93, histone H1.4 at serine 36 and histone H1.2 at serine 36 (Figure 31). Even though the mutants showed unique effects on phosphorylation of many substrates, phosphorylation of some substrates was affected equally for two mutants. Most analogies were observed for the d244-248+E249Q and the 200_201insV mutants, which had a similar effect on 28 substrates. Less similarities were seen for the L206R and the d244-248+E249Q mutants which shared the effect on 13 substrates and the L206R and the 200_201insV mutants which similarly affected 6 substrates. Interestingly several substrates were found hypophosphorylated by one mutant and hyperphosphorylated by another mutant. Most differences were observed between the d244-248+E249Q and the 200_201insV mutants with 17 conversely affected substrates. An opposite effect on phosphorylation of 6 or 5 substrates was shown for the L206R and the d244-248+E249Q or the 200_201insV mutants respectively. This highlights that every mutation has a specific effect on the substrate specificity of PKA Cα. Importantly, the substrates identified to be affected by a change in substrate

specificity of the mutants, were also found in lysates of the adrenal carcinoma cell line NCI-H295R.

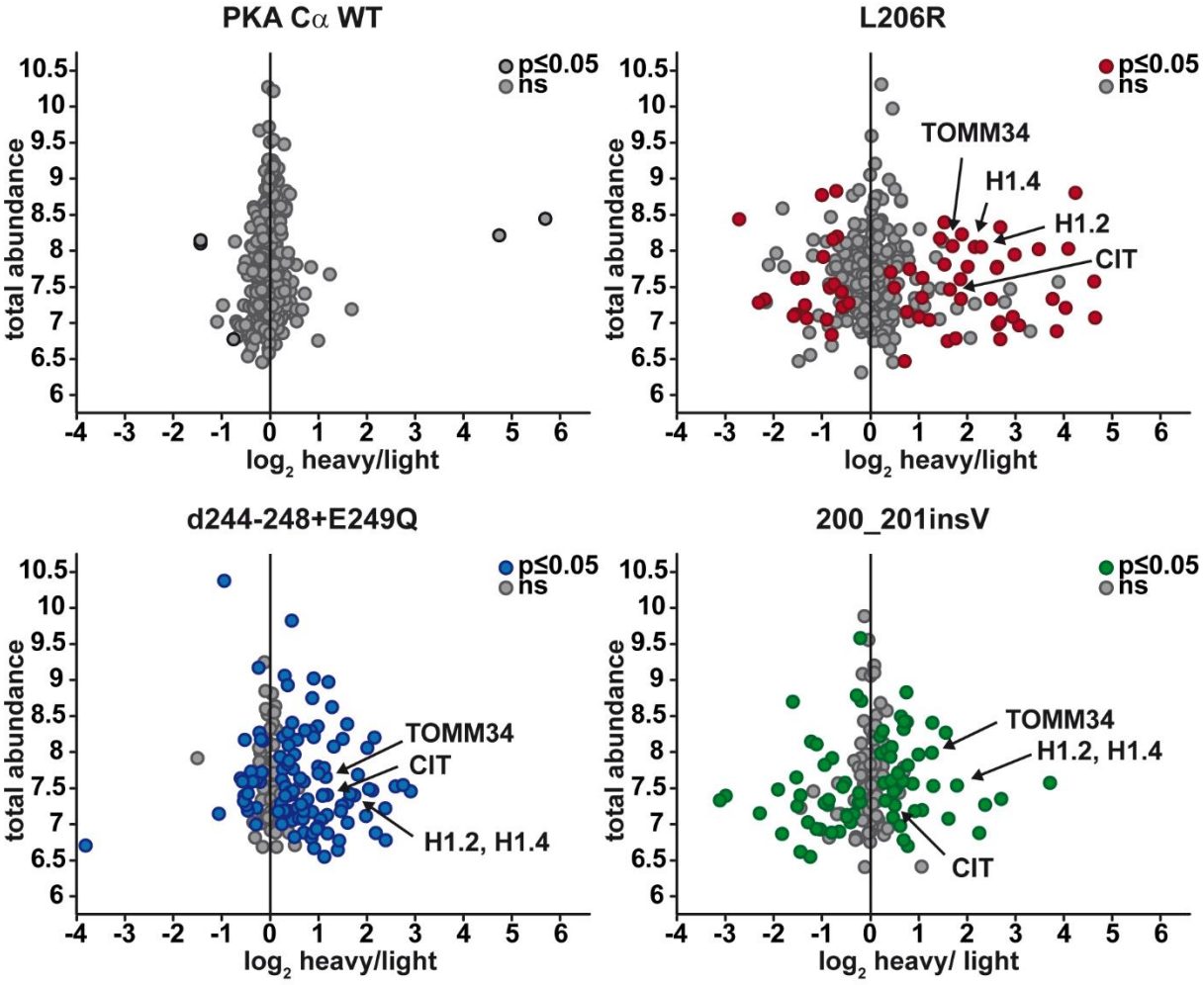

Figure 31: *PRKACA* mutations affect substrate specificity as revealed by phosphoproteomics analysis. HEK293A cells were co-transfected with RIIβ and either wild-type (WT) or mutant Cα subunits and labeled with light amino acids (WT) or heavy amino acids (mutant). Phosphopeptides were pulled down using a phospho-PKA substrate antibody recognizing the RRXpS/T consensus and analyzed by nanoLC-MS/MS. Depicted are scatter plots showing the abundance of the phosphopeptides in the mutant (heavy) relative to wild-type (light) samples of three independent experiments. Phosphopeptides to the right are preferred by the mutant and phosphopeptides shifted to the left are preferred by wild-type PKA Cα. Significantly hypo- or hyperphosphorylated peptides by the mutant are colored.

The sequences of these hypo- or hyperphosphorylated peptides were used to compute sequence logos for each tested PKA Cα mutant (Figure 32). These logos represent the probability of an amino acid at a given position in the substrate with respect to the total human proteome as background. Here, the amino acids above and below the x-axis represent over- and underrepresented amino acids, respectively. Additionally, the letter size of the amino acids corresponds to the relative frequency of this amino acid in this position. Both, the logos of hypo- and hyperphosphorylated peptide sequences, show relevant changes in comparison to the wild-type. For the L206R mutant, the logos revealed a reduction in the preference for a hydrophobic amino acid at the +1 position except for leucine and a strong acidic preference at the +2 position for the L206R mutant. The strongest effect was detected for the d244-248+E249Q as predicted by the *in silico* analysis. As predicted, the requirement for a phenylalanine at the +1 position was reduced. In contrast to the predicted increase of a glutamate or serine residue in this position, an increased requirement for valine was observed. The changes in the consensus sequence for the 200_201insV were not that striking. As predicted, there was a reduction for the requirement of a phenylalanine and an increase for a requirement of valine in the +1 position. Interestingly I also observed an increased requirement for proline at position +3. All these observations were in line for both hypo- and hyperphosphorlyated sequence logos. Therefore, if an increased preference for a specific amino acid in a position was observed in the hyperphosphorylated logo, a decreased preference of this amino acid in the same position was seen in the hypophosphorylated logo. This correlation was not observed for the preference for arginine in position -1 and the positions -7 until -4 for all the mutants, which was reduced for hyper- and hypophosphorylated peptides.

These results showed that the three tested mutants (L206R, the 200_201insV and the d244-248+E249Q), as predicted, have a major effect on the substrate specificity of PKA Cα. This leads to increased or decreased phosphorylation of specific PKA substrates.

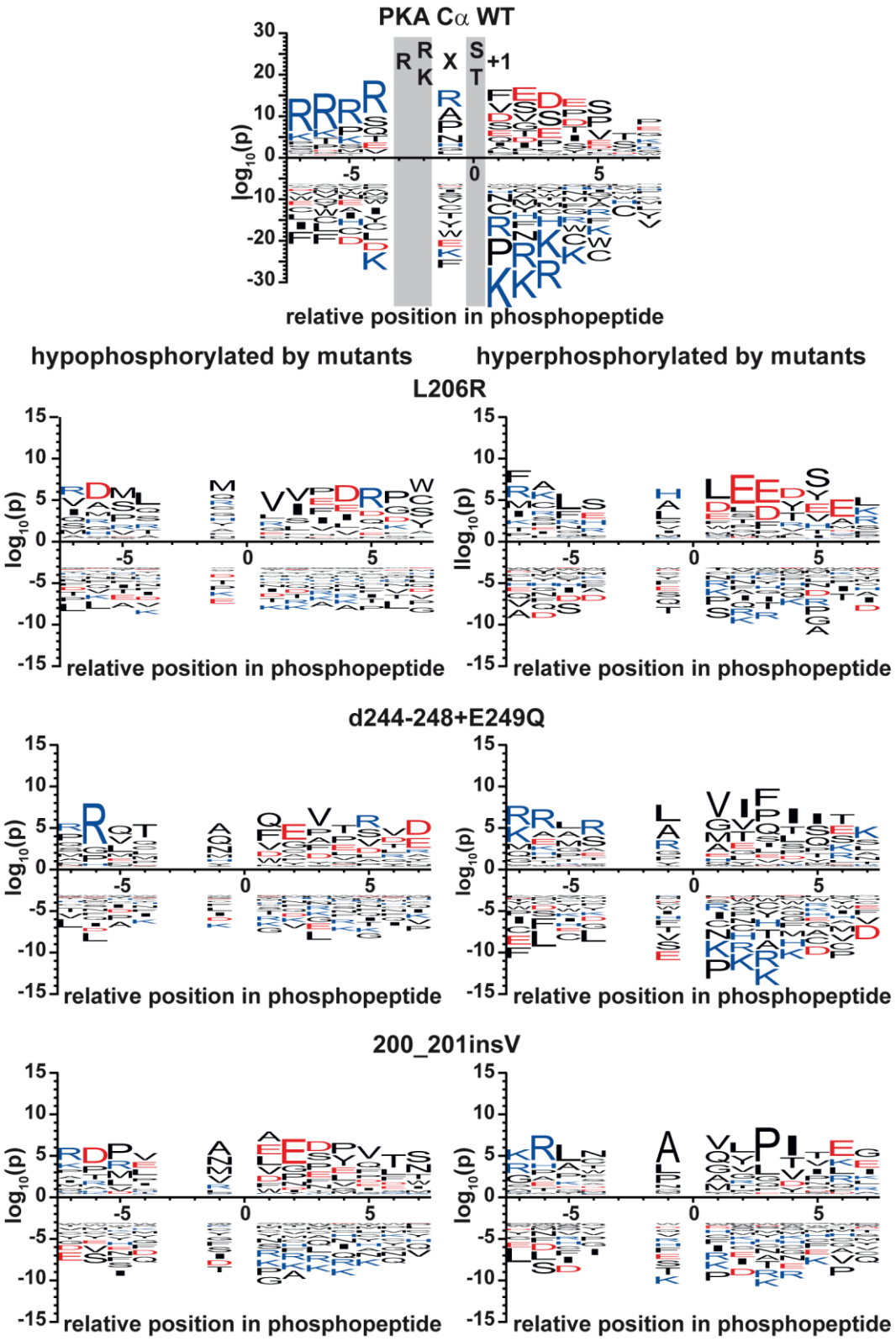

Figure 32: Sequence logos reporting the relative amino acid preferences around the consensus motif (RRXpS/T). Phosphosubstrates found in the phosphoproteomics experiment to be hypo- (left) and hyperphosphorylated (right) by the mutant were analyzed using pLogo. The size of the letters (y-axis), each corresponding to an amino acid, indicate their frequency relative to the total human proteome at a given position (x-axis). Values are represented as $\log_{10}$-odds of the significance of overrepresentation versus the significance of underrepresentation, which are calculated using the binomial probability of the residue frequency.

4.3.3 Histone H1.4 and H1.2 phosphorylation

Interestingly, two (of the total four) substrates hyperphosphorylated by the three mutants were histones. Therefore, to validate the phosphoproteomics results, I analyzed the phosphorylation of these histones in HEK293A cells co-transfected with RIIβ and either wild-type or mutant PKA Cα and in CPA tissue harboring the *PRKACA* L206R and d244-248+E249Q mutation. For this purpose, I acid extracted histones from these transfected cells as well as patient tumor samples and analyzed the purified histones by western blot analysis. Unfortunately, a phosphosite-specific antibody was available only for histone H1.4 and not for H1.2.

The results of the HEK293A cells confirmed the phosphoproteomics data (Figure 33A). Under stimulated condition, the L206R mutant showed significant hyperphosphorylation of H1.4 Ser36. The d244-248+E249Q and the 200_201insV mutant just showed a tendency to hyperphosphorylate H1.4 at serine 36. Interestingly, in basal state, only the L206R mutant showed hyperphosphorylation of H1.4 at serine 36. The results of the CPA tumor samples (Figure 33B) showed that in L206R mutated samples, H1.4 at serine 36 is significantly more phosphorylated than in wild-type tumors, which is in line with the observation under basal condition in HEK293A cells. For the d244-248+E249Q mutant, phosphorylation of H1.4 at serine 36 was not enhanced in the tissue samples.

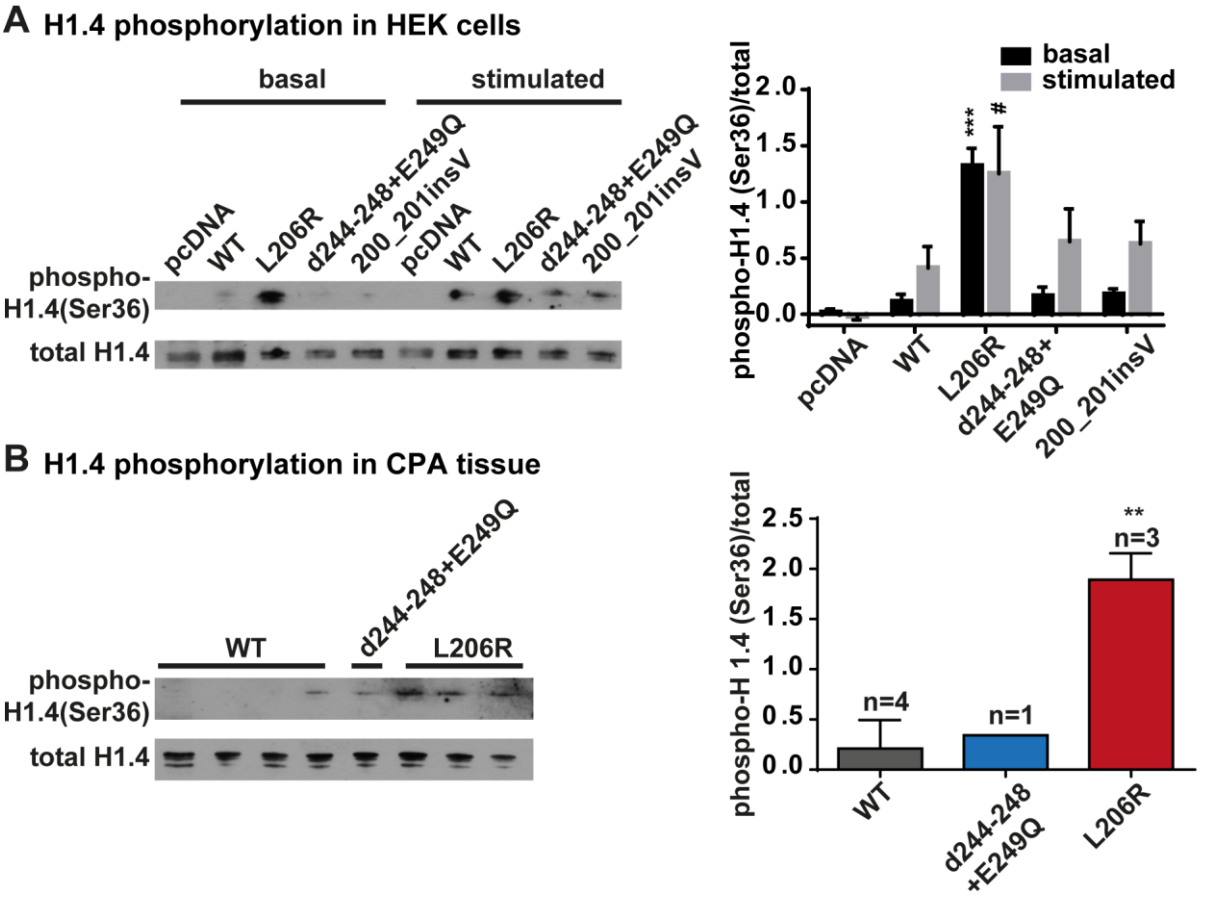

Figure 33: Effect of *PRKACA* mutation on histone H1.4 serine 36 phosphorylation. Immunoblot analysis of histone H1.4 phosphorylation in HEK293A cells transfected with PKA RIIβ and Cα mutants in basal and stimulated (10 μM forskolin for 30 min) condition (A) and tissue samples of CPAs carrying the L206R and the d244-248+E249Q *PRKACA* mutation (B). Shown are representative blots (left) and their corresponding quantification (right). Data in A are mean ± s.e.m. of three independent experiments. Differences are statistically significant by two-way ANOVA. *** P<0.001 vs. WT basal and # P<0.05 vs. WT stimulated by Bonferroni´s post hoc test. Data in B are tissue samples from different patients. Quantification is shown as mean ± s.e.m. Differences are statistically significant by Student's t-test **P<0.01 vs. WT.

Since there was no phosphosite-specific antibody available for H1.2 serine 36, I used Phos-tag gels to separate the phosphorylated and unphosphorylated H1.2. The results showed no significant increase in phosphorylation of H1.2 at serine 36 in HEK293A cells (Figure 34A). However, there was a trend that the L206R mutant hyperphosphorylates H1.2 at serine 36 under basal condition. Analysis of CPA tissue revealed that H1.2 serine 36 was more phosphorylated in *PRKACA* L206R mutated samples than by the *PRKACA* wild-type samples (Figure 34B). No difference was observed for the d244-248+E249Q mutant.

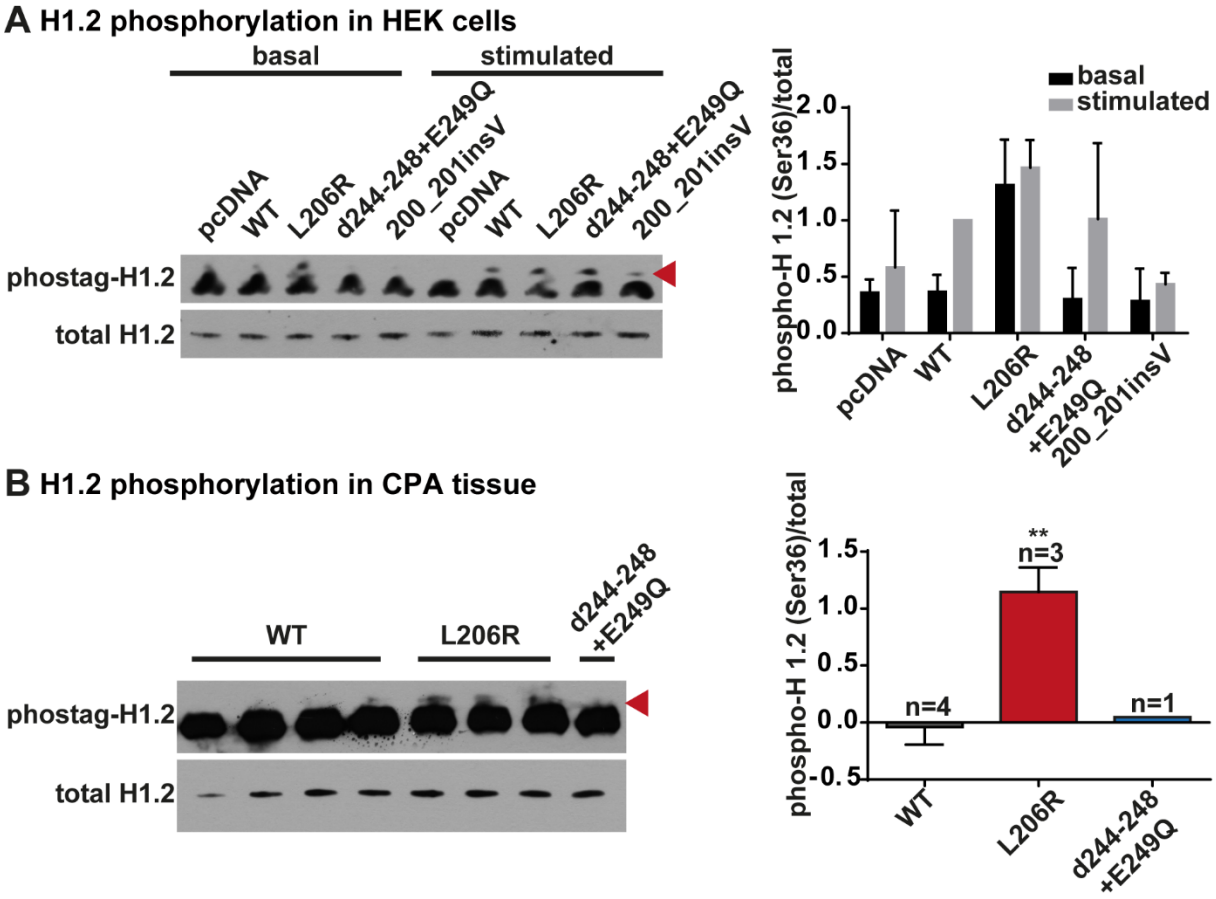

Figure 34: Effect of *PRKACA* mutation on histone H1.2 serine 36 phosphorylation. Immunoblot analysis of histone H1.2 phosphorylation at serine 36 in HEK293A cells transfected with PKA Cα mutants in basal and stimulated (10 μM forskolin for 30 min) condition (A) and tissue samples of CPAs carrying the L206R and the d244-248+E249Q *PRKACA* mutation (B). Shown are representative blots (left) with arrowheads indicating the position of the band of phosphorylated histone. The corresponding quantification is also shown (right). Data in A are mean ± s.e.m. of three independent experiments. Data in B are tissue samples from different patients. Quantification is shown as mean ± s.e.m. Differences are statistically significant by Student's t-test **P<0.01 vs. WT.

These experiments showed that the L206R mutant causes hyperphosphorylation of H1.4 and H1.2 on serine 36 in HEK293A cells and in CPA tumor tissue. The other two mutants (d244-248+E249Q and 200_201insV) showed a less prominent effect on phosphorylation of serine 36 of H1.2 and H1.4. In total hyperphosphorylation of serine 36 was more striking for H1.4.

4.3.4 TOM34 and CIT phosphorylation

In addition to the histone phosphorylation, I also investigated the two other substrates hyperphosphorylated by all three PKA Cα mutants (TOM34 and CIT) in the phosphoproteomics experiment. Therefore, I used IP to pull down TOM34 or CIT from cell lysates. I then would analyze the immunoprecipitated CIT or TOM34 for phosphorylation of the PKA motif by western blot analysis using an antibody detecting phosphorylated PKA substrates. Unfortunately, I was not able to obtain a robust IP of TOM34 (Figure 35A). Therefore, analysis of the phosphorylation status was not possible. For CIT, the IP worked, but I was not able to detect any phosphorylation in these samples (Figure 35B). Future studies will be required to confirm hyperphosphorylation of TOM34 and CIT by the PKA Cα mutants.

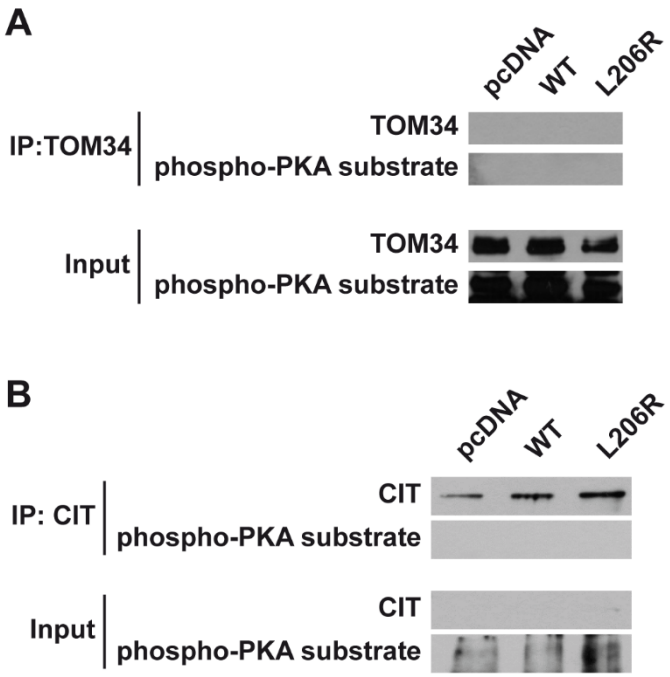

Figure 35: Immunoprecipitation of TOM34 and CIT. Immunoblot analysis of immunoprecipitated TOM34 (A) and CIT (B) in HEK293A cells transfected with PKA RIIβ and either empty vector (pcDNA), wild-type (WT) Cα or Cα L206R mutant upon stimulation (10 μM forskolin for 30 min). Shown are representative blots analyzing for the immunoprecipitated protein (TOM34 or CIT) and phosphorylation of PKA substrates.

4.4 Introduction of *PRKACA* L206R mutation in a cell line

To further study the effect of *PRKACA* mutations, we planned to generate a model for *PRKACA* mutated CPAs in the previously tested HEK293T cell line[167] as well as in a biologically relevant cell line. I decided to use the CRISPR/Cas9 system in a human adrenal cell line which is also capable of cortisol production. The only available cell line was the NCI-H295R cell line which exists as adherent and suspension cell line[189, 190]. For this purpose, I decided to generate a cell line harboring the most frequent L206R mutation.

For the generation of this cell line, I used the type II CRISPR/Cas9 system of *Streptococcus pyogenes*, which utilizes a single multi-functional protein, Cas9, for DNA targeting and degradation, guided by a natural dual-RNA heteroduplex consisting of a crRNA and a tracrRNA[176]. To set up the system, I chose a cell line which is easy to handle and was already used for modifications with CRISPR/Cas9: HEK293T[167].

I designed two guides and one repair template for both guides (Figure 21) and tested the indel efficiency for both guides, also in combination with the repair template. An indel is a random mutation as effect of a double strand break in the DNA. These indels can be detected in a surveyor assay by forming heteroduplexes of the indel and wild-type DNA. Those heteroduplexes are characterized by mismatches which can be detected by surveyor nuclease, a special enzyme that cuts at mismatches. This results in smaller DNA fragments in case of indels. As one can see in figure 36A, guide 1 was more efficient than guide 2. Therefore, I did further tests just with guide 1. I checked the efficiency of homology directed repair (HDR) of this guide in combination with the repair template (Figure 36B). This assay is based on the insertion of the repair template, which contains a silent modification coding for a cutting site for BssHII enzyme. If the repair template is inserted by HDR, digestion with BssHII reveals HDR efficiency. Here, HDR efficiency was 70% of the indel efficiency. Thus, I concluded that this guide 1-repair template pair was functional.

The next step was to obtain a clonal cell line from HEK293T cells to be sure that all cells have the same desired *PRKACA* L206R mutation. Due to the GFP-tagged SpCas9 construct, I was able to eliminate untransfected cells and to pick single cells by fluorescence activated cell sorting (FACS). Those single cells were cultured and tested if the repair template was inserted by BssHII digestion (Figure 37). I was able to show insertion of the repair template - in 2 cases just partially – in 20.5% of the single cell clones. Those clonal cell lines were cultured further.

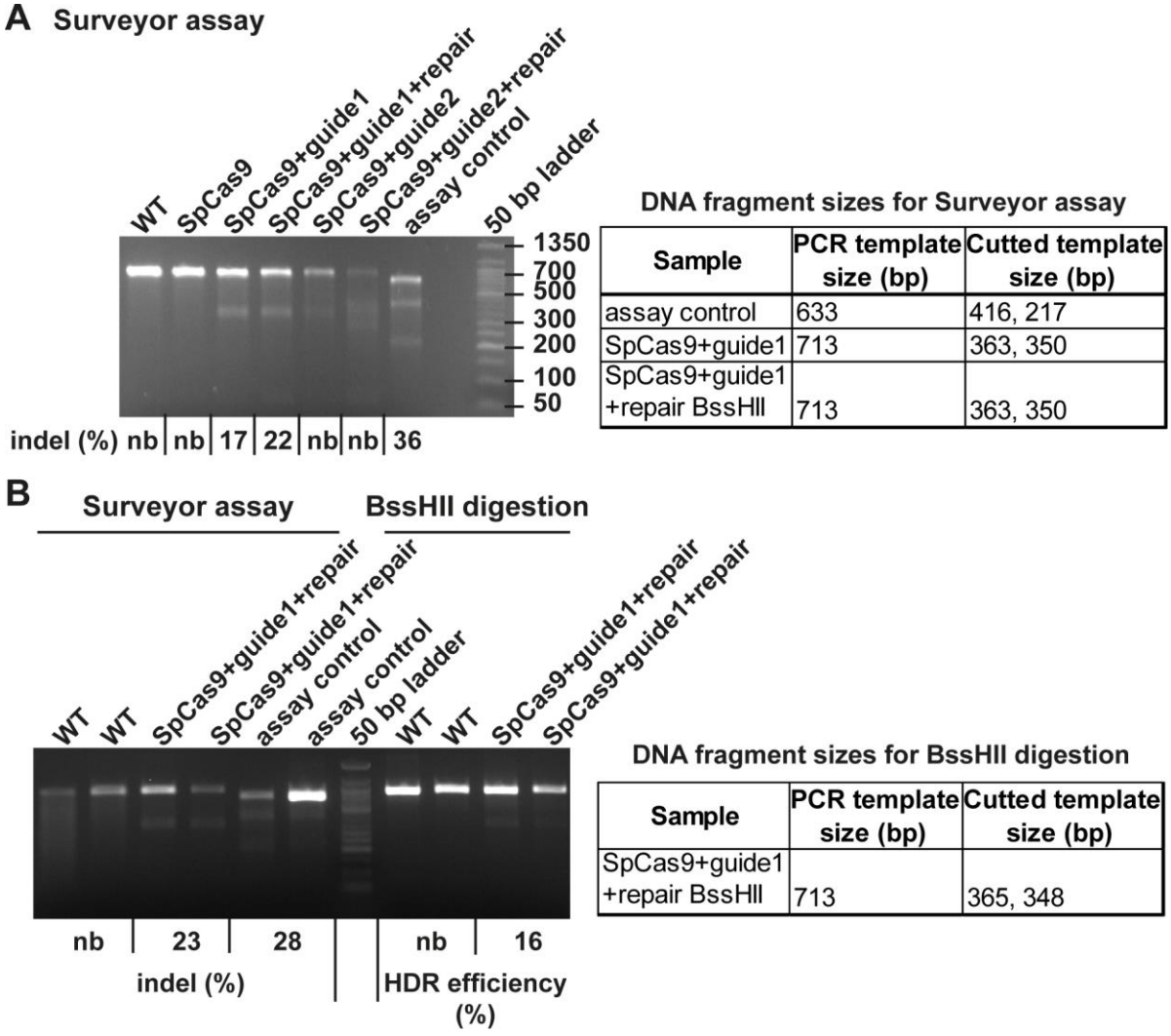

Figure 36: Cutting efficiency of guides. HEK293T cells were either non-transfected (WT), transfected with a plasmid encoding the SpCas9, co-transfected with the SpCas9 and a guide or co-transfected with a plasmid encoding for the SpCas9 and guide 1 and the repair template. Guides were tested for their indel efficiency by Surveyor (A) and indel efficiency was compared to HDR efficiency of the guide by BssHII digestion (B).

To be sure about the correct insertion of the repair template, I sequenced the region around the *PRKACA* L206R modification. An example (clone 49) for a positive, homozygous insertion is shown in figure 38A. Additionally I also checked the three most likely off-targets of guide 1 for modifications. The results for the homozygous clone 49 are shown in figure 38B-D. These show no modifications in the off-target regions. Additionally, a whole exome sequencing for *PRKACA* was performed by Dr. Sabine Herterich (Zentrallabor University Hospital Würzburg) to prove the preliminary sequencing results. These data did not show any other mutation in *PRKACA* additional to the mutation at the target locus in *PRKACA*.

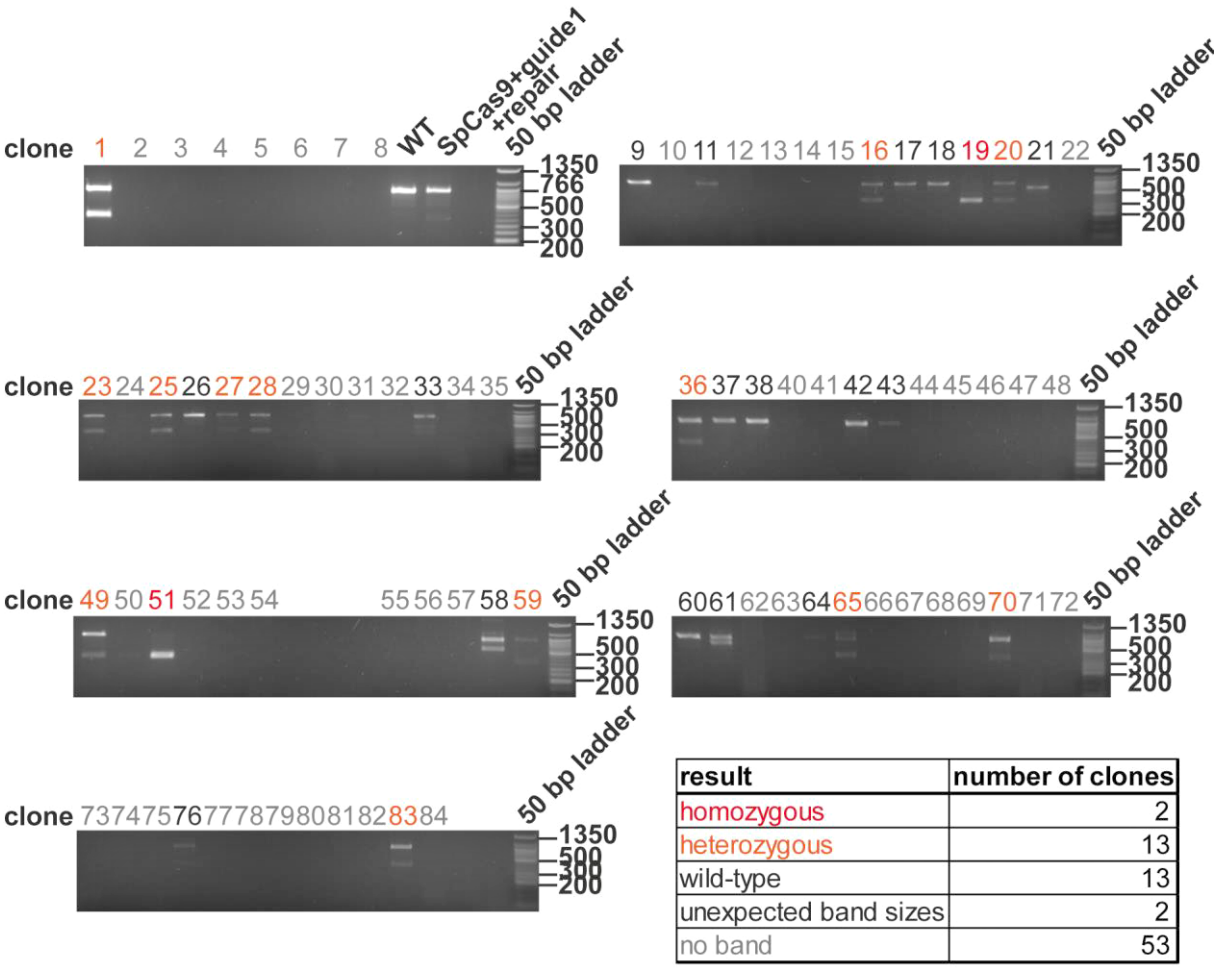

result	number of clones
homozygous	2
heterozygous	13
wild-type	13
unexpected band sizes	2
no band	53

Figure 37: HDR analysis of HEK293T single clones. HEK293T cells were co-transfected with the repair template and a plasmid encoding for SpCas9 and guide1. After FACS the resulting single cells were cultured and analyzed for efficient repair template insertion by BssHII digestion of the PCR product of the target region.

In table 10, all results for the clonal cell lines are summarized. I was able to generate two cell lines (clone 23 and 49) harboring the L206R mutation homozygous. Interestingly clone 23 harbors the BssHII cutting site heterozygous, indicating a partial repair template insertion. A cell line harboring the *PRKACA* L206R mutation heterozygous was not obtained. Off-target effects of the guide were detected in 5 out of 9 tested clones. For further experiments, the homozygous clone 49 was used.

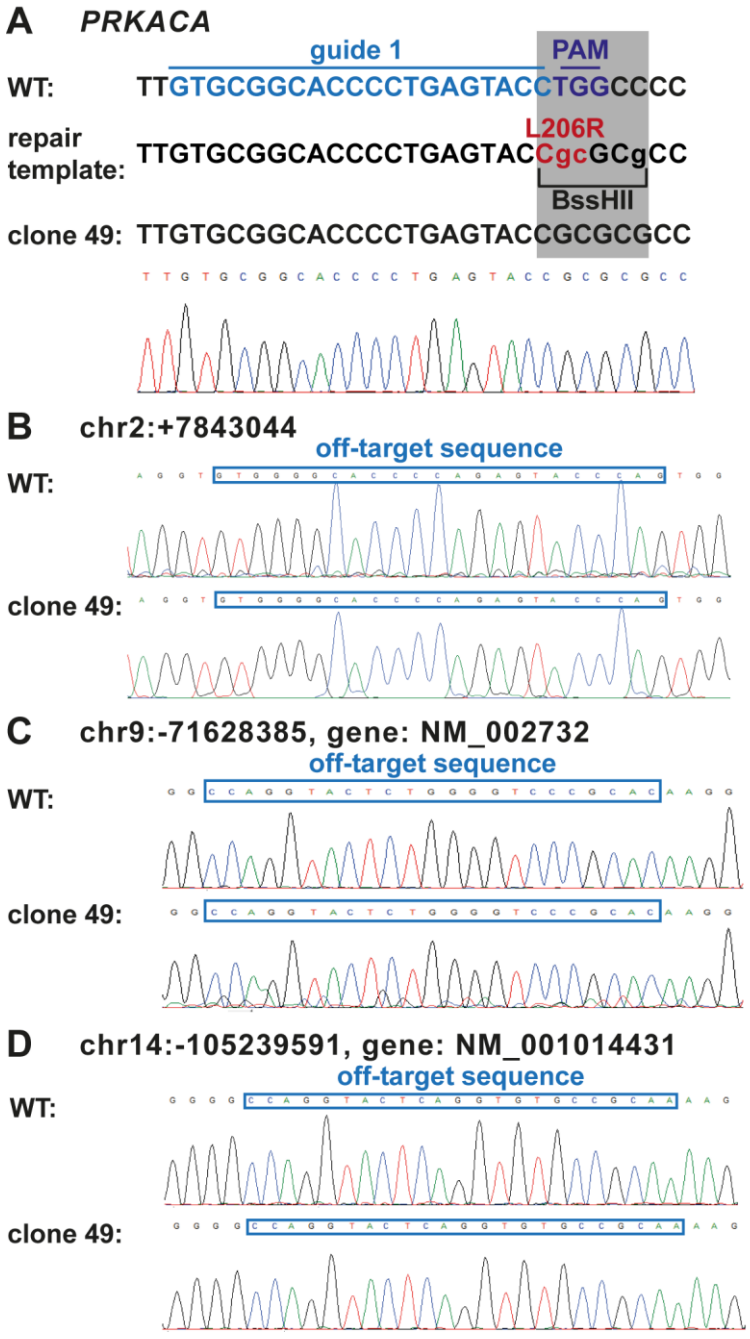

Figure 38: Sequencing of clone 49. DNA is extracted from a 10 cm plate of clone 49 and PCR was run for the target gene (A) and three off-target genes (B-D). The PCR templates were sequenced. Shown are comparisons between wild-type cell and clone 49. The mutation was inserted homozygous in the target gene (A). All analyzed off-targets were not affected (B-D).

Table 10: Summary of results for BssHII digestion, sequencing of target and off-target genes and whole exome sequencing of *PRKACA*.

Clone	BssHII digestion	Sequencing of target locus	Off-targets	*PRKACA* whole exome sequencing
1	heterozygous	indel	chr9 overlaying sequences	x
16	heterozygous	clone lost		
9	homozygous	heterozygous, low signal	ok	x
20	heterozygous	indel	chr9 3 base pair-exchanges	x
23	heterozygous	homozygous L206R, heterozygous BssHII	Chr 9 low signal, high noise	homozygous L206R, heterozygous BssHII
25	heterozygous	heterozygous	Chr 9 heterozygous G>C substitution	x
27	heterozygous	indel	x	x
28	heterozygous	indel	x	x
36	heterozygous	heterozygous	ok	overlaying sequences, indel
49	heterozygous	homozygous	ok	Homozygous insertion of L206R and BssHII
51	homozygous	heterozygous	Chr9 heterozygous T>A substitution	x
58	unexpected band size	indel	x	x
59	heterozygous	indel	x	x
61	unexpected band size	WT	x	x
65	heterozygous	indel	x	x
70	heterozygous	WT	x	x
83	heterozygous	heterozygous	ok	overlaying sequences, indel

To further characterize the new cell line, I compared expression levels of PKA Cα, phosphorylation of PKA targets and proliferation to wild-type HEK293T (Figure 39). Clone 49 showed an increased phosphorylation of PKA targets under basal and surprisingly also under stimulated (10 μM forskolin) condition. In all other assays, clone 49 showed no significant difference to wild-type HEK293T.

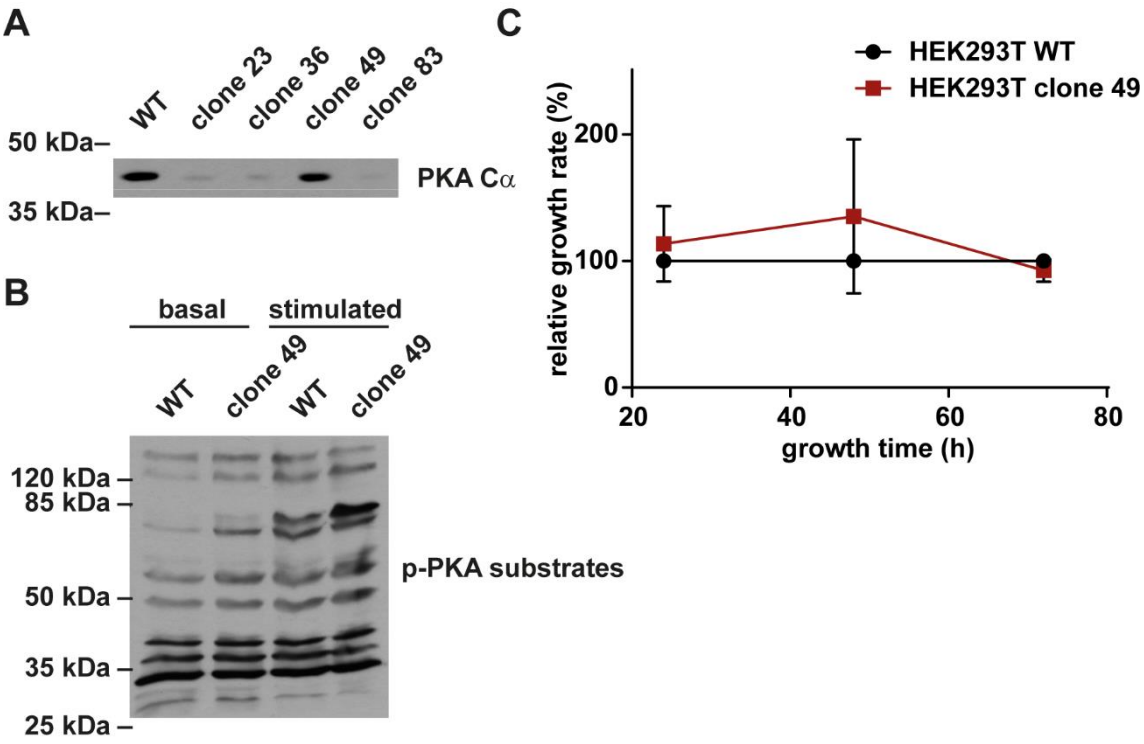

Figure 39: Characterization of HEK293T CRISPR clones. Shown are expression of PKA Cα (A), western blot of the phosphorylation of endogenous PKA substrates in basal and stimulated (10 μM forskolin for 30 min) (B) and cell proliferation measured by MTT assay (C).

After the successful modification of *PRKACA* of HEK293T cells I started with the adherent human adrenal carcinoma cell line NCI-H295R. Already transfections were less efficient with about 50% compared to HEK293T cells with 80%. In addition, to obtain growing single clones of NCI-H295R cells was not possible. I tried FACS and serial dilution with conditioned medium and coating (Nu-serum or matrigel) of the plates before seeding cells. But unfortunately, I was not able to obtain growing single clones of NCI-H295R cells.

In summary, I used the CRISPR/Cas9 system to generate a cellular model for L206R mutated tumors. I therefore used HEK293T cells to introduce the L206R mutation into the genome. The obtained cells were used to investigate the subcellular localization of the PKA subunits and to validate the higher nuclear translocation of PKA Cα L206R mutant under basal conditions.

4.5 Subcellular localization of PKA Cα mutants

Another important feature of the PKA Cα subunit is the nuclear translocation upon cAMP binding to the R subunit of the holoenzyme[191]. To analyze this, I transfected HEK293A cells with CFP-tagged R subunit and YFP-tagged C subunit and monitored their localization under basal and stimulated (10 μM forskolin for 30 min) condition. This experiment revealed an increased translocation to the nucleus under basal conditions for three mutants: L206R, 199_200insW, S213R+insIILR (Figure 40B). Upon stimulation, all PKA Cα mutants showed translocation to the nucleus. Interestingly, this effect just occurred in combination with RIIβ (Figure 40B). The Cα constructs co-transfected with RIα did not show any translocation to the nucleus, not even upon stimulation (Figure 40A). To verify this result I co-transfected YFP-tagged wild-type PKA Cα with either CFP-tagged RIIβ, CFP-tagged RIα or an empty vector (pcDNA3) and monitored the localization of Cα. The results showed that Cα translocated to the nucleus upon stimulation only when co-expressed with RIIβ (Figure 40C). In combination with an empty vector or RIα the Cα localization did not change upon forskolin stimulation. Moreover, in combination with RIα, the Cα was found to be present more in the cytosol, similar to the basal condition observed when co-expressed with RIIβ (Figure 40C). Contrary, the localization of the Cα in combination with the empty vector was comparable to the stimulated condition when expressed in combination with RIIβ (Figure 40C).

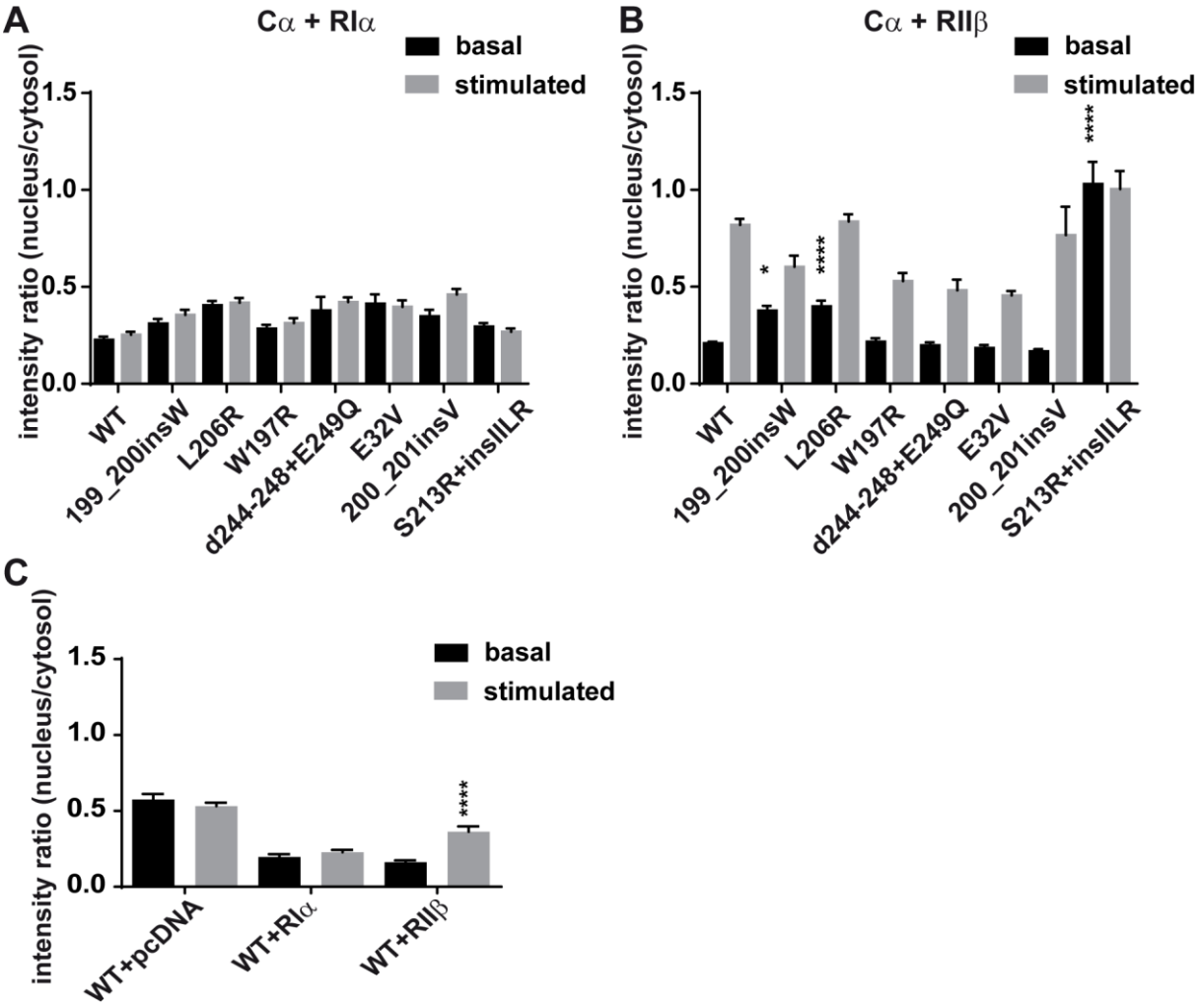

Figure 40: Nuclear translocation of PKA Cα mutants. HEK293A cells were co-transfected with CFP-RIα or CFP-RIIβ and either YFP-tagged -wild-type (WT) or -mutant Cα subunits. Confocal images were taken 48 hours post transfection under basal and stimulated (10uM forskolin for 30 min) conditions. The intensity ratios for the Cα subunit were plotted by measuring the mean grey value in the nucleus and the cytosol. The values were normalized to the wild-type sample in stimulated condition. Shown are the intensity ratios of the nucleus and cytosol of the YFP-PKA Cα mutants in combination with CFP-RIα (A) or CFP-RIIβ (B) and the effect of the CFP-R subunit on the YFP-Cα wild-type to control for nuclear translocation of Cα from different holoenzymes (C). Data are mean ± s.e.m. of two or more independent experiments. Data are statistically significant by two-way ANOVA. *P<0.05, ****P<0.0001 vs. WT basal by Bonferroni´s post hoc test.

To check that the higher amount of Cα in the nucleus is not due to technical reasons such as overexpression or transient transfections of the constructs, I used the HEK293T cells harboring the L206R mutation that I generated using CRISPR/Cas9 (section 4.4) and performed immunofluorescence experiments. Therefore, I first tested the antibodies for specificity and bleed-through in the other channel (Figure 41). The primary antibodies gave a strong and

specific signal and the anti-mouse Cy2-conjugated secondary antibody did not give a signal in the channel of the anti-rabbit Alexa Fluor 594 conjugated secondary antibody and vice versa.

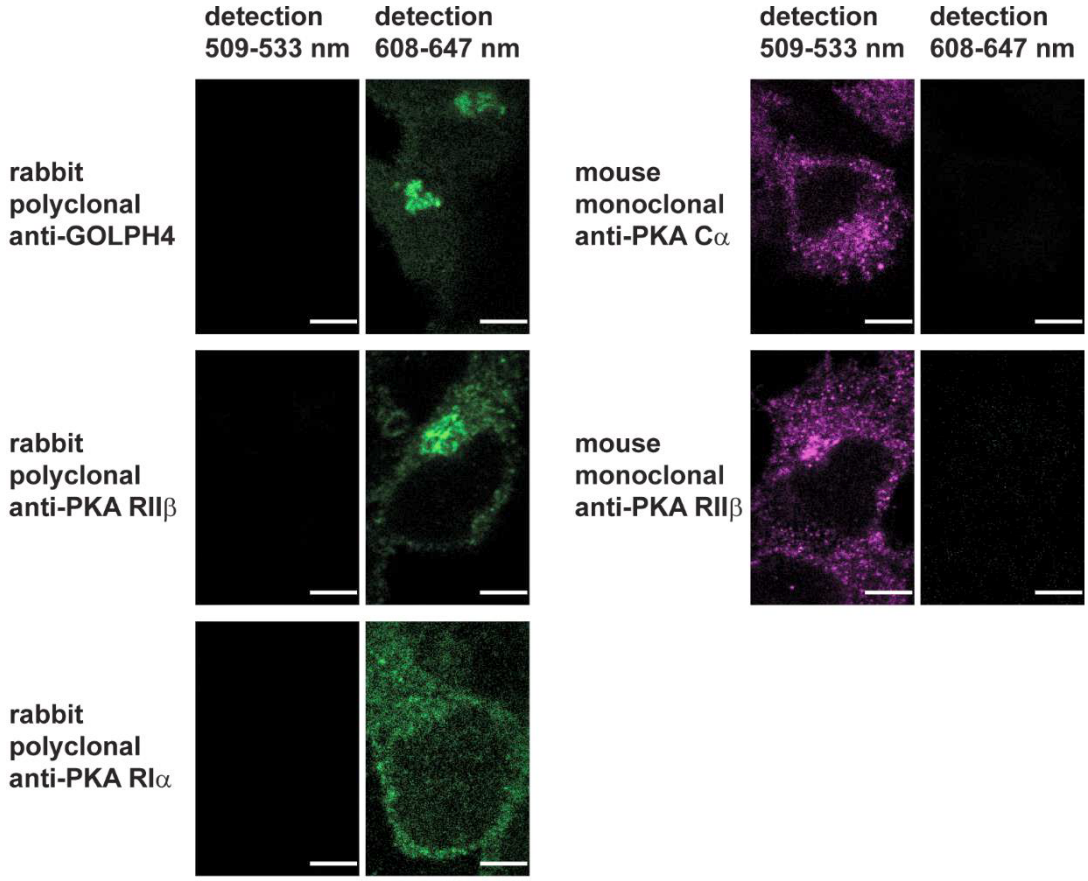

Figure 41: Setup of Immunofluorescence experiment. Shown are representative images of fixed HEK293T cells that were stained with the indicated primary antibodies. Secondary antibodies used are anti-mouse Cy2-conjugated and anti-rabbit Alexa Fluor 594 conjugated. Cy2 was excited using a 488 line of a 65 mW argon-ion laser set at 13% and detected in a range from 509-533 nm. Alexa 594 was excited using the 594-nm line of a HeNe594 laser and emission was detected in a range from 608-647 nm. Scale bars are 5 μm.

After confirming that there was no cross-talk or bleed through between the antibodies, I repeated the nuclear translocation experiment with the wild-type HEK293T cells and CRISPR/Cas9 generated *PRKACA* L206R mutated HEK293T cells under basal and stimulated (10 μM forskolin for 30 min) condition. There was a clear translocation of the L206R mutated Cα subunit to the nucleus in the basal state (Figure 42). Interestingly, RIα was seen to be dispersed throughout the cytosol, whereas RIIβ was mainly concentrated at the Golgi. Additionally, the Cα subunit also showed a higher concentration under basal condition in this perinuclear region in the wild-type HEK293T cells. Both R subunit locations were not changed upon stimulation (Figure 42).

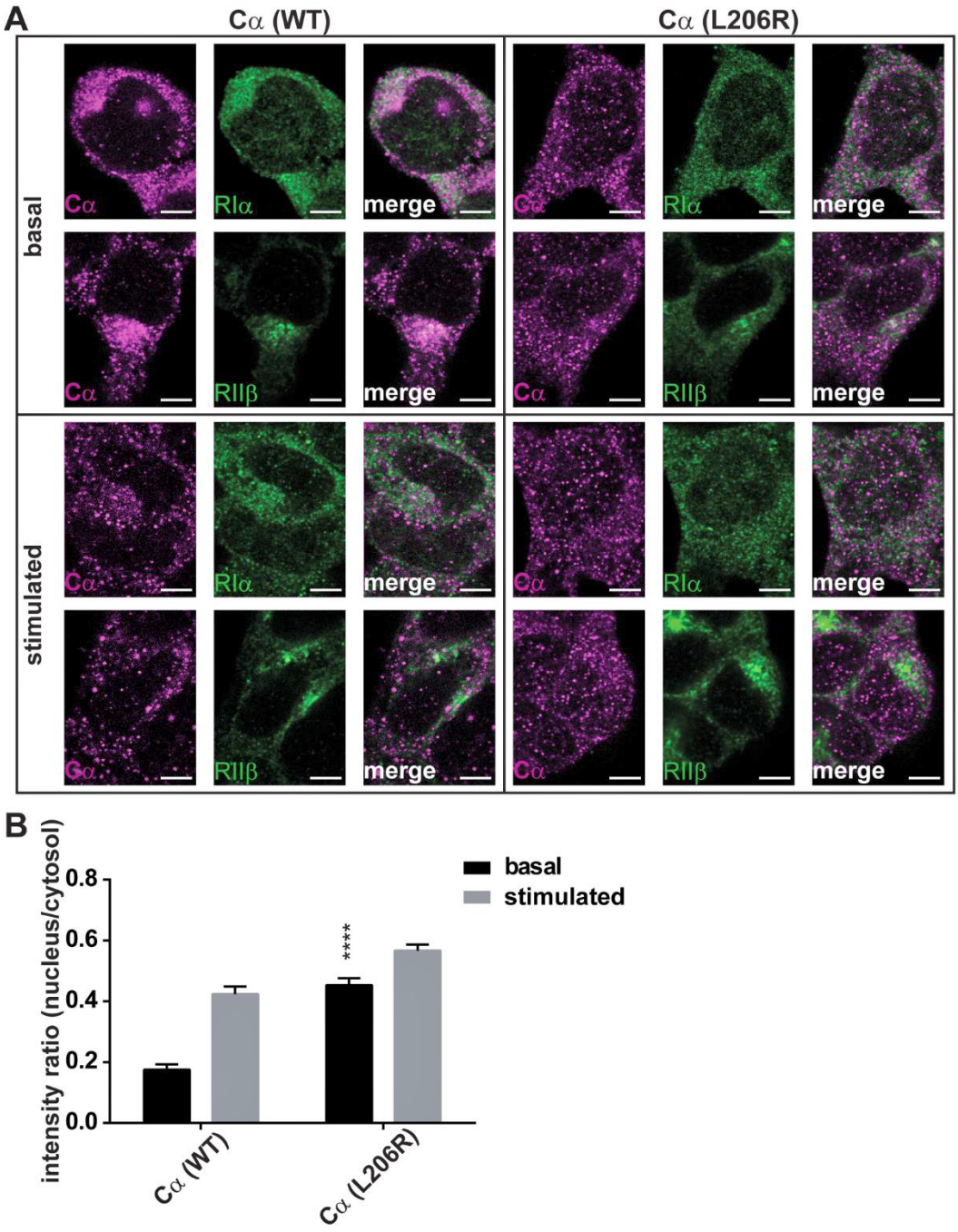

Figure 42: Nuclear translocation of endogenous PKA Cα. Immunofluorescence on either wild-type (WT) HEK293T cells or CRISPR/Cas9 generated *PRKACA* L206R mutated HEK293T cells was used to show the translocation of endogenous PKA Cα to the nucleus. To stain Cα, the mouse monoclonal anti-PKA Cα antibody was used in combination with a Cy2 conjugated secondary antibody. Emission of which was detected in a range from 509-533 nm. To detect R subunits, rabbit polyclonal anti-PKA RIα or RIIβ were used in combination with Alexa Fluor 594 conjugated secondary antibody. Emission of which was detected in a range from 608-647 nm. Shown are representative confocal images (A) and quantification of 10 cells (B) of basal and stimulated condition (10 μM forskolin for 30 min). Data are mean ± s.e.m. Data are statistically significant by two-way ANOVA. ****P<0.0001 vs. WT basal by Bonferroni´s post hoc test. Scale bars are 5 μm.

To show that RIIβ and wild-type PKA Cα are localized at the Golgi, I did another Immunofluorescence experiment with staining of the Golgi (Figure 43). As expected, both RIIβ and wild-type PKA Cα staining co-localized with the Golgi staining under basal condition. Upon stimulation or in *PRKACA* L206R mutated cells, this co-localization at the Golgi was absent for PKA Cα, but not for RIIβ.

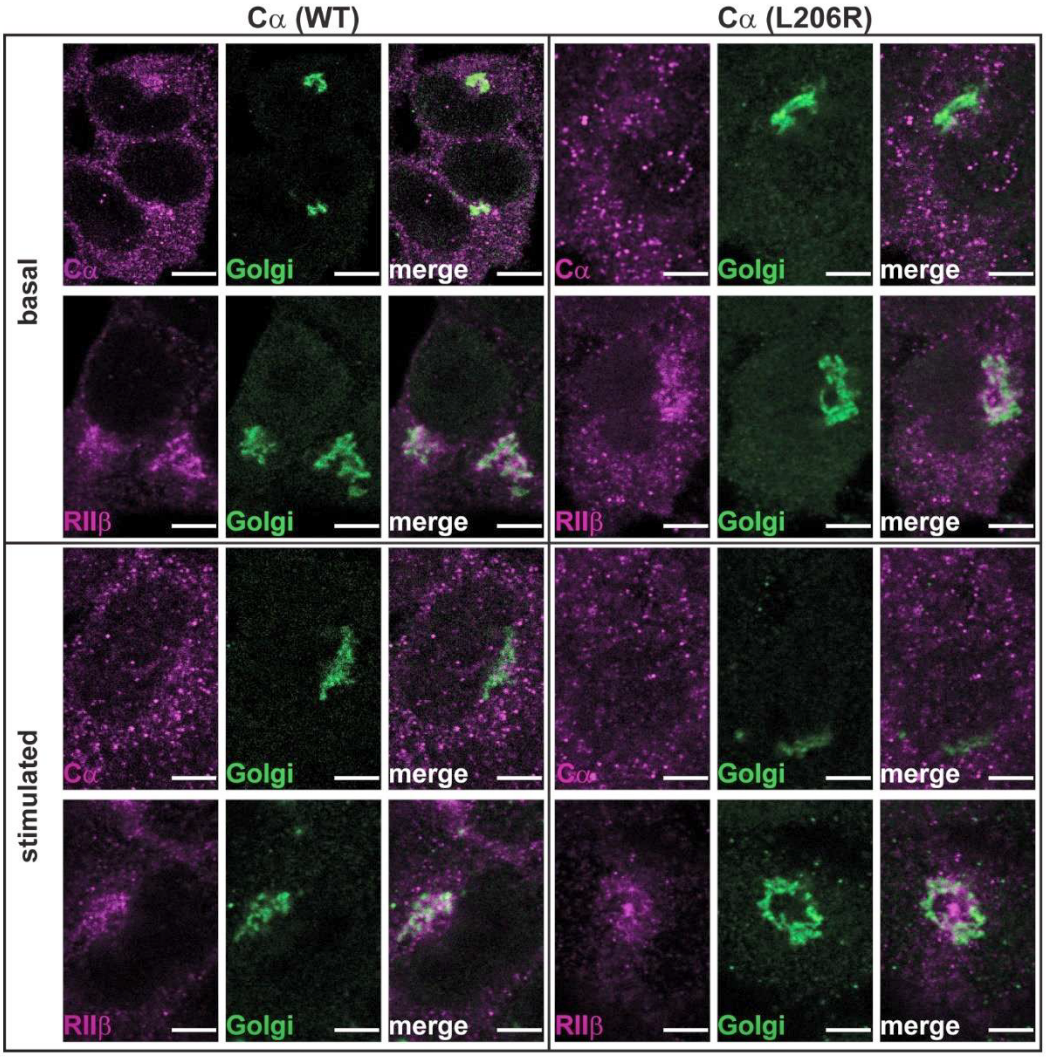

Figure 43: Localization of PKA subunits at the Golgi. Immunofluorescence was used to show the location of endogenous PKA subunits in the cell. To stain Cα the mouse monoclonal anti-PKA Cα antibody and for RIIβ subunit the mouse monoclonal anti-PKA RIIβ were used both in combination with a Cy2 conjugated secondary antibody, emission of which was detected in a range from 509-533 nm. To stain the Golgi the rabbit polyclonal anti-GOLPH4 antibody was used in combination Alexa Fluor 594 conjugated secondary antibody, emission of which was detected in a range from 608-647 nm. Either wild-type (WT) HEK293T cells or CRISPR/Cas9 modified HEK293T cells expressing the PKA Cα L206R mutant instead of wild-type were used. Shown are representative confocal images of basal and stimulated condition (10 μM forskolin for 3 min). Scale bars are 5 μm.

These results revealed that three mutations (199_200insW, L206R, S213R+insIILR) affect the cellular localization of the PKA Cα subunit in cells at a variable degree. Additionally, they indicated that the localization of the R subunits is not altered due to *PRKACA* L206R mutation.

In summary, I characterized PKA Cα mutants, which were identified in CPAs of Cushing's patients. Co-IP showed, that not all mutants have an impact on the interaction to the R subunit. Interestingly, for the d244-248+E249Q mutant I could observe a binding to the RIIβ but not to the RIα subunit. Also, not all the mutants showed constitutive activity in the kemptide assay. Results on the artificial substrate (kemptide) and endogenous substrates did not always correlate. For example, I showed that the 200_201insV mutant, which was not active in the kemptide assay phosphorylated endogenous PKA substrates. Additionally, nuclear translocation experiments – another marker for active PKA – gave different results. Here just three mutants (L206R, 199_200insW and S213R+insIILR) showed higher nuclear translocation under basal condition. All other mutants and the wild-type Cα showed translocation to the nucleus just upon stimulation. But this is true, just if co-transfected with the RIIβ subunit. In combination with RIα or an empty vector no translocation to the nucleus was observed. By showing different results for kemptide and endogenous substrates and different phosphorylation patterns in western blot, the activity assays indicated changes in substrate specificity of the PKA Cα mutants. Therefore, I used an algorithm to predict changes in substrate specificity of the PKA Cα mutants. The mutants predicted to have the major effect on substrate specificity were checked using phosphoproteomics. This experiment showed remarkable changes in the substrate specificity of the tested mutants. Interestingly the tested mutants just had four hyperphosphorylated substrates in common: CIT at serine 480, TOM34 at serine 93, H1.4 at serine 36 and H1.2 at serine 36. Those results were then cross-checked by phospho-specific western blot analysis of transfected HEK293A cells and tumor tissue of Cushing's patients having *PRKACA* wild-type or mutated (L206R and d244-248+E249Q). The results showed that both histones are hyperphosphorylated on the tested site in CPA tissue with *PRKACA* L206R mutation.

5 Discussion

My thesis investigated the mechanisms of action of *PRKACA* mutations recently identified in CPAs, which are believed to be the main cause of adrenal Cushing's syndrome[89, 90, 91, 92, 93, 94, 157, 158]. Until now, their mechanism of action was only partially known. Using a combination of optical and biochemical methods, including phosphoproteomics, I found that several mechanisms contribute to overall effects of these mutations. These include: interference with the formation of a stable holoenzyme, alteration of the subcellular localization of the mutated Cα subunit and a change in substrate specificity of PKA.

5.1 Interference with the formation of a stable PKA holoenzyme

A first important effect of the mutations was an impairment of the formation of a stable PKA holoenzyme. This lead to a constitutively active C subunit by removing the inhibitory signal normally provided by the R subunit. This mechanism seemed to play a role for all the mutants except E32V. For the L206R and the 199_200insW, this was in line with previous studies by our and other groups[146, 147]. As reported earlier, due to the lack of binding of the L206R mutant to the RIIβ subunit[146], the L206R mutant showed constitutive activity[89, 90, 91, 92, 146] in combination with both R subunits. Contrary to previous findings[147], the L206R mutant was efficiently inhibited by the PKI inhibitor peptide. Interestingly, the 199_200insW mutant, which also showed lack of binding to both R subunits and was reported to constitutively activate PKA[89, 146], was found to be constitutively active only in combination with RIIβ in the kemptide assay. In this assay, this mutant was not stimulated to a level higher than the basal in combination with RIα. Interestingly the previous data on constitutive activity of this mutant was just measured combination with RIIβ not with RIα[146]. Nevertheless, I would have expected constitutive activity of this mutant in combination with both R subunits, since also binding to both R subunits was lost. But interestingly, the phosphorylation of endogenous substrates showed the expected constitutive activity in combination with both R subunits. This was one of the findings that prompted me to investigate a possible change in substrate specificity (section 5.3).

The W197R mutant, which has been reported to negatively affect the binding of the R subunit[155], was able to form a holoenzyme with both tested R subunits and also bound the inhibitor peptide PKI in my experiments. However, it was reported that if the R subunit is stripped off of cAMP, the W197R was still able to form a holoenzyme[143]. The long washing

steps in this experiment might strip cAMP from the R subunit and therefore allow interaction with the W197R mutant. However, in intact cells, I would expect abolishment of holoenzyme formation. This was supported by the kemptide assay showing constitutive activity of this mutant in combination with both R subunits. Contrary to this, the endogenous substrates just showed a slight hyperphosphorylation compared to wild-type Cα. This again might be at least in theory due to changes in substrate specificity, even if this was not supported by the *in silico* prediction for this mutant. However, other possibilities cannot be excluded. For example, other inhibitors (e.g. other R subunits) could buffer the loss of interaction to RIα and RIIβ. Additionally, the mutation could cause a faster degradation of the protein in cells.

The selective abolishment of RIα binding by the d244-248+E249Q could be due to the differences in the RIα and RIIβ holoenzyme architectures[15, 97, 101], which revealed that there are unique interaction-sites for RI and RII subunits[115, 192]. Therefore, deletion of amino acids 244 to 248 and substitution of glutamic acid 249 with glutamine in the Cα subunit seemed to affect a region essential for RIα binding but not RIIβ binding. As expected from the Co-IP, in the kemptide assay, the d244-248+E249Q showed constitutive activity in combination with RIα subunit. Interestingly, it also presented this behavior in combination with RIIβ even though it still bound this R subunit. This could be an indication that the interaction with the RIIβ subunit was not as strong as with the wild-type Cα subunit. In contrast, binding to PKI inhibitor peptide seemed not to be affected by this mutation, since it was effectively able to inhibit activity. This was in line with the literature reporting distinct binding sites for PKI and the R subunits[143].

The E32V mutant did not affect binding to any tested R subunit, which is likely due to its position far away from interaction sites with the R subunit (Figure 11) and therefore showed comparable activity as wild-type Cα.

The position and type of the mutation of the 200_201insV mutant is very similar to the 199_200insW mutant which has been shown to affect R subunit binding[146]. Therefore, the 200_201insV mutant likewise, affected the holoenzyme formation, as suggested by Di Dalmazi *et al.*[93]. Controversial to this data, in the kemptide assay, the 200_201insV mutant did not show higher basal activity, nor could it be stimulated to a higher activity than the basal. Whereas it could be stimulated to the level of the wild-type using endogenous PKA substrate. This discrepancy could be due to a change in substrate specificity as shown for the L206R[148]. The mutation could therefore interfere with the recognition of kemptide as a substrate, which is supported by the *in silico* prediction and the phosphoproteomics experiment showing a change in substrate specificity for this mutant.

The S213R+insIILR mutant showed decreased binding to both R subunits that were tested here, as predicted by the literature[93]. This was supported by the kemptide assay showing constitutive activity of this mutant. However, in combination with RIIβ, this mutant showed a reduced interaction which could not be loosened by addition of cAMP. This was in line with the observation of a reduced maximal activity of this mutant in the western blot analysis. Due to the observation that the S213R+insIILR mutant showed no binding to RIα and overall reduced but persistent binding to the RIIβ subunit, it was likely that the affinity of the mutated Cα subunit to the RIIβ subunit was reduced compared to that of the wild-type Cα subunit. Additionally, the fact that PKI did not completely block the activity of this mutant indicated a lower affinity of the S213R+insIILR mutant to PKI. Therefore, I speculate that the affinity of this mutant to the RIIβ subunit might be reduced. When a holoenzyme is formed, dissociation of the latter is inhibited. Something similar was already observed for RIα mutants, which are kept in a conformation where they cannot bind to cAMP[87, 88] or cannot undergo the conformational change necessary to dissociate[114].

Interestingly, I observed higher basal activity of all Cα constructs, including the wild-type, in combination with RIα compared to RIIβ in both activity assays used. As mentioned in the introduction (section 1.2.1) the holoenzymes exhibit different sensitivity to the cAMP level. The $RI\alpha_2C\alpha_2$ holoenzyme was shown to be activated at 101 nM cAMP concentration [116], whereas the $RII\beta_2C\alpha_2$ holoenzyme was reported to be activated at 584 nM cAMP concentration [101]. Therefore, the PKA I holoenzyme already dissociates at lower cAMP concentrations, rendering the C subunit active[193]. Here, the endogenous cAMP concentration in the cell lysates already caused a response in the samples combined with RIα but was not sufficient to activate the $RII\beta_2C\alpha_2$ holoenzyme.

In summary, holoenzyme formation (at least with one R subunit) in intact cells was lost for all Cα mutants except the E32V, which rendered the Cα mutants constitutively active. This appears to be one important mechanism of action of the PKA Cα mutants.

5.2 Altered subcellular localization of PKA Cα by *PRKACA* mutation

Another finding of this study was that some mutants are mislocalized to the nucleus, which is likely a consequence of the reduced interaction with R subunits. This was expected to affect phosphorylation of nuclear PKA targets . As explained in the introduction (section 1.1.2), these nuclear targets include transcription factors[17] (e.g. CREB[17]) which play an important role in the transcription of key steroidogenic enzymes like StAR[29, 30] and Cyp11A1[28] (Figure 2). Therefore, increased localization of PKA Cα to the nucleus and thus increased phosphorylation of transcription factors could affect gene transcription leading to increased steroidogenesis. Therefore this was a second mechanism of action of the PKA Cα mutants.

To investigate this mechanism under endogenous PKA levels, I generated HEK293T cells carrying the most frequent *PRKACA* L206R mutation using the CRISPR/Cas9 system. To overcome the possibility that the chosen guide sequence might not efficiently target the Cas9 protein to the target locus in the DNA, I tested two guides for their cutting and HDR efficiency, as recommended by Ran *et al.*[167]. I was able to achieve a cutting efficiency of 17 to 23% and an HDR efficiency of 16% for the best guide. The indel efficiency varied from guide to guide, but the average of 20% indel efficiency was in line with other guides targeting the EMX1 locus in HEK293T cells[194]. Due to the fact that HDR is just active in dividing cells[195], the HDR efficiency was lower compared to the indel efficiency. With this combination of guide and repair template, I obtained 17 cell clones (20.5%) with modifications in the targeted region of the genome. Unfortunately, I was just able to verify a homozygous insertion in two clones (2.5%). However, this was close to the HDR efficiency of 3 to 8% reported for HEK293T cells[196]. To increase the HDR efficiency further, one could suppress the nonhomologous end-joining (NHEJ) mechanism in the cells[197, 198]. I detected off-target effects in 56% of the tested clones, which was in good agreement with the previously reported experimental values[194]. These off-target effects could be minimized by usage of nickases[199] or high fidelity nucleases[200]. Since the double-nicking did not work, I used the Cas9 nuclease. Insertion of the mutation and selection of clones was followed by functional characterization of clone 49, which was homozygous in L206R mutation and BssHII cutting site. This clone showed similar expression of PKA Cα compared to the wild-type HEK293T cells, no significant changes in proliferation but enhanced basal PKA activity as expected from HEK cells with transient transfection of PKA Cα L206R mutant.

Immunofluorescence staining of Cα, RIα, RIIβ and the Golgi in these *PRKACA* L206R mutated and in wild-type HEK293T cells, revealed nuclear translocation of the L206R mutant even with low cAMP level. Additionally, this confirmed earlier findings that RIα was present in the

cytosol[191] and RIIβ was localized to the Golgi[201]. Due to binding of wild-type Cα to RIIβ, Cα wild-type was also co-localized at the Golgi (Figure 43). Contrary to the wild type Cα, the L206R mutant did not co-localize at the Golgi, due to the loss of RIIβ binding (Figure 43). Consistent with findings of other groups no translocation of RIα to the nucleus was observed[191, 202]. Additionally, I did not observe translocation of RIIβ to the nucleus as reported earlier[202, 203, 204]. But my results are also consistent with the observation that RIIβ did not translocate to the nucleus upon forskolin stimulation but did so under ethanol treatment of the cells[205]. Ethanol was shown to stimulate the cAMP/PKA signaling pathway which then has an impact on consumption and the sensitivity to sedative effects of ethanol[206, 207, 208].

To investigate also the localization of the other PKA Cα mutants I used transiently transfected HEK293A cells. Interestingly, the PKA Cα subunit mutants – including the wild-type – just showed nuclear translocation upon stimulation in combination with RIIβ subunit. This has been already a matter of debate. Several groups showed that RIIβ and AKAPs play an important role in the nuclear translocation of the Cα subunit[209, 210]. Whereas others showed translocation of Cα to the nucleus upon dissociation from the type I holoenzyme[191, 211]. In 2002, Constantinescu *et al.* suggested that Cα from type II PKA holoenzymes is translocated to the nucleus upon stimulation and induces phosphorylation of CREB, whereas Cα from type I PKA is activated in the cytoplasm and responsible for downstream pathways other transcription factors[205]. This was in line with my observation that just the Cα constructs from the RIIβ holoenzyme translocate to the nucleus.

Interestingly, in combination with RIIβ, just three mutants (L206R, 199_200insW, S213R+insIILR) showed enhanced translocation to the nucleus under basal condition. This correlates with immunofluorescence experiments for the L206R mutant. Therefore, increased nuclear translocation due to overexpression can be excluded. The higher amount of the L206R and the 199_200insW mutant in the nucleus can be explained by the loss of binding to the R subunit, which lead to a higher amount of free C subunit which then diffuses to the nucleus[191]. This was also observed, when wild-type Cα was co-transfected with an empty vector (Figure 40C). Unexpectedly, the W197R, d244-248+E249Q and the 200_201insV mutant did not show any effect on nuclear localization even though R subunit binding was abolished. Therefore, abolishment of R subunit binding seemed not to be the only factor responsible for higher nuclear localization of L206R and 199_200insW. However, the effect for the S213R+insIILR mutant was significantly stronger. The insertion of four amino acids (isoleucine-isoleucine-leucine-arginine) leads to a stretch of basic amino acids that could form an additional nuclear localization sequence (here: RIILR) in the S213R+insIILR mutant. Therefore, in addition to the

diffusion of the free Cα subunit to the nucleus[212], an active mechanism could contribute to the higher nuclear localization of this mutant.

Interestingly, the E32V mutation is located in the N-terminal region of the Cα subunit, which is known to bind to AKIP1a, a nuclear AKAP that accumulates PKA Cα in the nucleus[213]. AKIP1a is present in HEK293A cells at low levels[214]. Abolishment of binding to the Cα subunit could lead to shorter presence of PKA Cα E32V in the nucleus due to faster export by PKI[215, 216]. This could not be investigated with persistent forskolin stimulation. However, investigating the interaction of the E32V mutant with the AKIP1a and the residence time of the Cα mutant in the nucleus would be an interesting starting point for further studies on this mutant.

In summary, I successfully used the CRISPR/Cas9 system to generate a HEK293T based cell line where the most frequently identified *PRKACA* L206R mutation was introduced into the genome. This cell line was used to investigate the subcellular localization of the PKA subunits. Overall, my results showed for the first time that mutations in *PRKACA* can alter the subcellular localization of the PKA Cα subunit. This enhanced nuclear translocation of the 199_200insW, L206R and S213R+insIILR mutants under basal condition was not only due to abolishment of R subunit binding but also other mechanisms might be involved.

5.3 Alteration in PKA substrate specificity by *PRKACA* mutations

In addition to the two aforementioned mechanisms affecting holoenzyme formation and subcellular localization of the Cα subunit, mutations can also have an impact on the substrate specificity of the kinase. My results showed clearly, that some mutations affect the substrate specificity due to the location of the mutation close to the active site of the enzyme. This change in substrate specificity could also play a role in the interference with the binding to the R subunit and therefore also in the altered subcellular localization.

In a first trial, the different phosphorylation patterns of the Cα mutants (Figure 28) could not be validated by investigating the phosphorylation status of the PKA phosphorylation sites in the known PKA substrates CREB, α/β-GSK and β-catenin. Therefore, I combined the use of a theoretical *in silico* prediction and a phosphoproteomics experiment to assess the question of altered substrate specificity in the PKA Cα mutants. My results showed for the first time, that a change in substrate specificity is a mechanism of action not only for the L206R mutant.

The results for the L206R mutant showed a reduced preference for a hydrophobic amino acid at the +1 position, which was in good agreement with the prediction and with a report analyzing the substrate specificity of the L206R mutant in *E.coli* [148]. In addition, the same study observed a strong acidic preference at the +2 position[148], which further corroborated my findings. The d244-248+E249Q mutant, which was predicted to have the strongest effect by my *in silico* analysis also showed the highest number of affected substrates by phosphoproteomics compared to the other mutants (116 vs. 62 for L206R and 75 for 200_201insV). Additionally, the biggest effect on substrate specificity (as shown by the sequence logos) was also detected. Interestingly, not all the predictions for this mutant could be verified. For example, I could not validate the increased preference for glutamate or serine around the phosphosite. According to the prediction, this mutant might also affect the preference for the amino acids of the PKA consensus sequence (RR/KXpS/T). In the phosphoproteomics experiment, I immunoprecipitated PKA substrates using an antibody against this consensus sequence. Therefore, we might not see all changes in substrate specificity with this phosphoproteomics setup. The results of the *in silico* prediction and the phosphoproteomics of the 200_201insV mutant were in good agreement. Both showed a reduction for the requirement of a phenylalanine and an increase of requirement for valine at the +1 position. Additionally, this mutant could also affect the consensus sequence of PKA (RR/KXpS/T), which could not be analyzed in this experimental setup. This mutant did not recognize the kemptide as substrate due to the change in the preferred amino acids around the phosphoacceptor site. This could explain why this mutant was found to be inactive in the kemptide activity assay.

Even though several PKA targets found to be hypo- or hyperphosphorylated by the PKA Cα mutants could play a role in the mechanism of action of the Cα mutants. I first wanted to investigate the mechanisms of action shared by the PKA Cα mutants. Therefore, I concentrated on the four substrates found to be commonly hyperphosphorylated by all three tested mutants. Those substrates were CIT (serine 480), TOMM34 (serine 93), H1.4 (serine 36) and H1.2 (serine 36). It is important to note that those substrates were also present in lysates of the adrenal carcinoma cell line NCI-H295R. Therefore, they could possibly play a role in downstream effects of *PRKACA* mutations in adrenal adenomas of Cushing's syndrome patients.

Since two of these substrates were histones, these substrates seemed to be particularly interesting. Phosphorylation of linker histones is known to be linked to mitosis[217]. H1.4 serine 36 was shown to be phosphorylated by PKA[218] and it was shown that the phosphorylation of this site dissociates the H1.4 from mitotic chromatin[218]. Due to the sharp increase of the phosphorylation status at prophase and the decrease in cytokinesis, it was believed that the phosphorylation of serine 36 of H1.4 may control mitotic entry or the transition from telophase to cytokinesis[218]. The knock-out of H1.4 decreased the number of mitotic cells, which could not be rescued by a phosphodeficient H1.4 S36A mutant[218]. It was also shown that the phosphorylation of serine 36 on H1.4 affects chromatin condensation in a way that ihhibition of PKA activity by H89 either blocks decondensation or induces condensation of chromatin [218]. This was supported by the finding that inhibition of PKA activity by PKI injection induced chromatin condensation regardless of the stage in the cell cycle. This effect could be rescued by injection of C subunit of PKA [219]. Therefore, it was believed that phosphorylation of H1.4 serine 36 contributes to the maintenance of optimal chromatin compaction during mitosis [218]. Evaluation of H1.4 phosphorylation in transiently transfected HEK293A cells, revealed hyperphosphorylation of the PKA phosphorylation site by the L206R mutant in basal and in stimulated condition. The d244-248+E249Q and the 200_201insV mutants just showed a trend of hyperphosphorylation of this site under stimulated condition. The discrepancy between the L206R and the two other mutants (d244-248+E249Q, 200_201insV) in basal condition might be due to the observed increased nuclear translocation of the L206R mutant compared to wild-type, d244-248+E249Q and 200_201insV mutated PKA Cα. The increased phosphorylation of H1.4 on serine 36 in the basal state was also shown in *PRKACA* L206R mutated CPA tissue. This could then affect the mitosis of *PRKACA* L206R mutated cells. Probably, the hyperphosphorylation of H1.4 at serine 36 would lead to an increased number of mitotic cells, since the loss of phosphorylation leads to fewer mitotic cells[218].

H1.2 was already shown to be phosphorylated on serine 36 by mass spectrometry before[220, 221], but the results showing that H1.2 on serine 36 is phosphorylated by PKA are new. The phosphosite around serine 36 in H1.4 is conserved for the histones 1.2, 1.3 and 1.4[220]. Therefore, even if phosphorylation of H1.2 by PKA has not been shown yet, it is likely that PKA is able to phosphorylate H1.2 and H1.3. Interestingly, H1.2 serine 36 phosphorylation was not as strongly affected by the mutants as the H1.4 serine 36 phosphorylation. The results on H1.2 and H1.4 phosphorylation were similar, both reflecting the increased nuclear translocation of the L206R mutant under basal condition. Interestingly, in this study I found that H1.2 serine 36 was hyperphosphorylated in HEK293A cells as well as in tumor CPA tissues by the PKA Cα L206R mutant, revealing a novel and hitherto unknown effect of this mutation. No function is known for this phosphosite on H1.2 but it could have a similar effect as the H1.4 serine 36 phosphorylation.

Phosphorylation of the other two proteins, CIT and TOM34, by PKA have not been shown yet. Both proteins possess a PKA consensus motif at the identified site. Unfortunately, I was not able to purify TOM34 by immunoprecipitation to analyze the phosphorylation of serine 174. TOM34 is localized at the surface of mitochondria and is involved in mitochondrial protein import[222]. It has been shown to be a cochaperone of heat shock protein (HSP) 70 and Hsp90 and assembles into a complex that shuttles proteins into the mitochondria[223]. Interestingly, yeast TOM70 has been shown to be phosphorylated by PKA on serine 174 which reduces its receptor activity and has a negative effect on mitochondrial protein import[224]. This region in yeast TOM70 is homologous to the region in TOM34 around serine 93[222]. Therefore, phosphorylation of serine 93 in human TOM34 could inhibit its receptor activity and therefore impair the import of metabolite carriers into mitochondria. As described in the introduction, some steps in hormone synthesis take place in the mitochondria. Therefore, affecting mitochondrial protein import could also have some impact on cortisol synthesis.

In contrast to TOM34, I was able to immunoprecipitate CIT. Unfortunately, I did not detect any phosphorylation of the protein. This could be due to the long IP protocol, where the phosphorylation could get lost. CIT is a serine/threonine-protein kinase[225] known to phosphorylate the light chain of myosin II, which is the primary motor protein responsible for cytokinesis[226]. It was shown that CIT is necessary for efficient cytokinesis[227] and that overexpression of CIT leads to increased cell proliferation[228]. Interestingly, CIT was shown to be overexpressed in human colon cancer tissues, which could be a reason for development of colon cancer[228]. The enhanced phosphorylation of serine 480 of CIT by PKA Cα mutants could influence activity or expression of CIT and therefore also play a role in cell proliferation.

In addition to these four substrates hyperphosphorylated by all three tested mutants, several other substrates were found to be hyper- or hypophosphorylated by the mutants (116 for d244-248+E249Q. 62 for L206R and 75 for 200_201insV). Also, these could be implicated in cortisol synthesis and in cell proliferation of adrenal cells. Therefore, it would be of interest to also investigate the other hypo- or hyperphosphorylated targets.

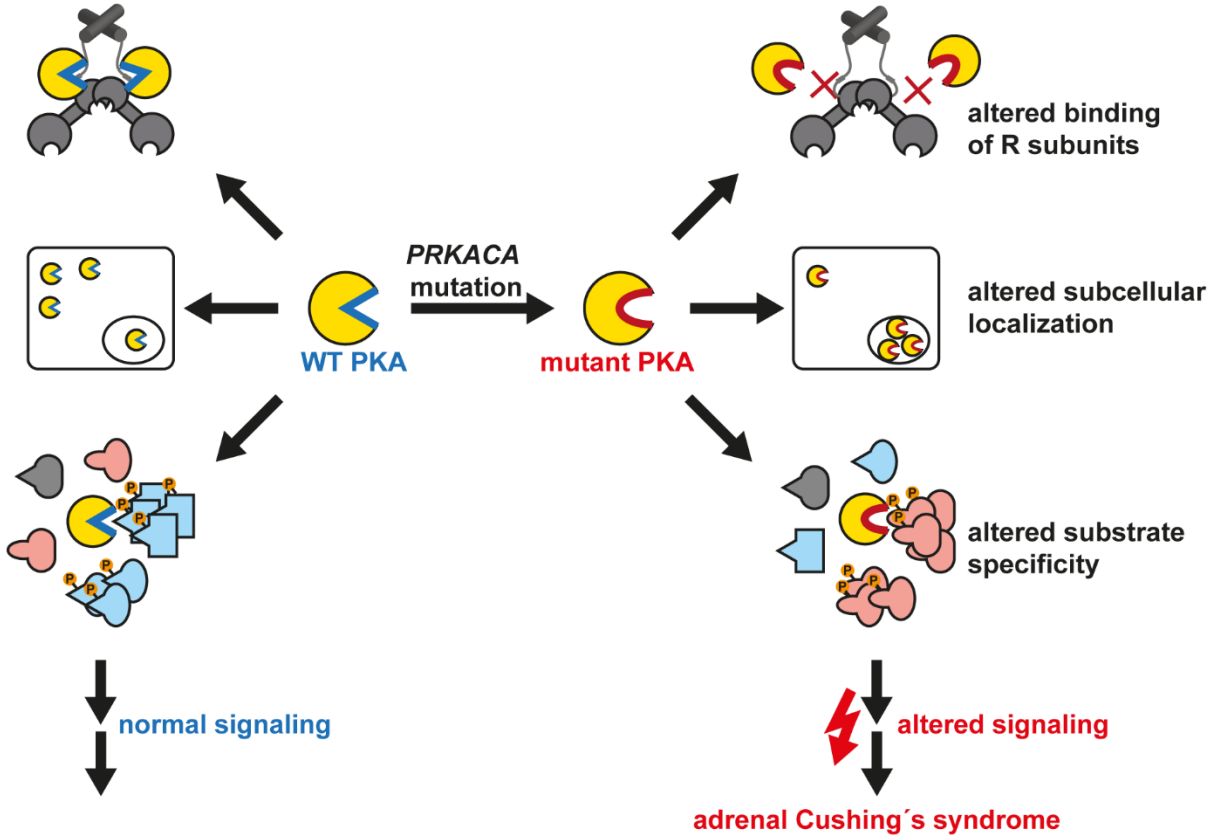

Figure 44: Contributing mechanisms leading to cortisol oversecretion and cell proliferation in adrenal Cushing's syndrome. *PRKACA* mutation can cause inhibition of binding to R subunits, which can also be specific for the type of R subunit, altered subcellular localization by enhanced translocation to the nucleus and a change in substrate specificity. Mutants can act via one mechanism or a combination of mechanisms ultimately leading to an altered signaling which contributes to cortisol oversecretion and increased cell proliferation in adrenal Cushing's syndrome.

In summary, my results showed for the first time that there are three mechanisms contributing to cortisol oversecretion and possibly cell proliferation in *PRKACA* mutated CPAs of Cushing's syndrome patients (Figure 44). Some Cα mutants might act via a combination of these mechanisms, others by just one. An important effect of the mutations was the inhibition of the formation of a stable PKA holoenzyme, which was observed for most of the mutants. This leads to a constitutively active C subunit by abolishing the regulation of the R subunit. A second

potential mechanism seemed to be an enhanced translocation to the nucleus despite a low cAMP level. This could be a consequence of the lost interaction with R subunits. However, since this was observed only for few mutants, other mechanisms might be at play. Increased nuclear translocation under basal condition would strongly affect phosphorylation of nuclear PKA targets and could therefore play an important role in gene transcription. Importantly my findings revealed that a change in PKA substrate specificity is another major mechanism. According to the *in silico* analysis, this effect is expected for a large fraction of mutants (five out of seven). This was verified by an experimental setup using phosphoproteomics for three mutants (L206R, 200_201insV, d244-248+E249Q). The phosphoproteomics revealed several targets affected by changes of substrate specificity, which differed among the mutants. Only four targets were hyperphosphorylated by all three mutants compared to wild-type Cα. Importantly two out of these four were H1 histones, which are known to be implicated in mitosis[217]. My results also confirmed hyperphosphorylation of these histones in CPAs carrying the *PRKACA* L206R mutation. Thus, confirming the change in substrate specificity and suggesting a possible downstream effect on cell proliferation.

6 Outlook

My data indicate that there are three mechanisms of action of the PKA Cα mutants, which can explain increased cell proliferation and cortisol secretion. These mechanisms include the interference with a formation of a stable PKA holoenzyme, a change in subcellular localization and a change in substrate specificity.

To investigate the subcellular localization, a model for *PRKACA* L206R mutated CPAs was generated using HEK293T cells. It would still be useful to generate such a cellular model in an adrenal cell line to investigate the effects on cortisol secretion and proliferation. Unfortunately, the NCI-H295R cell line was found to be particularly difficult to work with. To produce single clones, one should be able to get at least single isolated cells that grow in culture. The NCI-H295R cells need cell-cell contacts to grow efficiently. As a result, obtaining single cell clones in these cells was not possible. While other groups have generated stable cell lines using NCI-H295R cells, they have typically used bulk-cell lines selected by antibiotics[229]. This is unfortunately not possible using the CRISPR/Cas9 system because every cell in the bulk could harbor a unique modification, as seen with the HEK293T clones. Therefore, generation of a cellular model for adrenal adenomas harboring the *PRKACA* L206R mutation using NCI-H295R, was not possible. Thus, unfortunately, the investigation of the impact of *PRKACA* mutations on down-stream effects like expression of steroidogenic enzymes, glucocorticoid secretion and proliferation was not possible. To overcome the problems with this cell line, one could try other available human adrenocortical cell lines[230], like the SW-13 cell line[231]. Unfortunately, these cells do not produce glucocorticoids nor do they respond to ACTH[230], which would be a very poor model for cortisol secreting tumors. One cell line at least secreting glucocorticoids and steroidogenic enzymes is a pediatric adrenocortical adenoma derived cell line[232]. Unfortunately, this cell line was reported to reach just eight subculture passages[230], therefore using these cell for genome editing would be impossible. Growing the single clones would take too much time before one could use these cells as a model. Additional to the human adrenocortical cell lines, an adrenal mouse cell line (Y1) can also be investigated. Unfortunately, this cell line exhibits an abnormal steroid profile and developed unresponsiveness to ACTH over the culture period[189]. Due to these shortcomings, none of these alternative cell lines is an optimal model for CPAs. Therefore, generating a model using a biological relevant cell line might not be possible. An alternative would be to generate transgenic mice harboring the *PRKACA* L206R mutation to study the effect of the mutation *in vivo*.

Interestingly, in all the experiments in this study, one mutant (E32V) behaved like the wild-type Cα. Therefore, this mutant might even act via another mechanism. One possibility is that this mutation could alter the binding to a specific AKAP, AKIP1a. Abolishment of binding to this AKAP could lead to a faster export of the Cα from the nucleus[213]. Therefore, it would be useful to investigate its binding to AKIP1a and to analyze the retention time of this mutant in the nucleus. The binding to AKIP1a could be investigated by Co-IP as done for the association of the R and C subunits. Additionally, the retention time in the nucleus could be assessed by photoactivation. This method allows monitoring intracellular protein dynamics including nuclear export[233].

For the effect of the substrate specificity change of the Cα mutants, I focused on the investigation of substrates found to be hyperphosphorylated by all three tested mutants. But as the mutations are different from each other, every mutant showed a specific effect on substrate specificity. Even if a substrate is just affected by one mutant it could have a key-role in the specific mechanism of action of this mutant. Therefore, it could also be interesting to investigate the other substrates hypo- or hyperphosphorylated by the mutants. Unfortunately, for many of these substrates phosphosite-specific antibodies will not be available, as for TOM34 and CIT. Because of this, I used IP to analyze the phosphorylation status. This was unfortunately not successful. One could instead try using Phos-tag gels, as done for the analysis of H1.2. This does not allow identification of a specific phosphosite, but the total phosphorylation status of these proteins could be assessed. Identification of hyperphosphorylation of these three substrates in CPA tissue would strengthen their hypothetic role in cell proliferation and cortisol secretion.

Additionally, it would be worth determining the downstream effects of these substrate specificity changes. A good starting point would be the H1.4 serine 36 phosphosite, which is the best characterized until now. H1.4 serine 36 phosphorylation was shown to affect chromatin condensation and to be necessary in cell proliferation. It would be interesting to see whether the chromatin in CPAs with *PRKACA* mutation show a different compaction level than in *PRKACA* wild-type CPAs. Also, the HEK293T *PRKACA* L206R mutated cell line generated in this study could be used to investigate the effect of this mutation on chromatin compaction. As discussed in the introduction, PKA can have differing effects on cell proliferation. Therefore, assessment of the effect on proliferation should be studied in an adrenal cell line. It should also be considered that, in addition to the down-stream effects of H1.4 phosphorylation, other identified PKA targets could also have downstream effects leading to cortisol oversecretion and increased proliferation of adrenal cells. Therefore, the effect of phosphorylation of these phosphosites on the substrates also should be investigated. One could for example start with

generating phospho-deficient mutants of CIT, TOM34 and H1.2 (for example alanine substitution mutants) and investigate the lack of phosphorylation on cytokinesis, mitochondrial protein import and chromatin compaction respectively. Similarly, one would then investigate all the other PKA targets identified to be hypo- or hyperphosphorylated.

8 Side project: genome modification of mice using CRISPR/Cas9

Since I successfully introduced the CRISPR/Cas9 system in the lab to generate a model for L206R mutated CPAs, I took advantage of it and contributed to a project where we used this system to generate transgenic mice expressing a SNAPf-tagged metabotropic glutamate receptor 4 (mGlu4) as a basis for future studies in the lab.

8.1 Results

First, an mGlu4 construct, in which the mGlu4 signal peptide was substituted with the signal peptide of mGlu5 in combination with a HA-tag and a SNAPf-tag, was designed by me and Sana Siddig (AG Calebiro, Institute for Pharmacology, University of Würzburg) (Figure 45A). This construct was then tested for functionality by Dr. Marie-Lise Jobin (AG Calebiro, Institute for Pharmacology, University of Würzburg). In particular, inhibition of adenylate cyclase, one effector of the mGlu4, was monitored using FRET imaging of the Epac cAMP-sensor (Figure 45B). Upon cAMP production by adenylate cyclase (Figure 2), cAMP binds to the Epac cAMP-sensor, which lead to a decrease in FRET ratio[178]. The results (Figure 45B) showed a decrease of FRET ratio in response to agents inducing cAMP production, such as the adenylate cyclase activator forskolin. Inversely, in response to the activation of mGlu4 by glutamate (Glu), adenylate cyclase is inhibited, and cAMP level decreased, which in turn increased the FRET ratio. Comparison of FRET traces after stimulation of the wild-type mGlu4 receptor and the newly designed SNAPf-tagged mGlu4 receptor revealed no significant differences indicating that the new construct was functional.

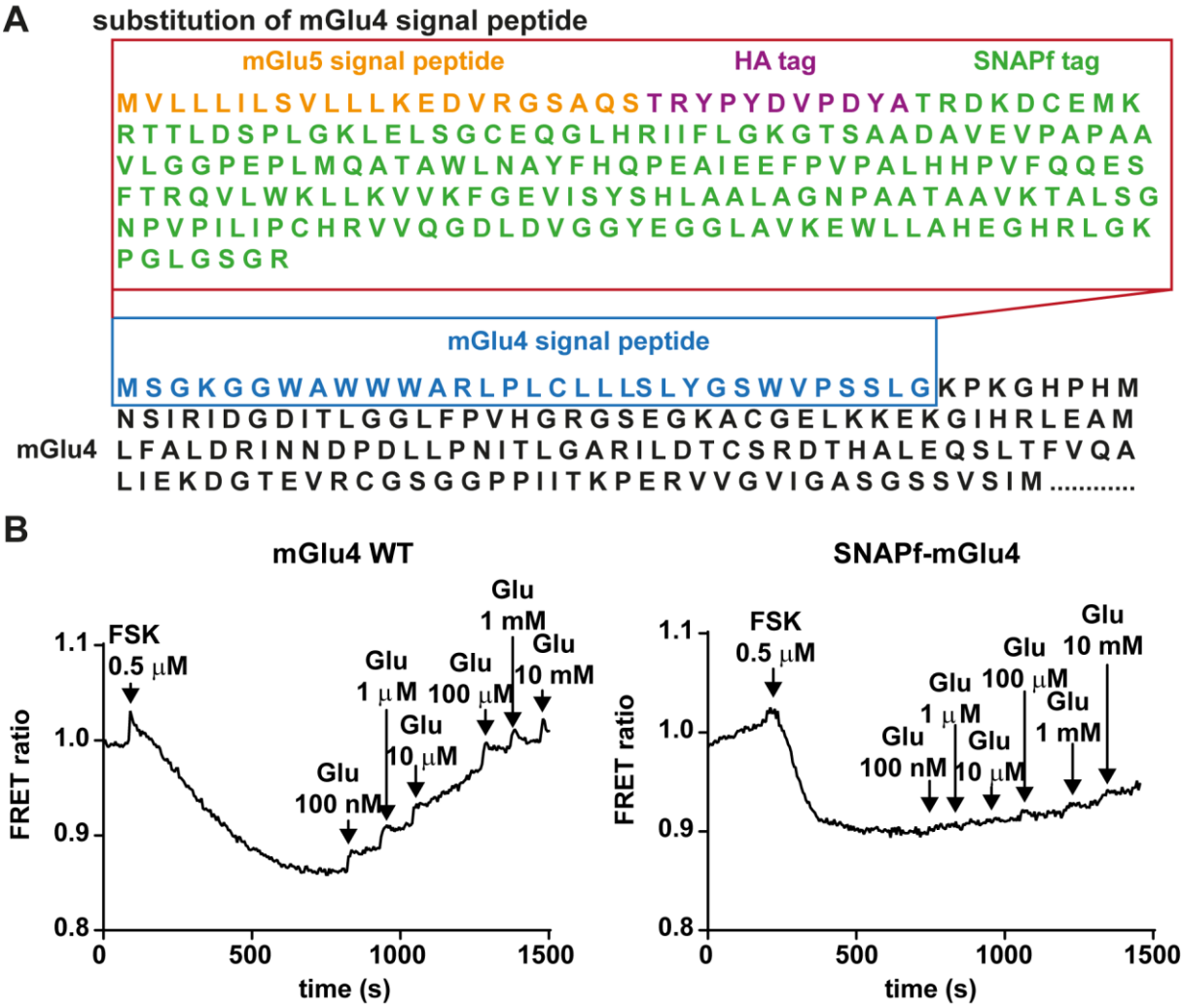

Figure 45: Functional test of mGlu4-SNAPf receptor. Shown are the sequence substitution of mGlu4 signal peptide for the generation of SNAPf -mGlu4 (A) and representative FRET traces for the functional testing of the new generated construct (right panel) in comparison with wild-type mGlu4 (left panel) using the Epac cAMP sensor (B).For maximal cAMP concentration the adenylate cyclase activator forskolin (FSK) was added. Then increasing concentration of glutamate (Glu) were added to decrease the cAMP level.

The next step was to design guides and check their efficiency. I was just able to show efficient cutting for guide 2, therefore just results for this guide are shown. First, the guides were tested for their cutting efficiency *in vitro* (Figure 46A), on PCR templates of the gene encoding for the mGlu4, and in the mouse cell line Hepa1-6 (Figure 46B). Both tests showed efficient cutting of guide 2 compared to the positive control targeting the gene encoding for hypoxanthine-guanine phosphoribosyltransferase (*HPRT*) and the control included in the EnGen Mutation Detection Kit.

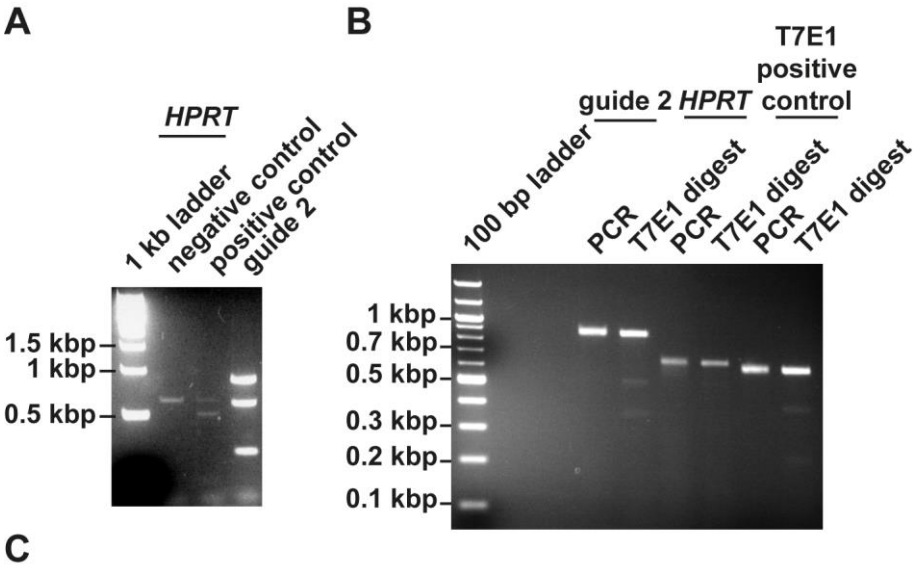

C

Sample	PCR template size (bp)	Cutted template size (bp)
guide 2	872	600, 272
HPRT control	647	512, 135
T7E1 control	600	400, 200

Figure 46: Test of guide 2 for cutting the mGlu4 gene. Shown are tests in vitro (A) and in Hepa1-6 cells transfected with an RNP complex carrying guide 2, or the positive control *HPRT* guide (B). The T7E1 positive control is a template included in the EnGen Mutation Detection Kit.

After successful tests in Hepa1-6 cells, injection of mouse zygotes (done by Daniela Östreich, Zentrum für Experimentelle Molekulare Medizin, University of Würzburg) with the repair template and the RNP complex containing the SpCas9 protein and the guide RNA was started. Those zygotes were implanted in foster mothers. Tissue samples of mice resulting from these pregnancies were taken and tested for repair template insertion. Therefore, a PCR covering the target locus was performed. The insertion of the repair template results in a larger PCR fragment than for the wild-type targeted genomic mGlu4 region. Therefore, no further digestion was necessary to reveal a successful insertion of the repair template. As shown in figure 47, one female mouse harboring the modification (S9) was obtained. It is likely that this mouse was mosaic, meaning that some tissues of this mouse harbor this modification and others not. The S9 mouse was then used for breeding to obtain mice harboring the heterozygous SNAPf-tagged mGlu4. These can then be paired to achieve homozygous mice.

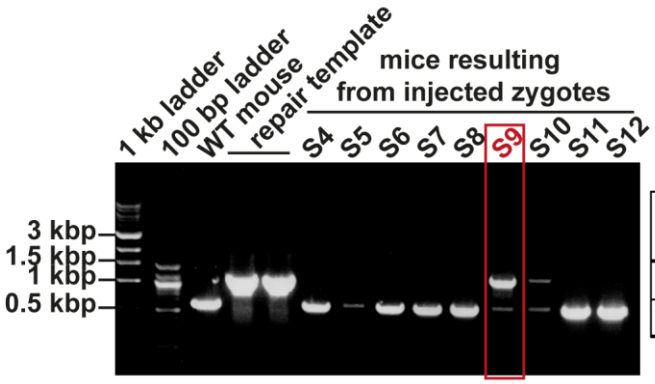

integration of repair template	PCR template size (bp)
No (WT mouse)	511 bp
Yes (SNAPf-mGlu4 mouse)	1200 bp

Figure 47: Selection of CRISPR/Cas9 modified mice. After injection of zygotes with CRISPR/Cas9, guide and repair template, zygotes were implanted in a foster mother. DNA was extracted from these progeny pups and PCR was carried out around the target locus. Insertion of the repair template results in a larger PCR fragment. Wild-type mouse was used as negative and repair template as positive control. Positive mouse (S9) is highlighted in red.

8.2 Discussion

After the successful establishment of the CRISPR/Cas9 system, we decided to generate transgenic mice expressing a SNAPf-tagged mGlu4 as a basis for future experiments in the lab. Such a mouse strain would be useful to further investigate the organization and function of mGlu4 in synapses. Therefore, it was first evaluated if the desired construct would be functional, which was assessed using FRET of an Epac cAMP-sensor. Even though, the FRET response of the tagged receptor was not as strong as the wild-type, the construct caused a reduction of cAMP which leaded to an increase in FRET of the Epac cAMP-sensor (Figure 45).

Like for genome modification in HEK293T cells, I then assessed the indel efficiency of two guides and selected the most putative. Contrary to the plasmid-based system used in HEK293T cells, we directly injected the repair template and the RNP complex comprised of the Cas9 protein, the guide and tracrRNA. This overcame the varying expression and transfection of plasmids and reduced off-targets due to the rapid degradation[234]. Out of 21 mice born after treatment of the zygotes with CRISPR/Cas9 we identified one (4.8%) with the intended insertion and two with a knock-out (9.5%). This was consistent with varying HDR efficiencies in treated zygotes[235, 236].

8.3 Outlook

Additionally, to the genome modification in HEK293T cells, I also contributed to the generation of a transgenic mouse expressing a SNAPf-tagged mGlu4, by planning the insertion and designing, testing and providing the necessary components of the CRIPSR/Cas9 system. Additionally, I was also involved in genotyping and sequencing of the resulting mice. The obtained knock-in mouse will be used for breeding to initiate a mouse strain. As soon as there are enough descendants harboring the same genomic mutation, one should investigate the expression of the SNAPf-mGlu4 in the brain of this mouse. Therefore, one would sacrifice the mouse and perform whole-animal perfusion with paraformaldehyde to fix the brain. Afterwards one would cut cerebellum slices and analyze the expression of the SNAPf-mGlu4 by immunofluorescence taking advantage of the inserted HA-tag. If the construct is expressed at comparable levels as the wild-type mGlu4 in wild-type mice and the mouse strain is stable, one would start cryo-conservation of embryos. This mouse model could then be used to investigate location and function of the mGlu4 at endogenous expression in native tissue.

9 Summary

Protein kinase A (PKA) is the main effector of cyclic-adenosine monophosphate (cAMP) and plays an important role in steroidogenesis and proliferation of adrenal cells. In a previous study we found two mutations (L206R, 199_200insW) in the main catalytic subunit of protein kinase A (PKA Cα) to be responsible for cortisol-producing adrenocortical adenomas (CPAs). These mutations interfere with the formation of a stable holoenzyme, thus causing constitutive PKA activation. More recently, we identified additional mutations affecting PKA Cα in CPAs associated with overt Cushing syndrome: S213R+insIILR, 200_201insV, W197R, d244-248+E249Q, E32V.

This study reports a functional characterization of those PKA Cα mutations linked to CPAs of Cushing's patients. All analyzed mutations except for E32V showed a reduced interaction with at least one tested regulatory (R) subunit. Interestingly the results of the activity differed among the mutants and between the assays employed. For three mutants (L206R, 199_200insW, S213R+insIILR), the results showed enhanced translocation to the nucleus. This was also observed in CRISPR/Cas9 generated *PRKACA* L206R mutated HEK293T cells. The enhanced nuclear translocation of this mutants could be due to the lack of R subunit binding, but also other mechanisms could be at play. Additionally, I used an algorithm, which predicted an effect of the mutation on substrate specificity for four mutants (L206R, 199_200insW, 200_201insV, d244-248+E249Q). This was proven using phosphoproteomics for three mutants (L206R, 200_201insV, d244-248+E249Q). In *PRKACA* L206R mutated CPAs this change in substrate specificity also caused hyperphosphorylation of H1.4 on serine 36, which has been reported to be implicated in mitosis. Due to these observations, I hypothesized, that there are several mechanisms of action of *PRKACA* mutations leading to increased cortisol secretion and cell proliferation in adrenal cells: interference with the formation of a stable holoenzyme, altered subcellular localization and a change in substrate specificity. My data indicate that some PKA Cα mutants might act via just one, others by a combination of these mechanisms. Altogether, these findings indicate that several mechanisms contribute to the development of CPAs caused by *PRKACA* mutations. Moreover, these findings provide a highly illustrative example of how alterations in a protein kinase can cause a human disease.

10 Zusammenfassung

Proteinkinase A (PKA) ist der Haupteffektor von cyclischem Adenosinmonophosphat (cAMP) und spielt eine wichtige Rolle bei der Synthese von Steroiden und der Proliferation von Nebennierenzellen. In einer vorangegangenen Studie fanden wir zwei Mutationen (L206R, 199_200insW) der wichtigsten katalytischen Untereinheit von PKA (PKA Cα), die für Kortisol sekretierende Nebennierenrindenadenome (CPAs) verantwortlich sind. Diese Mutationen stören die Bildung eines stabilen Holoenzyms und verursachen somit eine dauerhafte PKA Aktivierung. Vor Kurzem fanden wir weitere Mutationen der PKA Cα in CPAs von Patienten mit Cushing Syndrom: S213R+insIILR, 200_201insV, W197R, d244-248+E249Q, E32V.

In dieser Arbeit wurde eine funktionelle Charakterisierung dieser PKA Cα Mutanten, die im Zusammenhang mit CPAs von Cushing Patienten stehen, durchgeführt. Alle PKA Mutanten, mit Ausnahme von E32V, zeigten eine reduzierte Interaktion mit mindestens einer getesteten regulatorischen (R) Untereinheit. Interessanterweise hatten die Mutanten unterschiedliche Effekte auf die Aktivität der Kinase. Zusätzlich hatte die Analysemethode ebenfalls Einfluss auf die Aktivität der Mutanten. Für drei Mutanten (L206R, 199_200insW, S213R+insIILR) zeigten die Ergebnisse eine verstärkte Translokation der Cα Untereinheit in den Zellkern. Dies wurde auch in HEK293T Zellen bestätigt, in deren *PRKACA* Gen mittels CRISPR/Cas9 die L206R Mutation eingeführt wurde. Diese erhöhte Translokation kann durch die fehlende Bindung zur R-Untereinheit erklärt werden, aber auch andere Mechanismen könnten eine Rolle spielen. Außerdem zeigten die Ergebnisse eine Veränderung der Substratspezifität, die für vier Mutanten durch einen Algorithmus vorausberechnet wurde (L206R, 199_200insW, 200_201insV, d244-248+E249Q). Für drei dieser Mutanten (L206R, 200_201insV, d244-248+E249Q) wurde dieses Ergebnis mittels Phosphoproteomics nachgewiesen. Diese Änderung der Substratspezifität verursacht in *PRKACA* L206R mutierten CPAs auch eine Hyperphosphorylierung von H1.4 an Serin 36, welches eine wichtige Rolle in der Zellteilung spielt. Meine Ergebnisse weisen darauf hin, dass es mehrere Wirkungsmechanismen von *PRKACA* Mutationen gibt, die zu einer erhöhten Sekretion von Kortisol und Zellproliferation in Nebennierenzellen führen: Störung der Bildung eines stabilen Holoenzyms, Änderung der subzellulären Lokalisation und eine Veränderung der Substratspezifität. Meine Ergebnisse weisen darauf hin, dass einige PKA Cα-Mutanten durch nur einen, andere durch eine Kombination dieser Mechanismen wirken. Insgesamt zeigen diese Ergebnisse, dass *PRKACA* Mutationen durch mehrere Mechanismen zur Entwicklung von CPAs beitragen. Darüber hinaus liefern diese Ergebnisse ein anschauliches Beispiel dafür, wie Mutationen in einer Proteinkinase eine menschliche Krankheit verursachen können.

11 References

1. Cushing H. The Basophil Adenomas of the Pituitary Body and Their Clinical Manifestations (Pituitary Basophilism). *Obesity Research* **2**, 486-508 (1994).

2. Lonser R.R., Nieman L., Oldfield E.H. Cushing's disease: pathobiology, diagnosis, and management. *Journal of Neurosurgery* **126**, 404-417 (2017).

3. Arnaldi G., Angeli A., Atkinson A.B., Bertagna X., Cavagnini F., Chrousos G.P., Fava G.A., Findling J.W., Gaillard R.C., Grossman A.B., Kola B., Lacroix A., Mancini T., Mantero F., Newell-Price J., Nieman L.K., Sonino N., Vance M.L., Giustina A., Boscaro M. Diagnosis and complications of Cushing's syndrome: a consensus statement. *The Journal of Clinical Endocrinology & Metabolism* **88**, 5593-5602 (2003).

4. Boscaro M., Barzon L., Fallo F., Sonino N. Cushing's syndrome. *Lancet* **357**, 783-791 (2001).

5. Lindholm J., Juul S., Jorgensen J.O., Astrup J., Bjerre P., Feldt-Rasmussen U., Hagen C., Jorgensen J., Kosteljanetz M., Kristensen L., Laurberg P., Schmidt K., Weeke J. Incidence and late prognosis of cushing's syndrome: a population-based study. *The Journal of Clinical Endocrinology & Metabolism* **86**, 117-123 (2001).

6. Plotz C.M., Knowlton A.I., Ragan C. The natural history of Cushing's syndrome. *The American Journal of Medicine* **13**, 597-614 (1952).

7. Nussey S W.S. The adrenal gland. In: *Endocrinology: An Integrated Approach.* BIOS Scientific Publishers (2001).

8. Rosol T.J., Yarrington J.T., Latendresse J., Capen C.C. Adrenal gland: structure, function, and mechanisms of toxicity. *Toxicologic Pathology* **29**, 41-48 (2001).

9. Privalle C.T., Crivello J.F., Jefcoate C.R. Regulation of intramitochondrial cholesterol transfer to side-chain cleavage cytochrome P-450 in rat adrenal gland. *Proceedings of the National Academy of Sciences of the United States of America* **80**, 702-706 (1983).

10. Weber A., Kapas S., Hinson J., Grant D.B., Grossman A., Clark A.J.L. Functional characterization of the cloned human ACTH receptor: impaired responsiveness of a mutant receptor in familial glucocorticoid deficiency. *Biochemical and Biophysical Research Communications* **197**, 172-178 (1993).

11. Buckley D.I., Ramachandran J. Characterization of corticotropin receptors on adrenocortical cells. *Proceedings of the National Academy of Sciences of the United States of America* **78**, 7431-7435 (1981).

12. Robison G.A., Butcher R.W., Sutherland E.W. Cyclic AMP. *Annual Review of Biochemistry* **37**, 149-174 (1968).

13. Klainer L.M., Chi Y.M., Freidberg S.L., Rall T.W., Sutherland E.W. Adenyl cyclase. IV. The effects of neurohormones on the formation of adenosine 3',5'-phosphate by preparations from brain and other tissues. *The Journal of Biological Chemistry* **237**, 1239-1243 (1962).

14. Corbin J.D., Keely S.L., Park C.R. The distribution and dissociation of cyclic adenosine 3':5'-monophosphate-dependent protein kinases in adipose, cardiac, and other tissues. *The Journal of Biological Chemistry* **250**, 218-225 (1975).

15. Kim C., Cheng C.Y., Saldanha S.A., Taylor S.S. PKA-I holoenzyme structure reveals a mechanism for cAMP-dependent activation. *Cell* **130**, 1032-1043 (2007).

16. Arakane F., King S.R., Du Y., Kallen C.B., Walsh L.P., Watari H., Stocco D.M., Strauss J.F., 3rd. Phosphorylation of steroidogenic acute regulatory protein (StAR) modulates its steroidogenic activity. *The Journal of Biological Chemistry* **272**, 32656-32662 (1997).

17. Gonzalez G.A., Montminy M.R. Cyclic AMP stimulates somatostatin gene transcription by phosphorylation of CREB at serine 133. *Cell* **59**, 675-680 (1989).

18. Simpson E.R., Waterman M.R. Regulation of the synthesis of steroidogenic enzymes in adrenal cortical cells by ACTH. *Annual Review of Physiology* **50**, 427-440 (1988).

19. Faust J.R., Goldstein J.L., Brown M.S. Receptor-mediated uptake of low density lipoprotein and utilization of its cholesterol for steroid synthesis in cultured mouse adrenal cells. *The Journal of Biological Chemistry* **252**, 4861-4871 (1977).

20. Manna P.R., Cohen-Tannoudji J., Counis R., Garner C.W., Huhtaniemi I., Kraemer F.B., Stocco D.M. Mechanisms of action of hormone-sensitive lipase in mouse Leydig cells: its role in the regulation of the steroidogenic acute regulatory protein. *The Journal of Biological Chemistry* **288**, 8505-8518 (2013).

21. Stocco D.M. StAR protein and the regulation of steroid hormone biosynthesis. *Annual Review of Physiology* **63**, 193-213 (2001).

22. Tremblay J.J., Hamel F., Viger R.S. Protein kinase A-dependent cooperation between GATA and CCAAT/enhancer-binding protein transcription factors regulates steroidogenic acute regulatory protein promoter activity. *Endocrinology* **143**, 3935-3945 (2002).

23. Sewer M.B., Waterman M.R. Insights into the Transcriptional Regulation of Steroidogenic Enzymes and StAR. *Reviews in Endocrine and Metabolic Disorders* **2**, 269-274 (2001).

24. Chedrese P.J., Schott D., Zhang D., Murphy B.D. The Signal Transduction System in Luteotrophic Stimulation of Expression of the 3β-HSD Gene in Porcine Granulosa Cells in Culture. In: *Signaling Mechanisms and Gene Expression in the Ovary* (Ed. Gibori G.). Springer New York (1991).

25. Kagawa N., Waterman M.R. Purification and Characterization of a Transcription Factor Which Appears to Regulate Camp Responsiveness of the Human Cyp21b Gene. *The Journal of Biological Chemistry* **267**, 25213-25219 (1992).

26. Sewer M.B., Nguyen V.Q., Huang C.J., Tucker P.W., Kagawa N., Waterman M.R. Transcriptional activation of human CYP17 in H295R adrenocortical cells depends on complex formation among p54(nrb)/NonO, protein-associated splicing factor, and SF-1, a complex that also participates in repression of transcription. *Endocrinology* **143**, 1280-1290 (2002).

27. Wang X.L., Bassett M., Zhang Y., Yin S., Clyne C., White P.C., Rainey W.E. Transcriptional regulation of human 11beta-hydroxylase (hCYP11B1). *Endocrinology* **141**, 3587-3594 (2000).

28. John M.E., Simpson E.R., Waterman M.R., Mason J.I. Regulation of cholesterol side-chain cleavage cytochrome P-450 gene expression in adrenal cells in monolayer culture. *Molecular and Cellular Endocrinology* **45**, 197-204 (1986).

29. Pescador N., Houde A., Stocco D.M., Murphy B.D. Follicle-stimulating hormone and intracellular second messengers regulate steroidogenic acute regulatory protein messenger ribonucleic acid in luteinized porcine granulosa cells. *Biology of Reproduction* **57**, 660-668 (1997).

30. Balasubramanian K., LaVoie H.A., Garmey J.C., Stocco D.M., Veldhuis J.D. Regulation of porcine granulosa cell steroidogenic acute regulatory protein (StAR) by insulin-like growth factor I: synergism with follicle-stimulating hormone or protein kinase A agonist. *Endocrinology* **138**, 433-439 (1997).

31. Fujita T., Meguro T., Fukuyama R., Nakamuta H., Koida M. New signaling pathway for parathyroid hormone and cyclic AMP action on extracellular-regulated kinase and cell proliferation in bone cells. Checkpoint of modulation by cyclic AMP. *The Journal of Biological Chemistry* **277**, 22191-22200 (2002).

32. de Rooij J., Zwartkruis F.J., Verheijen M.H., Cool R.H., Nijman S.M., Wittinghofer A., Bos J.L. Epac is a Rap1 guanine-nucleotide-exchange factor directly activated by cyclic AMP. *Nature* **396**, 474-477 (1998).

33. Vossler M.R., Yao H., York R.D., Pan M.G., Rim C.S., Stork P.J.S. cAMP activates MAP kinase and Elk-1 through a B-Raf- and Rap1-dependent pathway. *Cell* **89**, 73-82 (1997).

34. Schmitt J.M., Stork P.J. PKA phosphorylation of Src mediates cAMP's inhibition of cell growth via Rap1. *Molecular Cell* **9**, 85-94 (2002).

35. Takahashi H., Honma M., Miyauchi Y., Nakamura S., Ishida-Yamamoto A., Iizuka H. Cyclic AMP differentially regulates cell proliferation of normal human keratinocytes through ERK activation depending on the expression pattern of B-Raf. *Archives of Dermatological Research* **296**, 74 (2004).

36. Morice C., Nothias F., König S., Vernier P., Baccarini M., Vincent J.-D., Barnier J.V. Raf-1 and B-Raf proteins have similar regional distributions but differential subcellular localization in adult rat brain. *European Journal of Neuroscience* **11**, 1995-2006 (1999).

37. Dugan L.L., Kim J.S., Zhang Y., Bart R.D., Sun Y., Holtzman D.M., Gutmann D.H. Differential effects of cAMP in neurons and astrocytes. Role of B-raf. *The Journal of Biological Chemistry* **274**, 25842-25848 (1999).

38. Kievit P., Lauten J.D., Maurer R.A. Analysis of the role of the mitogen-activated protein kinase in mediating cyclic-adenosine 3',5'-monophosphate effects on prolactin promoter activity. *Molecular Endocrinology* **15**, 614-624 (2001).

39. Iacovelli L., Capobianco L., Salvatore L., Sallese M., D'Ancona G.M., De Blasi A. Thyrotropin activates mitogen-activated protein kinase pathway in FRTL-5 by a cAMP-

dependent protein kinase A-independent mechanism. *Molecular Pharmacology* **60**, 924-933 (2001).

40. Buscà R., Abbe P., Mantoux F., Aberdam E., Peyssonnaux C., Eychène A., Ortonne J.-P., Ballotti R. Ras mediates the cAMP-dependent activation of extracellular signal-regulated kinases (ERKs) in melanocytes. *The EMBO Journal* **19**, 2900-2910 (2000).

41. Wojnowski L., Zimmer A.M., Beck T.W., Hahn H., Bernal R., Rapp U.R., Zimmer A. Endothelial apoptosis in Braf-deficient mice. *Nature Genetics* **16**, 293 (1997).

42. Chen T., Cho R.W., Stork P.J.S., Weber M.J. Elevation of Cyclic Adenosine 3′,5′-Monophosphate Potentiates Activation of Mitogen-activated Protein Kinase by Growth Factors in LNCaP Prostate Cancer Cells. *Cancer Research* **59**, 213-218 (1999).

43. Stork P.J., Schmitt J.M. Crosstalk between cAMP and MAP kinase signaling in the regulation of cell proliferation. *Trends in Cell Biology* **12**, 258-266 (2002).

44. Sevetson B.R., Kong X., Lawrence J.C., Jr. Increasing cAMP attenuates activation of mitogen-activated protein kinase. *Proceedings of the National Academy of Sciences of the United States of America* **90**, 10305-10309 (1993).

45. New M., Yau M., Lekarev O., Lin-Su K., Parsa A., Pina C., Yuen T., Khattab A. Congenital Adrenal Hyperplasia. In: *Endotext* (Ed. De Groot L. J.*, et al.*). MDText.com, Inc. (2000).

46. Elias L.L., Huebner A., Pullinger G.D., Mirtella A., Clark A.J.L. Functional characterization of naturally occurring mutations of the human adrenocorticotropin receptor: poor correlation of phenotype and genotype. *The Journal of Clinical Endocrinology & Metabolism* **84**, 2766-2770 (1999).

47. Metherell L.A., Chapple J.P., Cooray S., David A., Becker C., Ruschendorf F., Naville D., Begeot M., Khoo B., Nurnberg P., Huebner A., Cheetham M.E., Clark A.J.L. Mutations in MRAP, encoding a new interacting partner of the ACTH receptor, cause familial glucocorticoid deficiency type 2. *Nature Genetics* **37**, 166 (2005).

48. Clark A.J.L., Chan L.F., Chung T.-T., Metherell L.A. The genetics of familial glucocorticoid deficiency. *Best Practice & Research Clinical Endocrinology & Metabolism* **23**, 159-165 (2009).

49. Chida D., Nakagawa S., Nagai S., Sagara H., Katsumata H., Imaki T., Suzuki H., Mitani F., Ogishima T., Shimizu C., Kotaki H., Kakuta S., Sudo K., Koike T., Kubo M., Iwakura Y. Melanocortin 2 receptor is required for adrenal gland development, steroidogenesis, and neonatal gluconeogenesis. *Proceedings of the National Academy of Sciences of the United States of America* **104**, 18205-18210 (2007).

50. Yaswen L., Diehl N., Brennan M.B., Hochgeschwender U. Obesity in the mouse model of pro-opiomelanocortin deficiency responds to peripheral melanocortin. *Nature Medicine* **5**, 1066 (1999).

51. Coll A.P., Challis B.G., Yeo G.S., Snell K., Piper S.J., Halsall D., Thresher R.R., O'Rahilly S. The effects of proopiomelanocortin deficiency on murine adrenal development and responsiveness to adrenocorticotropin. *Endocrinology* **145**, 4721-4727 (2004).

52. Karpac J., Ostwald D., Bui S., Hunnewell P., Shankar M., Hochgeschwender U. Development, maintenance, and function of the adrenal gland in early postnatal proopiomelanocortin-null mutant mice. *Endocrinology* **146**, 2555-2562 (2005).

53. E. S.P. Hypophysectomy and a replacement therapy in the rat. *American Journal of Anatomy* **45**, 205-273 (1930).

54. Dallman M.F., Engeland W.C., Holzwarth M.A., Scholz P.M. Adrenocorticotropin inhibits compensatory adrenal growth after unilateral adrenalectomy. *Endocrinology* **107**, 1397-1404 (1980).

55. Ramachandran J., Suyama A.T. Inhibition of replication of normal adrenocortical cells in culture by adrenocorticotropin. *Proceedings of the National Academy of Sciences of the United States of America* **72**, 113-117 (1975).

56. Masui H., Garren L.D. Inhibition of replication in functional mouse adrenal tumor cells by adrenocorticotropic hormone mediated by adenosine 3':5'-cyclic monophosphate. *Proceedings of the National Academy of Sciences of the United States of America* **68**, 3206-3210 (1971).

57. Hornsby P.J., Gill G.N. Hormonal-Control of Adrenocortical Cell-Proliferation - Desensitization to Acth and Interaction between Acth and Fibroblast Growth-Factor in Bovine Adrenocortical Cell-Cultures. *Journal of Clinical Investigation* **60**, 342-352 (1977).

58. Propper D.J., Saunders M.P., Salisbury A.J., Long L., O'Byrne K.J., Braybrooke J.P., Dowsett M., Taylor M., Talbot D.C., Ganesan T.S., Harris A.L. Phase I study of the novel cyclic AMP (cAMP) analogue 8-chloro-cAMP in patients with cancer: toxicity, hormonal, and immunological effects. *Clinical Cancer Research* **5**, 1682-1689 (1999).

59. Cho-Chung Y.S., Clair T., Tortora G., Yokozaki H., Pepe S. Suppression of malignancy targeting the intracellular signal transducing proteins of cAMP: The use of site-selective cAMP analogs, antisense strategy, and gene transfer. *Life Sciences* **48**, 1123-1132 (1991).

60. Cho-Chung Y.S., Clair T., Tagliaferri P., Ally S., Katsaros D., Tortora G., Neckers L., Avery T.L., Crabtree G.W., Robins R.K. Site-Selective Cyclic AMP Analogs as New Biological Tools in Growth Control, Differentiation, and Proto-oncogene Regulation. *Cancer Investigation* **7**, 161-177 (1989).

61. Fassnacht M., Hahner S., Hansen I.A., Kreutzberger T., Zink M., Adermann K., Jakob F., Troppmair J., Allolio B. N-terminal proopiomelanocortin acts as a mitogen in adrenocortical tumor cells and decreases adrenal steroidogenesis. *The Journal of Clinical Endocrinology & Metabolism* **88**, 2171-2179 (2003).

62. Lania A.G., Mantovani G., Spada A. Mechanisms of disease: Mutations of G proteins and G-protein-coupled receptors in endocrine diseases. *Nature Clinical Practice Endocrinology & Metabolism* **2**, 681-693 (2006).

63. Lyons J., Landis C.A., Harsh G., Vallar L., Grunewald K., Feichtinger H., Duh Q.Y., Clark O.H., Kawasaki E., Bourne H.R., et al. Two G protein oncogenes in human endocrine tumors. *Science* **249**, 655-659 (1990).

64. Parma J., Duprez L., Van Sande J., Cochaux P., Gervy C., Mockel J., Dumont J., Vassart G. Somatic mutations in the thyrotropin receptor gene cause hyperfunctioning thyroid adenomas. *Nature* **365**, 649-651 (1993).

65. Vallar L., Spada A., Giannattasio G. Altered Gs and adenylate cyclase activity in human GH-secreting pituitary adenomas. *Nature* **330**, 566-568 (1987).

66. Landis C.A., Masters S.B., Spada A., Pace A.M., Bourne H.R., Vallar L. GTPase inhibiting mutations activate the alpha chain of Gs and stimulate adenylyl cyclase in human pituitary tumours. *Nature* **340**, 692-696 (1989).

67. Weinstein L.S., Shenker A., Gejman P.V., Merino M.J., Friedman E., Spiegel A.M. Activating mutations of the stimulatory G protein in the McCune-Albright syndrome. *New England Journal of Medicine* **325**, 1688-1695 (1991).

68. Carney J.A., Young W.F., Stratakis C.A. Primary bimorphic adrenocortical disease: cause of hypercortisolism in McCune-Albright syndrome. *The American Journal of Surgical Pathology* **35**, 1311-1326 (2011).

69. Kirschner L.S., Carney J.A., Pack S.D., Taymans S.E., Giatzakis C., Cho Y.S., Cho-Chung Y.S., Stratakis C.A. Mutations of the gene encoding the protein kinase A type I-alpha regulatory subunit in patients with the Carney complex. *Nature Genetics* **26**, 89-92 (2000).

70. Espiard S., Ragazzon B., Bertherat J. Protein kinase A alterations in adrenocortical tumors. *Hormone and Metabolic Research* **46**, 869-875 (2014).

71. Shenker A., Laue L., Kosugi S., Merendino Jr J.J., Minegishi T., Cutler Jr G.B. A constitutively activating mutation of the luteinizing hormone receptor in familial male precocious puberty. *Nature* **365**, 652 (1993).

72. Kremer H., Mariman E., Otten B.J., Moll J.G.W., Stoellnga G.B.A., Wit J.M., Jansen M., Drop S.L., Faas B., Ropers H.-H., Brunner H.G. Cosegregation of missense mutations of the luteinizing hormone receptor gene with familial male-limited precocious puberty. *Human Molecular Genetics* **2**, 1779-1783 (1993).

73. Abramowicz M.J., Duprez L., Parma J., Vassart G., Heinrichs C. Familial congenital hypothyroidism due to inactivating mutation of the thyrotropin receptor causing profound hypoplasia of the thyroid gland. *Journal of Clinical Investigation* **99**, 3018-3024 (1997).

74. Sunthornthepvarakui T., Gottschalk M.E., Hayashi Y., Refetoff S. Brief report: resistance to thyrotropin caused by mutations in the thyrotropin-receptor gene. *New England Journal of Medicine* **332**, 155-160 (1995).

75. Fragoso M.C., Domenice S., Latronico A.C., Martin R.M., Pereira M.A., Zerbini M.C., Lucon A.M., Mendonca B.B. Cushing's syndrome secondary to adrenocorticotropin-independent macronodular adrenocortical hyperplasia due to activating mutations of *GNAS1* gene. *The Journal of Clinical Endocrinology & Metabolism* **88**, 2147-2151 (2003).

76. Hu Q., Shokat K.M. Disease-Causing Mutations in the G Protein Galphas Subvert the Roles of GDP and GTP. *Cell* **173**, 1254-1264 e1211 (2018).

77. Weinstein L.S., Gejman P.V., Friedman E., Kadowaki T., Collins R.M., Gershon E.S., Spiegel A.M. Mutations of the Gs alpha-subunit gene in Albright hereditary osteodystrophy detected by denaturing gradient gel electrophoresis. *Proceedings of the National Academy of Sciences of the United States of America* **87**, 8287-8290 (1990).

78. McCune D.J. Osteodystrophia Fibrosa. *American Journal of Diseases of Children* **54**, 806 (1937).

79. Sutherland E.W., Rall T.W. Fractionation and characterization of a cyclic adenine ribonucleotide formed by tissue particles. *The Journal of Biological Chemistry* **232**, 1077-1092 (1958).

80. Szarek E., Stratakis C.A. Phosphodiesterases and adrenal Cushing in mice and humans. *Hormone and Metabolic Research* **46**, 863-868 (2014).

81. Horvath A., Boikos S., Giatzakis C., Robinson-White A., Groussin L., Griffin K.J., Stein E., Levine E., Delimpasi G., Hsiao H.P., Keil M., Heyerdahl S., Matyakhina L., Libe R., Fratticci A., Kirschner L.S., Cramer K., Gaillard R.C., Bertagna X., Carney J.A., Bertherat J., Bossis I., Stratakis C.A. A genome-wide scan identifies mutations in the gene encoding phosphodiesterase 11A4 (PDE11A) in individuals with adrenocortical hyperplasia. *Nature Genetics* **38**, 794 (2006).

82. Carney J.A., Gordon H., Carpenter P.C., Shenoy B.V., Go V.L. The complex of myxomas, spotty pigmentation, and endocrine overactivity. *Medicine (Baltimore)* **64**, 270-283 (1985).

83. Greene E.L., Horvath A.D., Nesterova M., Giatzakis C., Bossis I., Stratakis C.A. In vitro functional studies of naturally occurring pathogenic *PRKAR1A* mutations that are not subject to nonsense mRNA decay. *Human Mutation* **29**, 633-639 (2008).

84. Bataille M.G., Rhayem Y., Sousa S.B., Libe R., Dambrun M., Chevalier C., Nigou M., Auzan C., North M.O., Sa J., Gomes L., Salpea P., Horvath A., Stratakis C.A., Hamzaoui N., Bertherat J., Clauser E. Systematic screening for *PRKAR1A* gene rearrangement in Carney complex: identification and functional characterization of a new in-frame deletion. *European Journal of Endocrinology* **170**, 151-160 (2014).

85. Groussin L., Jullian E., Perlemoine K., Louvel A., Leheup B., Luton J.P., Bertagna X., Bertherat J. Mutations of the *PRKAR1A* gene in Cushing's syndrome due to sporadic primary pigmented nodular adrenocortical disease. *The Journal of Clinical Endocrinology & Metabolism* **87**, 4324-4329 (2002).

86. Meoli E., Bossis I., Cazabat L., Mavrakis M., Horvath A., Stergiopoulos S., Shiferaw M.L., Fumey G., Perlemoine K., Muchow M., Robinson-White A., Weinberg F., Nesterova M., Patronas Y., Groussin L., Bertherat J., Stratakis C.A. Protein kinase A effects of an expressed *PRKAR1A* mutation associated with aggressive tumors. *Cancer Research* **68**, 3133-3141 (2008).

87. Linglart A., Menguy C., Couvineau A., Auzan C., Gunes Y., Cancel M., Motte E., Pinto G., Chanson P., Bougneres P., Clauser E., Silve C. Recurrent *PRKAR1A* mutation in acrodysostosis with hormone resistance. *New England Journal of Medicine* **364**, 2218-2226 (2011).

88. Rhayem Y., Le Stunff C., Abdel Khalek W., Auzan C., Bertherat J., Linglart A., Couvineau A., Silve C., Clauser E. Functional Characterization of *PRKAR1A* Mutations Reveals a Unique Molecular Mechanism Causing Acrodysostosis but Multiple Mechanisms Causing Carney Complex. *The Journal of Biological Chemistry* **290**, 27816-27828 (2015).

89. Beuschlein F., Fassnacht M., Assié G., Calebiro D., Stratakis C.A., Osswald A., Ronchi C.L., Wieland T., Sbiera S., Faucz F.R., Schaak K., Schmittfull A., Schwarzmayr T., Barreau O., Vezzosi D., Rizk-Rabin M., Zabel U., Szarek E., Salpea P., Forlino A., Vetro A., Zuffardi O., Kisker C., Diener S., Meitinger T., Lohse M.J., Reincke M., Bertherat J., Strom T.M., Allolio B. Constitutive activation of PKA catalytic subunit in adrenal Cushing's syndrome. *New England Journal of Medicine* **370**, 1019-1028 (2014).

90. Cao Y., He M., Gao Z., Peng Y., Li Y., Li L., Zhou W., Li X., Zhong X., Lei Y., Su T., Wang H., Jiang Y., Yang L., Wei W., Yang X., Jiang X., Liu L., He J., Ye J., Wei Q., Li Y., Wang W., Wang J., Ning G. Activating hotspot L205R mutation in *PRKACA* and adrenal Cushing’s syndrome. *Science* **344**, 913-917 (2014).

91. Goh G., Scholl U.I., Healy J.M., Choi M., Prasad M.L., Nelson-Williams C., Kunstman J.W., Korah R., Suttorp A.C., Dietrich D., Haase M., Willenberg H.S., Stalberg P., Hellman P., Akerstrom G., Bjorklund P., Carling T., Lifton R.P. Recurrent activating

mutation in *PRKACA* in cortisol-producing adrenal tumors. *Nature Genetics* **46**, 613-617 (2014).

92. Sato Y., Maekawa S., Ishii R., Sanada M., Morikawa T., Shiraishi Y., Yoshida K., Nagata Y., Sato-Otsubo A., Yoshizato T., Suzuki H., Shiozawa Y., Kataoka K., Kon A., Aoki K., Chiba K., Tanaka H., Kume H., Miyano S., Fukayama M., Nureki O., Homma Y., Ogawa S. Recurrent somatic mutations underlie corticotropin-independent Cushing's syndrome. *Science* **344**, 917-920 (2014).

93. Di Dalmazi G., Kisker C., Calebiro D., Mannelli M., Canu L., Arnaldi G., Quinkler M., Rayes N., Tabarin A., Laure Jullie M., Mantero F., Rubin B., Waldmann J., Bartsch D.K., Pasquali R., Lohse M., Allolio B., Fassnacht M., Beuschlein F., Reincke M. Novel somatic mutations in the catalytic subunit of the protein kinase A as a cause of adrenal Cushing's syndrome: a European multicentric study. *The Journal of Clinical Endocrinology & Metabolism* **99**, E2093-2100 (2014).

94. Ronchi C.L., Di Dalmazi G., Faillot S., Sbiera S., Assie G., Weigand I., Calebiro D., Schwarzmayr T., Appenzeller S., Rubin B., Waldmann J., Scaroni C., Bartsch D.K., Mantero F., Mannelli M., Kastelan D., Chiodini I., Bertherat J., Reincke M., Strom T.M., Fassnacht M., Beuschlein F. Genetic Landscape of Sporadic Unilateral Adrenocortical Adenomas Without *PRKACA* p.Leu206Arg Mutation. *The Journal of Clinical Endocrinology & Metabolism* **101**, 3526-3538 (2016).

95. Honeyman J.N., Simon E.P., Robine N., Chiaroni-Clarke R., Darcy D.G., Lim, II, Gleason C.E., Murphy J.M., Rosenberg B.R., Teegan L., Takacs C.N., Botero S., Belote R., Germer S., Emde A.K., Vacic V., Bhanot U., LaQuaglia M.P., Simon S.M. Detection of a recurrent *DNAJB1-PRKACA* chimeric transcript in fibrolamellar hepatocellular carcinoma. *Science* **343**, 1010-1014 (2014).

96. Pierce K.L., Premont R.T., Lefkowitz R.J. Seven-transmembrane receptors. *Nature Reviews Molecular Cell Biology* **3**, 639-650 (2002).

97. Taylor S.S., Ilouz R., Zhang P., Kornev A.P. Assembly of allosteric macromolecular switches: lessons from PKA. *Nature Reviews Molecular Cell Biology* **13**, 646-658 (2012).

98. Diskar M., Zenn H.-M., Kaupisch A., Kaufholz M., Brockmeyer S., Sohmen D., Berrera M., Zaccolo M., Boshart M., Herberg F.W., Prinz A. Regulation of cAMP-dependent

protein kinases: The human protein kinase X (PrKX) reveals the role of the catalytic subunit αH-αI loop. *The Journal of Biological Chemistry* **285**, 35910-35918 (2010).

99. Zimmermann B., Chiorini J.A., Ma Y.L., Kotin R.M., Herberg F.W. PrKX is a novel catalytic subunit of the cAMP-dependent protein kinase regulated by the regulatory subunit type I. *The Journal of Biological Chemistry* **274**, 5370-5378 (1999).

100. Taylor S.S., Buechler J.A., Yonemoto W. cAMP-dependent protein kinase: framework for a diverse family of regulatory enzymes. *Annual Review of Biochemistry* **59**, 971-1005 (1990).

101. Zhang P., Smith-Nguyen E.V., Keshwani M.M., Deal M.S., Kornev A.P., Taylor S.S. Structure and allostery of the PKA RIIbeta tetrameric holoenzyme. *Science* **335**, 712-716 (2012).

102. Bossis I., Stratakis C.A. Minireview: *PRKAR1A*: normal and abnormal functions. *Endocrinology* **145**, 5452-5458 (2004).

103. Johnson D.A., Akamine P., Radzio-Andzelm E., Madhusudan M., Taylor S.S. Dynamics of cAMP-dependent protein kinase. *Chemical Reviews* **101**, 2243-2270 (2001).

104. Knighton D.R., Zheng J.H., Ten Eyck L.F., Ashford V.A., Xuong N.H., Taylor S.S., Sowadski J.M. Crystal structure of the catalytic subunit of cyclic adenosine monophosphate-dependent protein kinase. *Science* **253**, 407-414 (1991).

105. Taylor S.S., Zhang P., Steichen J.M., Keshwani M.M., Kornev A.P. PKA: lessons learned after twenty years. *Biochimica et Biophysica Acta (BBA) - Proteins and Proteomics* **1834**, 1271-1278 (2013).

106. Carr D.W., Stofko-Hahn R.E., Fraser I.D., Bishop S.M., Acott T.S., Brennan R.G., Scott J.D. Interaction of the regulatory subunit (RII) of cAMP-dependent protein kinase with RII-anchoring proteins occurs through an amphipathic helix binding motif. *The Journal of Biological Chemistry* **266**, 14188-14192 (1991).

107. Kinderman F.S., Kim C., von Daake S., Ma Y., Pham B.Q., Spraggon G., Xuong N.H., Jennings P.A., Taylor S.S. A dynamic mechanism for AKAP binding to RII isoforms of cAMP-dependent protein kinase. *Molecular Cell* **24**, 397-408 (2006).

108. Herberg F.W., Maleszka A., Eide T., Vossebein L., Tasken K. Analysis of A-kinase anchoring protein (AKAP) interaction with protein kinase A (PKA) regulatory subunits: PKA isoform specificity in AKAP binding. *Journal of Molecular Biology* **298**, 329-339 (2000).

109. Carr D.W., Stofko-Hahn R.E., Fraser I.D., Cone R.D., Scott J.D. Localization of the cAMP-dependent protein kinase to the postsynaptic densities by A-kinase anchoring proteins. Characterization of AKAP 79. *The Journal of Biological Chemistry* **267**, 16816-16823 (1992).

110. Means C.K., Lygren B., Langeberg L.K., Jain A., Dixon R.E., Vega A.L., Gold M.G., Petrosyan S., Taylor S.S., Murphy A.N., Ha T., Santana L.F., Tasken K., Scott J.D. An entirely specific type I A-kinase anchoring protein that can sequester two molecules of protein kinase A at mitochondria. *Proceedings of the National Academy of Sciences of the United States of America* **108**, E1227-E1235 (2011).

111. Burgers P.P., Ma Y., Margarucci L., Mackey M., van der Heyden M.A., Ellisman M., Scholten A., Taylor S.S., Heck A.J. A small novel A-kinase anchoring protein (AKAP) that localizes specifically protein kinase A-regulatory subunit I (PKA-RI) to the plasma membrane. *The Journal of Biological Chemistry* **287**, 43789-43797 (2012).

112. Bachmann V.A., Mayrhofer J.E., Ilouz R., Tschaikner P., Raffeiner P., Röck R., Courcelles M., Apelt F., Lu T.-W., Baillie G.S., Thibault P., Aanstad P., Stelzl U., Taylor S.S., Stefan E. Gpr161 anchoring of PKA consolidates GPCR and cAMP signaling. *Proceedings of the National Academy of Sciences of the United States of America* **113**, 7786-7791 (2016).

113. Huang L.J.S., Durick K., Weiner J.A., Chun J., Taylor S.S. Identification of a novel protein kinase A anchoring protein that binds both type I and type II regulatory subunits. *The Journal of Biological Chemistry* **272**, 8057-8064 (1997).

114. Kim C., Xuong N.H., Taylor S.S. Crystal structure of a complex between the catalytic and regulatory (RIalpha) subunits of PKA. *Science* **307**, 690-696 (2005).

115. Cheng X., Phelps C., Taylor S.S. Differential binding of cAMP-dependent protein kinase regulatory subunit isoforms Ialpha and IIbeta to the catalytic subunit. *The Journal of Biological Chemistry* **276**, 4102-4108 (2001).

116. Herberg F.W., Taylor S.S., Dostmann W.R. Active site mutations define the pathway for the cooperative activation of cAMP-dependent protein kinase. *Biochemistry* **35**, 2934-2942 (1996).

117. Smith C.M., Radzio-Andzelm E., Madhusudan, Akamine P., Taylor S.S. The catalytic subunit of cAMP-dependent protein kinase: prototype for an extended network of communication. *Progress in Biophysics & Molecular Biology* **71**, 313-341 (1999).

118. Uchiyama T., Uchida T., Wen J.W., Walker D.H. Demonstration of heat-labile and heat-stable epitopes of Rickettsia japonica on ultrathin sections. *Laboratory Investigation* **71**, 432-437 (1994).

119. Hanks S.K., Quinn A.M., Hunter T. The protein kinase family: conserved features and deduced phylogeny of the catalytic domains. *Science* **241**, 42-52 (1988).

120. Barker W.C., Dayhoff M.O. Viral src gene products are related to the catalytic chain of mammalian cAMP-dependent protein kinase. *Proceedings of the National Academy of Sciences of the United States of America* **79**, 2836-2839 (1982).

121. Bastidas A.C., Deal M.S., Steichen J.M., Guo Y., Wu J., Taylor S.S. Phosphoryl transfer by protein kinase A is captured in a crystal lattice. *Journal of the American Chemical Society* **135**, 4788-4798 (2013).

122. Bastidas A.C., Wu J., Taylor S.S. Molecular Features of Product Release for the PKA Catalytic Cycle. *Biochemistry* **54**, 2-10 (2015).

123. Das A., Gerlits O., Parks J.M., Langan P., Kovalevsky A., Heller W.T. Protein Kinase A Catalytic Subunit Primed for Action: Time-Lapse Crystallography of Michaelis Complex Formation. *Structure* **23**, 2331-2340 (2015).

124. Yonemoto W., Garrod S.M., Bell S.M., Taylor S.S. Identification of phosphorylation sites in the recombinant catalytic subunit of cAMP-dependent protein kinase. *The Journal of Biological Chemistry* **268**, 18626-18632 (1993).

125. Shoji S., Titani K., Demaille J.G., Fischer E.H. Sequence of two phosphorylated sites in the catalytic subunit of bovine cardiac muscle adenosine 3':5'-monophosphate-dependent protein kinase. *The Journal of Biological Chemistry* **254**, 6211-6214 (1979).

126. Toner-Webb J., van Patten S.M., Walsh D.A., Taylor S.S. Autophosphorylation of the catalytic subunit of cAMP-dependent protein kinase. *The Journal of Biological Chemistry* **267**, 25174-25180 (1992).

127. Shen J., Smith R.A., Stoll V.S., Edalji R., Jakob C., Walter K., Gramling E., Dorwin S., Bartley D., Gunasekera A., Yang J., Holzman T., Johnson R.W. Characterization of protein kinase A phosphorylation: multi-technique approach to phosphate mapping. *Analytical Biochemistry* **324**, 204-218 (2004).

128. Yonemoto W., McGlone M.L., Grant B., Taylor S.S. Autophosphorylation of the catalytic subunit of cAMP-dependent protein kinase in Escherichia coli. *Protein Engineering* **10**, 915-925 (1997).

129. Breitenlechner C., Engh R.A., Huber R., Kinzel V., Bossemeyer D., Gassel M. The typically disordered N-terminus of PKA can fold as a helix and project the myristoylation site into solution. *Biochemistry* **43**, 7743-7749 (2004).

130. Taylor S.S., Yang J., Wu J., Haste N.M., Radzio-Andzelm E., Anand G. PKA: a portrait of protein kinase dynamics. *Biochimica et Biophysica Acta (BBA) - Proteins and Proteomics* **1697**, 259-269 (2004).

131. Herberg F.W., Taylor S.S. Physiological inhibitors of the catalytic subunit of cAMP-dependent protein kinase: effect of MgATP on protein-protein interactions. *Biochemistry* **32**, 14015-14022 (1993).

132. Corbin J.D., Keely S.L., Soderling T.R., Park C.R. Hormonal regulation of adenosine 3',5'-monophosphate-dependent protein kinase. *Advances in Cyclic Nucleotide Research* **5**, 265-279 (1975).

133. Kovalevsky A.Y., Johnson H., Hanson B.L., Waltman M.J., Fisher S.Z., Taylor S., Langan P. Low- and room-temperature X-ray structures of protein kinase A ternary complexes shed new light on its activity. *Acta Crystallographica Section D Biological Crystallography* **68**, 854-860 (2012).

134. Cheng X., Shaltiel S., Taylor S.S. Mapping substrate-induced conformational changes in cAMP-dependent protein kinase by protein footprinting. *Biochemistry* **37**, 14005-14013 (1998).

135. Madhusudan, Akamine P., Xuong N.H., Taylor S.S. Crystal structure of a transition state mimic of the catalytic subunit of cAMP-dependent protein kinase. *Nature Structural Biology* **9**, 273-277 (2002).

136. Gerlits O., Tian J., Das A., Langan P., Heller W.T., Kovalevsky A. Phosphoryl Transfer Reaction Snapshots in Crystals: insights into the mechanism of protein kinase A catalytic subunit. *The Journal of Biological Chemistry* **290**, 15538-15548 (2015).

137. Valiev M., Kawai R., Adams J.A., Weare J.H. The role of the putative catalytic base in the phosphoryl transfer reaction in a protein kinase: first-principles calculations. *Journal of the American Chemical Society* **125**, 9926-9927 (2003).

138. Cheng Y., Zhang Y., McCammon J.A. How does the cAMP-dependent protein kinase catalyze the phosphorylation reaction: an ab initio QM/MM study. *Journal of the American Chemical Society* **127**, 1553-1562 (2005).

139. Valiev M., Yang J., Adams J.A., Taylor S.S., Weare J.H. Phosphorylation reaction in cAPK protein kinase-free energy quantum mechanical/molecular mechanics simulations. *The Journal of Physical Chemistry B* **111**, 13455-13464 (2007).

140. Khavrutskii I.V., Grant B., Taylor S.S., McCammon J.A. A transition path ensemble study reveals a linchpin role for Mg(2+) during rate-limiting ADP release from protein kinase A. *Biochemistry* **48**, 11532-11545 (2009).

141. Zhou J., Adams J.A. Participation of ADP dissociation in the rate-determining step in cAMP-dependent protein kinase. *Biochemistry* **36**, 15733-15738 (1997).

142. Grant B.D., Adams J.A. Pre-steady-state kinetic analysis of cAMP-dependent protein kinase using rapid quench flow techniques. *Biochemistry* **35**, 2022-2029 (1996).

143. Gibson R.M., Taylor S.S. Dissecting the cooperative reassociation of the regulatory and catalytic subunits of cAMP-dependent protein kinase. Role of Trp-196 in the catalytic subunit. *The Journal of Biological Chemistry* **272**, 31998-32005 (1997).

144. Rhayem Y., Perez-Rivas L.G., Dietz A., Bathon K., Gebhard C., Riester A., Mauracher B., Gomez-Sanchez C., Eisenhofer G., Schwarzmayr T., Calebiro D., Strom T.M., Reincke M., Beuschlein F. *PRKACA* Somatic Mutations Are Rare Findings in Aldosterone-Producing Adenomas. *The Journal of Clinical Endocrinology & Metabolism* **101**, 3010-3017 (2016).

145. Espiard S., Knape M.J., Bathon K., Assie G., Rizk-Rabin M., Faillot S., Luscap-Rondof W., Abid D., Guignat L., Calebiro D., Herberg F.W., Stratakis C.A., Bertherat J. Activating *PRKACB* somatic mutation in cortisol-producing adenomas. *JCI Insight* **3**, (2018).

146. Calebiro D., Hannawacker A., Lyga S., Bathon K., Zabel U., Ronchi C., Beuschlein F., Reincke M., Lorenz K., Allolio B., Kisker C., Fassnacht M., Lohse M.J. PKA catalytic subunit mutations in adrenocortical Cushing's adenoma impair association with the regulatory subunit. *Nature Communications* **5**, 5680 (2014).

147. Cheung J., Ginter C., Cassidy M., Franklin M.C., Rudolph M.J., Robine N., Darnell R.B., Hendrickson W.A. Structural insights into mis-regulation of protein kinase A in human tumors. *Proceedings of the National Academy of Sciences of the United States of America* **112**, 1374-1379 (2015).

148. Lubner J.M., Dodge-Kafka K.L., Carlson C.R., Church G.M., Chou M.F., Schwartz D. Cushing's syndrome mutant PKA(L205R) exhibits altered substrate specificity. *FEBS Letters* **591**, 459-467 (2017).

149. Luzi N.M., Lyons C.E., Peterson D.L., Ellis K.C. Kinetics and inhibition studies of the L205R mutant of cAMP-dependent protein kinase involved in Cushing's syndrome. *FEBS Open Bio* **8**, 606-613 (2018).

150. Lee S.R., Sang L., Yue D.T. Uncovering aberrant mutant PKA function with flow cytometric FRET. *Cell reports* **14**, 3019-3029 (2016).

151. Mantovani G., Lania A.G., Bondioni S., Peverelli E., Pedroni C., Ferrero S., Pellegrini C., Vicentini L., Arnaldi G., Bosari S., Beck-Peccoz P., Spada A. Different expression of protein kinase A (PKA) regulatory subunits in cortisol-secreting adrenocortical tumors: relationship with cell proliferation. *Experimental Cell Research* **314**, 123-130 (2008).

152. Vincent-Dejean C., Cazabat L., Groussin L., Perlemoine K., Fumey G., Tissier F., Bertagna X., Bertherat J. Identification of a clinically homogenous subgroup of benign cortisol-secreting adrenocortical tumors characterized by alterations of the protein kinase A (PKA) subunits and high PKA activity. *European Journal of Endocrinology* **158**, 829-839 (2008).

153. Weigand I., Ronchi C.L., Rizk-Rabin M., Dalmazi G.D., Wild V., Bathon K., Rubin B., Calebiro D., Beuschlein F., Bertherat J., Fassnacht M., Sbiera S. Differential

expression of the protein kinase A subunits in normal adrenal glands and adrenocortical adenomas. *Scientific Reports* **7**, 49 (2017).

154. Calebiro D., Di Dalmazi G., Bathon K., Ronchi C.L., Beuschlein F. cAMP signaling in cortisol producing adrenal adenoma. *European Journal of Endocrinology* **173**, M99-106 (2015).

155. Orellana S.A., McKnight G.S. Mutations in the catalytic subunit of cAMP-dependent protein kinase result in unregulated biological activity. *Proceedings of the National Academy of Sciences of the United States of America* **89**, 4726-4730 (1992).

156. Orellana S.A., Amieux P.S., Zhao X., McKnight G.S. Mutations in the catalytic subunit of the cAMP-dependent protein kinase interfere with holoenzyme formation without disrupting inhibition by protein kinase inhibitor. *The Journal of Biological Chemistry* **268**, 6843-6846 (1993).

157. Thiel A., Reis A.C., Haase M., Goh G., Schott M., Willenberg H.S., Scholl U.I. *PRKACA* mutations in cortisol-producing adenomas and adrenal hyperplasia: a single-center study of 60 cases. *European Journal of Endocrinology* **172**, 677-685 (2015).

158. Nakajima Y., Okamura T., Gohko T., Satoh T., Hashimoto K., Shibusawa N., Ozawa A., Ishii S., Tomaru T., Horiguchi K., Okada S., Takata D., Rokutanda N., Horiguchi J., Tsushima Y., Oyama T., Takeyoshi I., Yamada M. Somatic mutations of the catalytic subunit of cyclic AMP-dependent protein kinase (*PRKACA*) gene in Japanese patients with several adrenal adenomas secreting cortisol. *Endocrine Journal* **61**, 825-832 (2014).

159. El-Serag H.B., Davila J.A. Is fibrolamellar carcinoma different from hepatocellular carcinoma? A US population-based study. *Hepatology* **39**, 798-803 (2004).

160. Weeda V.B., Murawski M., McCabe A.J., Maibach R., Brugieres L., Roebuck D., Fabre M., Zimmermann A., Otte J.B., Sullivan M., Perilongo G., Childs M., Brock P., Zsiros J., Plaschkes J., Czauderna P., Aronson D.C. Fibrolamellar variant of hepatocellular carcinoma does not have a better survival than conventional hepatocellular carcinoma--results and treatment recommendations from the Childhood Liver Tumour Strategy Group (SIOPEL) experience. *European Journal of Cancer* **49**, 2698-2704 (2013).

161. Engelholm L.H., Riaz A., Serra D., Dagnaes-Hansen F., Johansen J.V., Santoni-Rugiu E., Hansen S.H., Niola F., Frodin M. CRISPR/Cas9 Engineering of Adult Mouse Liver Demonstrates That the *Dnajb1-Prkaca* Gene Fusion Is Sufficient to Induce Tumors

162

Resembling Fibrolamellar Hepatocellular Carcinoma. *Gastroenterology* **153**, 1662-1673.e1610 (2017).

162. Mulatero P., Stowasser M., Loh K.C., Fardella C.E., Gordon R.D., Mosso L., Gomez-Sanchez C.E., Veglio F., Young W.F., Jr. Increased diagnosis of primary aldosteronism, including surgically correctable forms, in centers from five continents. *The Journal of Clinical Endocrinology & Metabolism* **89**, 1045-1050 (2004).

163. Schirpenbach C., Reincke M. Primary aldosteronism: current knowledge and controversies in Conn's syndrome. *Nature Clinical Practice Endocrinology & Metabolism* **3**, 220-227 (2007).

164. Rossi G.P., Bernini G., Caliumi C., Desideri G., Fabris B., Ferri C., Ganzaroli C., Giacchetti G., Letizia C., Maccario M., Mallamaci F., Mannelli M., Mattarello M.J., Moretti A., Palumbo G., Parenti G., Porteri E., Semplicini A., Rizzoni D., Rossi E., Boscaro M., Pessina A.C., Mantero F. A prospective study of the prevalence of primary aldosteronism in 1,125 hypertensive patients. *Journal of the American College of Cardiology* **48**, 2293-2300 (2006).

165. Cox S., Taylor S.S. Holoenzyme interaction sites in the cAMP-dependent protein kinase. Histidine 87 in the catalytic subunit complements serine 99 in the type I regulatory subunit. *The Journal of Biological Chemistry* **269**, 22614-22622 (1994).

166. Zaccolo M., Pozzan T. Discrete microdomains with high concentration of cAMP in stimulated rat neonatal cardiac myocytes. *Science* **295**, 1711-1715 (2002).

167. Ran F.A., Hsu P.D., Wright J., Agarwala V., Scott D.A., Zhang F. Genome engineering using the CRISPR-Cas9 system. *Nature Protocols* **8**, 2281-2308 (2013).

168. Shechter D., Dormann H.L., Allis C.D., Hake S.B. Extraction, purification and analysis of histones. *Nature Protocols* **2**, 1445-1457 (2007).

169. Kinoshita E., Kinoshita-Kikuta E., Takiyama K., Koike T. Phosphate-binding Tag, a New Tool to Visualize Phosphorylated Proteins. *Molecular & Cellular Proteomics* **5**, 749-757 (2006).

170. Ishino Y., Shinagawa H., Makino K., Amemura M., Nakata A. Nucleotide sequence of the iap gene, responsible for alkaline phosphatase isozyme conversion in Escherichia coli, and identification of the gene product. *Journal of Bacteriology* **169**, 5429-5433 (1987).

171. Bolotin A., Quinquis B., Sorokin A., Ehrlich S.D. Clustered regularly interspaced short palindrome repeats (CRISPRs) have spacers of extrachromosomal origin. *Microbiology* **151**, 2551-2561 (2005).

172. Mojica F.J., Diez-Villasenor C., Garcia-Martinez J., Soria E. Intervening sequences of regularly spaced prokaryotic repeats derive from foreign genetic elements. *Journal of Molecular Evolution* **60**, 174-182 (2005).

173. Horvath P., Barrangou R. CRISPR/Cas, the immune system of bacteria and archaea. *Science* **327**, 167-170 (2010).

174. Jinek M., Chylinski K., Fonfara I., Hauer M., Doudna J.A., Charpentier E. A programmable dual-RNA-guided DNA endonuclease in adaptive bacterial immunity. *Science* **337**, 816-821 (2012).

175. Cong L., Ran F.A., Cox D., Lin S., Barretto R., Habib N., Hsu P.D., Wu X., Jiang W., Marraffini L.A., Zhang F. Multiplex genome engineering using CRISPR/Cas systems. *Science* **339**, 819-823 (2013).

176. Makarova K.S., Haft D.H., Barrangou R., Brouns S.J.J., Charpentier E., Horvath P., Moineau S., Mojica F.J.M., Wolf Y.I., Yakunin A.F., van der Oost J., Koonin E.V. Evolution and classification of the CRISPR–Cas systems. *Nature Reviews Microbiology* **9**, 467-477 (2011).

177. Gasiunas G., Barrangou R., Horvath P., Siksnys V. Cas9–crRNA ribonucleoprotein complex mediates specific DNA cleavage for adaptive immunity in bacteria. *Proceedings of the National Academy of Sciences of the United States of America* **109**, E2579-E2586 (2012).

178. Nikolaev V.O., Bunemann M., Hein L., Hannawacker A., Lohse M.J. Novel single chain cAMP sensors for receptor-induced signal propagation. *The Journal of Biological Chemistry* **279**, 37215-37218 (2004).

179. Sarma R., Barney B.M., Keable S., Dean D.R., Seefeldt L.C., Peters J.W. Insights into substrate binding at FeMo-cofactor in nitrogenase from the structure of an alpha-70(Ile) MoFe protein variant. *Journal of Inorganic Biochemistry* **104**, 385-389 (2010).

180. Safaei J., Manuch J., Gupta A., Stacho L., Pelech S. Prediction of 492 human protein kinase substrate specificities. *Proteome Science* **9**, 1-13 (2011).

181. Cox J., Mann M. MaxQuant enables high peptide identification rates, individualized p.p.b.-range mass accuracies and proteome-wide protein quantification. *Nature Biotechnology* **26**, 1367-1372 (2008).

182. Tokuji Ikenaka (Sakai) T.M.Y., Yasuki Hamazume (Obama) Peptide derivatives and activity measuring method of physiologically active substances using the same as substrates Patent 5120644 (1992).

183. Berthon A., Sahut-Barnola I., Lambert-Langlais S., de Joussineau C., Damon-Soubeyrand C., Louiset E., Taketo M.M., Tissier F., Bertherat J., Lefrancois-Martinez A.M., Martinez A., Val P. Constitutive beta-catenin activation induces adrenal hyperplasia and promotes adrenal cancer development. *Human Molecular Genetics* **19**, 1561-1576 (2010).

184. Tadjine M., Lampron A., Ouadi L., Horvath A., Stratakis C.A., Bourdeau I. Detection of somatic beta-catenin mutations in primary pigmented nodular adrenocortical disease (PPNAD). *Clinical Endocrinology* **69**, 367-373 (2008).

185. Tissier F., Cavard C., Groussin L., Perlemoine K., Fumey G., Hagnere A.M., Rene-Corail F., Jullian E., Gicquel C., Bertagna X., Vacher-Lavenu M.C., Perret C., Bertherat J. Mutations of beta-catenin in adrenocortical tumors: activation of the Wnt signaling pathway is a frequent event in both benign and malignant adrenocortical tumors. *Cancer Research* **65**, 7622-7627 (2005).

186. Morin P.J. β-catenin signaling and cancer. *BioEssays* **21**, 1021-1030 (1999).

187. Fang X., Yu S.X., Lu Y., Bast R.C., Jr., Woodgett J.R., Mills G.B. Phosphorylation and inactivation of glycogen synthase kinase 3 by protein kinase A. *Proceedings of the National Academy of Sciences of the United States of America* **97**, 11960-11965 (2000).

188. Taurin S., Sandbo N., Qin Y., Browning D., Dulin N.O. Phosphorylation of beta-catenin by cyclic AMP-dependent protein kinase. *The Journal of Biological Chemistry* **281**, 9971-9976 (2006).

189. Rainey W.E., Saner K., Schimmer B.P. Adrenocortical cell lines. *Molecular and Cellular Endocrinology* **228**, 23-38 (2004).

190. Hantel C., Beuschlein F. Xenograft models for adrenocortical carcinoma. *Molecular and Cellular Endocrinology* **421**, 28-33 (2016).

191. Meinkoth J.L., Ji Y., Taylor S.S., Feramisco J.R. Dynamics of the distribution of cyclic AMP-dependent protein kinase in living cells. *Proceedings of the National Academy of Sciences of the United States of America* **87**, 9595-9599 (1990).

192. Brown S.H.J., Wu J., Kim C., Alberto K., Taylor S.S. Novel isoform-specific interfaces revealed by PKA RIIbeta holoenzyme structures. *Journal of Molecular Biology* **393**, 1070-1082 (2009).

193. Brown S.H.J., Cheng C.Y., Saldanha S.A., Wu J., Cottam H.B., Sankaran B., Taylor S.S. Implementing fluorescence anisotropy screening and crystallographic analysis to define PKA isoform-selective activation by cAMP analogs. *American Chemical Society Chemical Biology* **8**, 2164-2172 (2013).

194. Hsu P.D., Scott D.A., Weinstein J.A., Ran F.A., Konermann S., Agarwala V., Li Y., Fine E.J., Wu X., Shalem O., Cradick T.J., Marraffini L.A., Bao G., Zhang F. DNA targeting specificity of RNA-guided Cas9 nucleases. *Nature Biotechnology* **31**, 827-832 (2013).

195. Saleh-Gohari N., Helleday T. Conservative homologous recombination preferentially repairs DNA double-strand breaks in the S phase of the cell cycle in human cells. *Nucleic Acids Research* **32**, 3683-3688 (2004).

196. Mali P., Yang L., Esvelt K.M., Aach J., Guell M., DiCarlo J.E., Norville J.E., Church G.M. RNA-guided human genome engineering via Cas9. *Science* **339**, 823-826 (2013).

197. Chu V.T., Weber T., Wefers B., Wurst W., Sander S., Rajewsky K., Kühn R. Increasing the efficiency of homology-directed repair for CRISPR-Cas9-induced precise gene editing in mammalian cells. *Nature Biotechnology* **33**, 543 (2015).

198. Maruyama T., Dougan S.K., Truttmann M.C., Bilate A.M., Ingram J.R., Ploegh H.L. Increasing the efficiency of precise genome editing with CRISPR-Cas9 by inhibition of nonhomologous end joining. *Nature Biotechnology* **33**, 538 (2015).

199. Ran F.A., Hsu P.D., Lin C.Y., Gootenberg J.S., Konermann S., Trevino A.E., Scott D.A., Inoue A., Matoba S., Zhang Y., Zhang F. Double nicking by RNA-guided CRISPR Cas9 for enhanced genome editing specificity. *Cell* **154**, 1380-1389 (2013).

200. Kleinstiver B.P., Pattanayak V., Prew M.S., Tsai S.Q., Nguyen N.T., Zheng Z., Joung J.K. High-fidelity CRISPR–Cas9 nucleases with no detectable genome-wide off-target effects. *Nature* **529**, 490 (2016).

201. R.M. R., C. C., S.M. L., M. B., G. K. Identification of a high affinity binding protein for the regulatory subunit RII beta of cAMP-dependent protein kinase in Golgi enriched membranes of human lymphoblasts. *The EMBO Journal* **11**, 1723-1731 (1992).

202. Ally S., Tortora G., Clair T., Grieco D., Merlo G., Katsaros D., Ogreid D., Døskeland S.O., Jahnsen T., Cho-Chung Y.S. Selective modulation of protein kinase isozymes by the site-selective analog 8-chloroadenosine 3',5'-cyclic monophosphate provides a biological means for control of human colon cancer cell growth. *Proceedings of the National Academy of Sciences of the United States of America* **85**, 6319-6322 (1988).

203. Coghlan V.M., Langeberg L.K., Fernandez A., Lamb N.J., Scott J.D. Cloning and characterization of AKAP 95, a nuclear protein that associates with the regulatory subunit of type II cAMP-dependent protein kinase. *The Journal of Biological Chemistry* **269**, 7658-7665 (1994).

204. Budillon A., Cereseto A., Kondrashin A., Nesterova M., Merlo G., Clair T., Cho-Chung Y.S. Point mutation of the autophosphorylation site or in the nuclear location signal causes protein kinase A RII beta regulatory subunit to lose its ability to revert transformed fibroblasts. *Proceedings of the National Academy of Sciences of the United States of America* **92**, 10634-10638 (1995).

205. Constantinescu A., Gordon A.S., Diamond I. cAMP-dependent protein kinase types I and II differentially regulate cAMP response element-mediated gene expression: implications for neuronal responses to ethanol. *The Journal of Biological Chemistry* **277**, 18810-18816 (2002).

206. Thiele T.E., Willis B., Stadler J., Reynolds J.G., Bernstein I.L., McKnight G.S. High ethanol consumption and low sensitivity to ethanol-induced sedation in protein kinase A-mutant mice. *Journal of Neuroscience* **20**, RC75 (2000).

207. Wand G., Levine M., Zweifel L., Schwindinger W., Abel T. The cAMP–Protein Kinase A Signal Transduction Pathway Modulates Ethanol Consumption and Sedative Effects of Ethanol. *The Journal of Neuroscience* **21**, 5297-5303 (2001).

208. Hoffman P.L., Tabakoff B. Ethanol and guanine nucleotide binding proteins: a selective interaction. *The FASEB Journal* **4**, 2612-2622 (1990).

209. Paolillo M., Feliciello A., Porcellini A., Garbi C., Bifulco M., Schinelli S., Ventra C., Stabile E., Ricciardelli G., Schettini G., Avvedimento E.V. The type and the localization of cAMP-dependent protein kinase regulate transmission of cAMP signals to the

nucleus in cortical and cerebellar granule cells. *The Journal of Biological Chemistry* **274**, 6546-6552 (1999).

210. Feliciello A., Li Y., Avvedimento E.V., Gottesman M.E., Rubin C.S. A-kinase anchor protein 75 increases the rate and magnitude of cAMP signaling to the nucleus. *Current Biology* **7**, 1011-1014 (1997).

211. Neary C.L., Cho-Chung Y.S. Nuclear translocation of the catalytic subunit of protein kinase A induced by an antisense oligonucleotide directed against the RIalpha regulatory subunit. *Oncogene* **20**, 8019-8024 (2001).

212. Harootunian A.T., Adams S.R., Wen W., Meinkoth J.L., Taylor S.S., Tsien R.Y. Movement of the free catalytic subunit of cAMP-dependent protein kinase into and out of the nucleus can be explained by diffusion. *Molecular Biology of the Cell* **4**, 993-1002 (1993).

213. Sastri M., Barraclough D.M., Carmichael P.T., Taylor S.S. A-kinase-interacting protein localizes protein kinase A in the nucleus. *Proceedings of the National Academy of Sciences of the United States of America* **102**, 349-354 (2005).

214. Sastri M., Haushalter K.J., Panneerselvam M., Chang P., Fridolfsson H., Finley J.C., Ng D., Schilling J.M., Miyanohara A., Day M.E., Hakozaki H., Petrosyan S., Koller A., King C.C., Darshi M., Blumenthal D.K., Ali S.S., Roth D.M., Patel H.H., Taylor S.S. A kinase interacting protein (AKIP1) is a key regulator of cardiac stress. *Proceedings of the National Academy of Sciences of the United States of America* **110**, E387-E396 (2013).

215. Fantozzi D.A., Harootunian A.T., Wen W., Taylor S.S., Feramisco J.R., Tsien R.Y., Meinkoth J.L. Thermostable inhibitor of cAMP-dependent protein kinase enhances the rate of export of the kinase catalytic subunit from the nucleus. *The Journal of Biological Chemistry* **269**, 2676-2686 (1994).

216. Wiley J.C., Wailes L.A., Idzerda R.L., McKnight G.S. Role of regulatory subunits and protein kinase inhibitor (PKI) in determining nuclear localization and activity of the catalytic subunit of protein kinase A. *The Journal of Biological Chemistry* **274**, 6381-6387 (1999).

217. Sarg B., Helliger W., Talasz H., Forg B., Lindner H.H. Histone H1 phosphorylation occurs site-specifically during interphase and mitosis: identification of a novel

phosphorylation site on histone H1. *The Journal of Biological Chemistry* **281**, 6573-6580 (2006).

218. Chu C.S., Hsu P.H., Lo P.W., Scheer E., Tora L., Tsai H.J., Tsai M.D., Juan L.J. Protein kinase A-mediated serine 35 phosphorylation dissociates histone H1.4 from mitotic chromosome. *The Journal of Biological Chemistry* **286**, 35843-35851 (2011).

219. Lamb N.J., Cavadore J.C., Labbe J.C., Maurer R.A., Fernandez A. Inhibition of cAMP-dependent protein kinase plays a key role in the induction of mitosis and nuclear envelope breakdown in mammalian cells. *The EMBO Journal* **10**, 1523-1533 (1991).

220. Wisniewski J.R., Zougman A., Kruger S., Mann M. Mass spectrometric mapping of linker histone H1 variants reveals multiple acetylations, methylations, and phosphorylation as well as differences between cell culture and tissue. *Molecular & Cellular Proteomics* **6**, 72-87 (2007).

221. Garcia B.A., Busby S.A., Barber C.M., Shabanowitz J., Allis C.D., Hunt D.F. Characterization of phosphorylation sites on histone H1 isoforms by tandem mass spectrometry. *Journal of Proteome Research* **3**, 1219-1227 (2004).

222. Nuttall S.D., Hanson B.J., Mori M., Hoogenraad N.J. hTom34: a novel translocase for the import of proteins into human mitochondria. *DNA and Cell Biology* **16**, 1067-1074 (1997).

223. Faou P., Hoogenraad N.J. Tom34: A cytosolic cochaperone of the Hsp90/Hsp70 protein complex involved in mitochondrial protein import. *Biochimica et Biophysica Acta (BBA) - Molecular Cell Research* **1823**, 348-357 (2012).

224. Schmidt O., Harbauer A.B., Rao S., Eyrich B., Zahedi R.P., Stojanovski D., Schonfisch B., Guiard B., Sickmann A., Pfanner N., Meisinger C. Regulation of mitochondrial protein import by cytosolic kinases. *Cell* **144**, 227-239 (2011).

225. Di Cunto F., Calautti E., Hsiao J., Ong L., Topley G., Turco E., Dotto G.P. Citron rho-interacting kinase, a novel tissue-specific ser/thr kinase encompassing the Rho-Rac-binding protein Citron. *The Journal of Biological Chemistry* **273**, 29706-29711 (1998).

226. Yamashiro S., Totsukawa G., Yamakita Y., Sasaki Y., Madaule P., Ishizaki T., Narumiya S., Matsumura F. Citron kinase, a Rho-dependent kinase, induces di-phosphorylation of regulatory light chain of myosin II. *Molecular Biology of the Cell* **14**, 1745-1756 (2003).

227. Gruneberg U., Neef R., Li X., Chan E.H., Chalamalasetty R.B., Nigg E.A., Barr F.A. KIF14 and citron kinase act together to promote efficient cytokinesis. *The Journal of Cell Biology* **172**, 363-372 (2006).

228. Wu Z., Zhu X., Xu W., Zhang Y., Chen L., Qiu F., Zhang B., Wu L., Peng Z., Tang H. Up-regulation of CIT promotes the growth of colon cancer cells. *Oncotarget* **8**, 71954-71964 (2017).

229. Kanczkowski W., Tymoszuk P., Chavakis T., Janitzky V., Weirich T., Zacharowski K., Ehrhart-Bornstein M., Bornstein S.R. Upregulation of TLR2 and TLR4 in the human adrenocortical cells differentially modulates adrenal steroidogenesis. *Molecular and Cellular Endocrinology* **336**, 41-46 (2011).

230. Wang T., Rainey W.E. Human adrenocortical carcinoma cell lines. *Molecular and Cellular Endocrinology* **351**, 58-65 (2012).

231. Leibovitz A., McCombs W.M., 3rd, Johnston D., McCoy C.E., Stinson J.C. New human cancer cell culture lines. I. SW-13, small-cell carcinoma of the adrenal cortex. *Journal of the National Cancer Institute* **51**, 691-697 (1973).

232. Almeida M.Q., Fragoso M.C., Lotfi C.F., Santos M.G., Nishi M.Y., Costa M.H., Lerario A.M., Maciel C.C., Mattos G.E., Jorge A.A., Mendonca B.B., Latronico A.C. Expression of insulin-like growth factor-II and its receptor in pediatric and adult adrenocortical tumors. *The Journal of Clinical Endocrinology & Metabolism* **93**, 3524-3531 (2008).

233. Patterson G.H., Lippincott-Schwartz J. A Photoactivatable GFP for Selective Photolabeling of Proteins and Cells. *Science* **297**, 1873-1877 (2002).

234. Kim S., Kim D., Cho S.W., Kim J., Kim J.S. Highly efficient RNA-guided genome editing in human cells via delivery of purified Cas9 ribonucleoproteins. *Genome Research* **24**, 1012-1019 (2014).

235. Zhang L., Jia R., Palange N.J., Satheka A.C., Togo J., An Y., Humphrey M., Ban L., Ji Y., Jin H., Feng X., Zheng Y. Large genomic fragment deletions and insertions in mouse using CRISPR/Cas9. *PLoS One* **10**, e0120396 (2015).

236. Wang L., Shao Y., Guan Y., Li L., Wu L., Chen F., Liu M., Chen H., Ma Y., Ma X., Liu M., Li D. Large genomic fragment deletion and functional gene cassette knock-in via Cas9 protein mediated genome editing in one-cell rodent embryos. *Scientific Reports* **5**, 17517 (2015).

12 Annex

12.1 Amino acid standard abbreviations

Amino acid	3-letter code	1-letter code
Alanine	Ala	A
Arginine	Arg	R
Asparagine	Asn	N
Aspartic acid	Asp	D
Cysteine	Cys	C
Glutamic acid	Glu	E
Glutamine	Gln	Q
Glycine	Gly	G
Histidine	His	H
Isoleucine	Ile	I
Leucine	Leu	L
Lysine	Lys	K
Methionine	Met	M
Phenylalanine	Phe	F
Proline	Pro	P
Serine	Ser	S
Threonine	Thr	T
Tryptophan	Trp	W
Tyrosine	Tyr	Y
Valine	Val	V
Any amino acid		X

12.2 Nucleobases standard abbreviations

Nucleobase	1-letter code
Adenine	A
Guanine	G
Cytosine	C
Thymine	T

12.3 Plasmid maps

12.3.1 Regulatory subunit

The architecture is the same for both RIα and RIIβ subunit.

Regulatory subunit without tags:

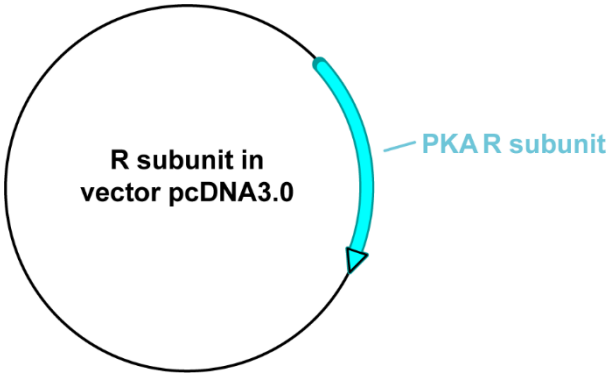

Regulatory subunit with FLAG-tag:

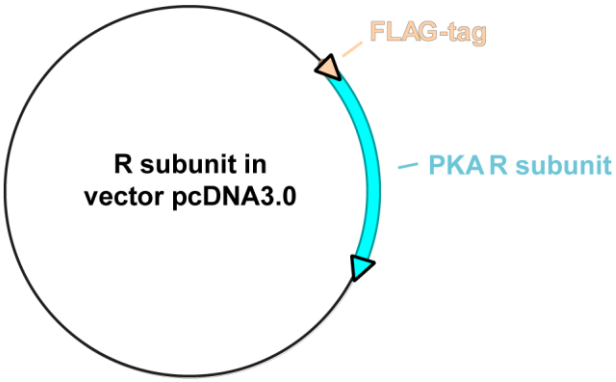

Regulatory subunit with CFP-tag:

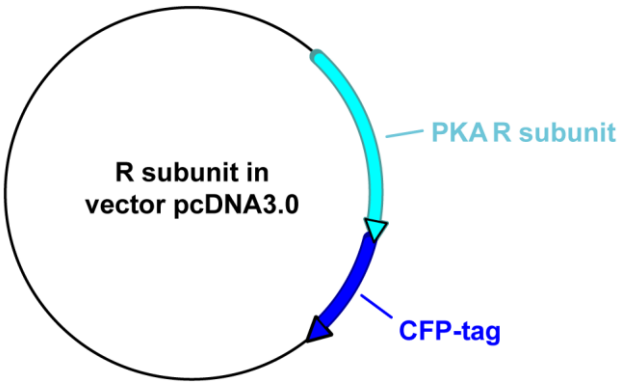

12.3.2 Catalytic subunit

The architecture is the same Cα wild-type and mutants.

Cα subunit without tags:

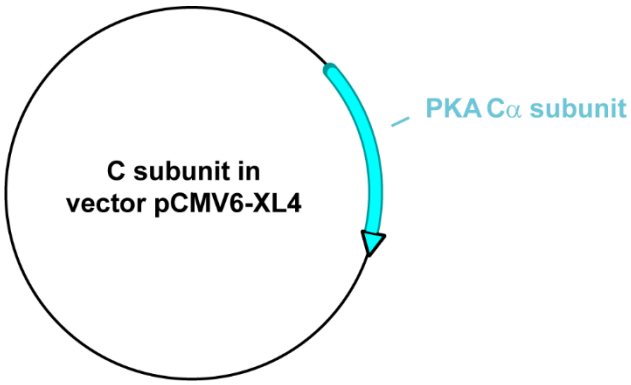

Cα subunit with YFP-tag:

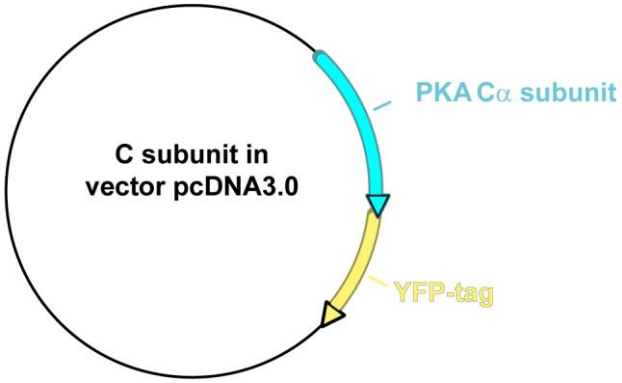

12.3.3 CRISPR/Cas9

PX458-pSpCas9(BB)-2A-GFP for CRISPR/Cas9 genome modification of cells:

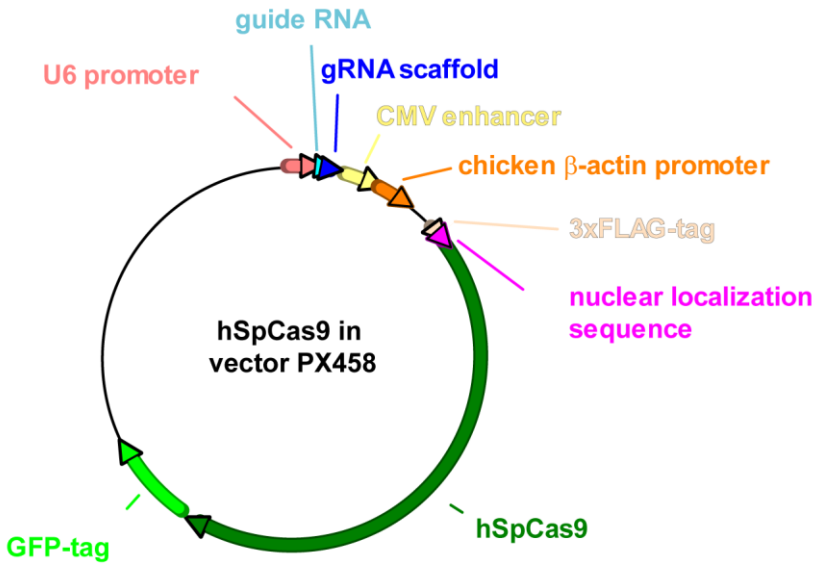

12.3.4 mGlu4 constructs

mGlu4 wild-type:

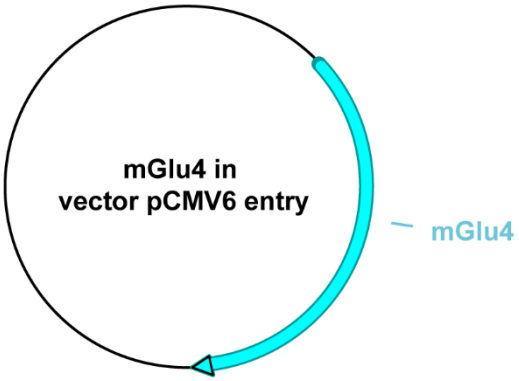

mGlu4-SNAPf:

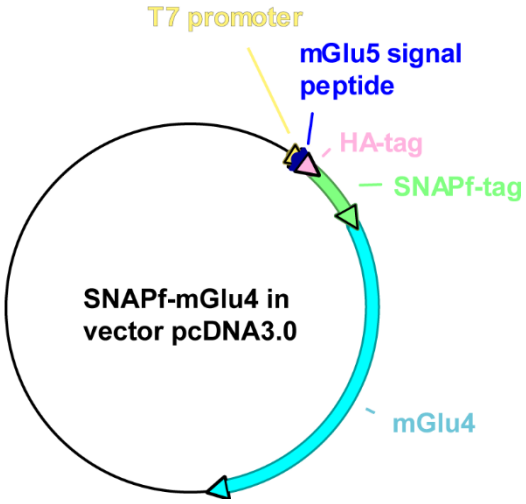

13 Curriculum Vitae

Publications

Espiard S., Knape M.J., **Bathon K.**, Assié G., Rizk-Rabin M., Faillot S., Luscap-Rondof W., Abid D., Guignat L., Calebiro D., Herberg F.W., Stratakis C.A. and Bertherat J. Activating *PRKACB* somatic mutation in cortisol-producing adenomas. *JCI Insight*, 2018, **3**.

Weigand I., Ronchi C.L., Rizk-Rabin M., Dalmazi G.D., Wild V., **Bathon K.**, Rubin B., Calebiro D., Beuschlein F., Bertherat J., Fassnacht M., and Sbiera S. Differential Expression of the Protein Kinase a Subunits in Normal Adrenal Glands and Adrenocortical Adenomas. *Scientific Reports,* 2017, **7**, 49

Calebiro D., **Bathon K.** & Weigand I. Mechanisms of Aberrant PKA Activation by Cα Subunit Mutations. *Hormone and Metabolic Research,* 2016.

Calebiro D., Grassi E.S., Eszlinger M., Ronchi C.L., Godbole A., **Bathon K.**, Guizzardi F., de Filippis T., Krohn K., Jaeschke H., Schwarzmayr T., Bircan R., Gozu H.I., Sancak S., Niedziela M., Strom T.M., Fassnacht M., Persani L. & Paschke R. Recurrent EZH1 mutations are a second hit in autonomous thyroid adenomas. *Journal of Clinical Investigation,* 2016, **126**, 3383-3388.

Rhayem Y., Perez-Rivas L.G., Dietz A., **Bathon K.**, Gebhard C., Riester A., Mauracher B., Gomez-Sanchez C., Eisenhofer G., Schwarzmayr T., Calebiro D., Strom T.M., Reincke M. & Beuschlein F. *PRKACA* Somatic Mutations Are Rare Findings in Aldosterone-Producing Adenomas. *Journal of Clinical Endocrinology and Metabolism,* 2016, **101**, 3010-3017.

Calebiro D., Di Dalmazi G., **Bathon K.**, Ronchi C.L. & Beuschlein F. cAMP signaling in cortisol-producing adrenal adenoma. *European Journal of Endocrinology,* 2015, **173**, M99-106.

Calebiro D., Hannawacker A., Lyga S., **Bathon K.**, Zabel U., Ronchi C., Beuschlein F.,Reincke M., Lorenz K., Allolio B., Kisker C., Fassnacht M. & Lohse M.J. PKA catalytic subunit mutations in adrenocortical Cushing's adenoma impair association with the regulatory subunit. *Nature Communications,* 2014, **5**, 5680.

Conference contributions

Oral presentations

15th Scientific Symposium of the European Network for the Study of Adrenal Tumours (ENSAT) in Birmingham, Great Britain: 'Functional characterization of *PRKACA* mutations in adrenal Cushing'

18th European Congress of Endocrinology (ECE) in Munich, Germany: '*PRKACA* mutations in adrenal Cushing impair association with the PKA regulatory subunit'

4th International Workshop on cAMP Signaling, Protein Kinase A, and Phosphodiesterases: from genetics to function and human diseases in Kayseri, Turkey: '*PRKACA* mutations in adrenal Cushing impair association with the PKA regulatory subunit'

1st Improving Outcome of Cushing's Syndrome (IMPROCUSH) in Munich, Germany: 'Mutations of PKA catalytic subunit in adrenocortical Cushing´s adenomas impair association with the regulatory subunit'

Posters

20th European Congress of Endocrinology (ECE) in Barcelona, Spain: '*PRKACA* mutations in adrenal Cushing induce histone H1.4 hyperphosphorylation'

European Pharma Summit in Berlin, Germany: '*PRKACA* mutations in adrenal Cushing induce histone H1.4 phosphorylation at serine 36'

19th European Congress of Endocrinology (ECE) in Lisbon, Portugal: '*PRKACA* mutations in adrenal Cushing can alter substrate specificity'

60th Deutscher Kongress für Endokrinologie in Würzburg, Germany: 'PRKACA mutations in adrenal Cushing act via different mechanisms'

Awards

ESE poster prize 2017

Bathon K., Weigand I., Vanselow J.T., Ronchi C.L., Di Dalmazi G., Beuschlein F., Sbiera S., Schlosser A., Fassnacht M., Calebiro D. '*PRKACA* mutations in adrenal Cushing can alter substrate specificity', 19th European Congress of Endocrinology (ECE), 2017, Lisbon, Portugal

DGE poster prize 2017

Bathon K., Weigand I., Ronchi C.L., Di Dalmazi G., Beuschlein F., Sbiera S., Fassnacht M., Calebiro D. '*PRKACA* mutations in adrenal Cushing act via different mechanisms', 60th Deutscher Kongress für Endokrinologie, 2017, Würzburg, Germany

Würzburg, …… ……..

Date Kerstin Bathon

14 Acknowledgements

First, I would like to thank my primary supervisor Prof. Davide Calebiro for the great possibility to work on this interesting project. His guidance and support were of great help for me throughout the whole project.

My thanks also go to my secondary and third supervisor, Prof. Martin Fassnacht and Prof. Caroline Kisker, for the helpful discussions and their support not only during my annual meetings.

Additionally, I would like to thank Dr. Isabel Weigand for the good collaboration on our two linked projects and Dr. Cristina Ronchi and Dr. Silviu Sbiera for helpful discussions during our ‘PKA meetings’.

Many thanks also to former and current members of the AG Calebiro for the great support, scientific advices and discussions. Especially, I would like to thank Bianca Klüpfel, Christin Misigaiski and Ines Elsner for their help and technical support in the lab. Special thanks also to Dr. Amod Godbole, Dr. Marie Lise Jobin, Kerstin Seier and Sana Siddig for their support and help. Overall, I would like to thank all members of AG Calebiro for the supportive atmosphere and some nice years.

Additionally, I would like to thank Prof. Andreas Schlosser and Dr. Jens T. Vanselow for their help with the mass spectrometry.

Finally, I would like to thank my family and friends for their emotional support and patience.